UNIVERSIDADE DE LISBOA

FACULDADE DE CIÊNCIAS

DEPARTAMENTO DE GEOLOGIA

THE INTERACTION BETWEEN THE MACROFAUNA AND GEOLOGIC FEATURES IN THE GULF OF CADIZ

DISSERTAÇÃO DE MESTRADO EM CIÊNCIAS DO MAR

Cristiana Pereira da Cunha

Dissertação orientada por:

Professor Doutor Filipe Medeiros Rosas

Professora Doutora Maria Marina Pais Ribeiro da Cunha

2016

As metas que se traçam sem dor e sem sacrifícios,

Nunca serão saboreadas como aquelas

Em que Lutar até ao último segundo,

É acreditar que sempre se pode ir mais longe.

Afinal, superarmo-nos a nós próprios é saber que não há limites,

Que tudo pode acontecer mesmo quando todos à nossa volta

Nos arrastam contra o precipício.

Cristiana Cunha

RESUMO

O Golfo de Cádis encontra-se localizado numa complexa área tectónica a oeste do Estreito de Gibraltar, sudoeste da Ibéria e noroeste de Marrocos. Este está posicionado numa área de transição entre a falha transformante da Gloria, delineando a fronteira entre as placas Africana e Euroasiática, e a parte mais oeste da cintura orogénica Alpina, marcada pelo Arco de Gibraltar. O Golfo de Cádis é uma região sismicamente ativa e como tal, pensasse ter sido o epicentro do Grande Terramoto de Lisboa, Portugal, de 1755, que atingiu um magnitude de 8.5 a 8.7 na escala de Richter. O terramoto originou o maior *tsunami* decorrido até agora na zona oeste da Europa, levando à destruição da cidade de Lisboa. Esta atividade tectónica ocorre no fundo do mar em estruturas responsáveis pelo escape de fluidos, como *pockmarks* (pequenas depressões no fundo do mar), cristas diapíricas, *carbonate mud mounds* e vulcões de lama. Os vulcões de lama são estruturas sedimentares localizadas no fundo do mar, criadas pela rápida advecção de fluidos e lamas saturadas de metano, provenientes das camadas sobre pressionadas de sedimentos do fundo do mar. Estes devido a exalação de fluidos geológicos, permitem a existência de comunidades biológicas quimiossintéticas.

O principal objetivo deste trabalho consiste em compreender a influência das falhas SWIM e dos vulcões de lama na distribuição da macrofauna no Golfo de Cádis. Vários passos foram realizados de forma a tornar possível a sua concretização, assim como a consulta de artigos publicados, onde se recolheram 122 espécies do filo Annelida, Mollusca, Arthropoda, e Echinodermata, o uso da batimetria multifeixe e da refletividade do fundo do mar (backscatter) com o intuito de se obter informação espacial detalhada sobre as estruturas em estudo, a localização geográfica, a distância das falhas SWIM e a sua associação com os vulcões de lama, e a examinação das correntes oceanográficas locais. Das espécies em estudo, 29 são quimiotróficas (18 da classe Poliqueta e 11 da classe Bivalvia) e 93 heterotróficas (17 da ordem Tanaidacea, 16 da classe Ophiuroidea, 56 da classe Gastropoda e 3 da classe Bivalvia). As espécies heterotróficas incluem todos os organismos que obtêm energia para o seu metabolismo a partir de fontes de carbono orgânico, em oposição encontram-se as espécies autotróficas que fixam o carbono inorgânico usando a luz do sol (fotoautotróficos) ou energia química (quimioautotróficos). Os seres quimioautotróficos (neste trabalho denominados de quimiotróficos), devido à ausência de luz, são os únicos organismos a habitarem o fundo do mar. Estes organismos normalmente vivem em fontes hidrotermais, fontes frias e outros ambientes redutores, e podem ser, ou não, simbiontes. As fontes hidrotermais, na sua maioria, estão localizadas ao longo do oceano onde fluidos a elevadas temperaturas se libertam do fundo do mar. Estas podem ser distinguidas entre dois tipos principais: as fumarolas negras e as brancas. As fumarolas negras emitem colunas de fumo quente, por volta dos 370 ºC, e são compostas por partículas pretas e finas de sulfureto. Este fluido mistura-se rapidamente com a água de fundo (bottom water) rica em oxigénio, resultante da precipitação de grandes quantidades de sulfureto e silicato, formando assim as chaminés hidrotermais. No geral, as fumarolas brancas encontram-se nas margens dos montes e descarga de fluidos, exibindo temperaturas entre os 265 e 300 ºC. Devido as suas baixas temperaturas, quando comparadas com as fumarolas negras, as fumarolas brancas estão incrustadas de tubos de vermes e outos organismos. As fontes frias são sistemas geológico e geoquímico ativos localizados onde o enxofre e o metano reduzido emergem dos

sedimentos do fundo do mar, que se formam devido à migração ascendente de hidrocarbonetos dissolvidos e/ou gasosos. As fontes frias ocorrem nas margens passivas e ativas do mundo inteiro e apresentam uma grande variação temporal e espacial de fluxo. As suas expressões superficiais incluem vulcões de lama, pockmarks, piscinas de água salgada, óleo e infiltrações de asfalto, sendo os vulcões de lama e os pockmarks os mais comuns.

Os dados utilizados neste trabalho foram compilados a partir da bibliografia mais relevante sobre a macrofauna dos vulcões de lama do Golfo de Cádis, incluindo vários artigos publicados recentemente (Dworschak and Cunha 2007; Génio *et al*. 2008, 2013; Hilário and Cunha 2008; Rodrigues *et al*. 2008; Blażewicz-Paszkowycz *et al*. 2011a, 2011b; Oliver *et al*. 2011; Rodrigues *et al*. 2011, 2013). As amostras foram recolhidas utilizando diferentes equipamentos (p.e.: Gravity Corer - GC, FLUFO Lander - FLUFO, USNEL Box Corer - USNEL, Multi Corer - MUC, Geology Dredge - GD, Kasten Corer - KC, BIGO Lander - BIGO, TV-Grab - Gr, Suction Sampler ROV - SUS, Push Corer ROV - PUC, NIOZ Box Corer - NIOZ) dependendo do objetivo específico da cada campanha, da natureza geológica do fundo do mar amostrado e da disponibilidade de equipamentos do navio.

No ArcMap, o componente principal do ArcGis (Sistema de Informação Geográfico) foi criada uma base de dados geográfica usando-se o ArcCatalog, de nome Biodata, para armazenar todos os dados espaciais e tabulares. Os dados foram organizados em *layers*: *Feature Classes* e *Raster Dataset*, dando origem aos mapas utilizados ao longo desde trabalho. Todos os mapas foram projetados utilizando-se o sistema de coordenadas UTM Zona 29N *Datum* WGS84.

No total foram analisadas 122 espécies recolhidas em 105 estações, 18 pertencem à família Siboglinidae (filo Annelida, classe Polychaeta), 14 à classe Bivalvia (filo Mollusca), 56 à classe Gastropoda (filo Mollusca), 17 à ordem Tanaidacea (filo Arthropoda, Subfilo Crustacea, classe Malacostraca), uma à ordem Decapoda (filo Arthropoda, subfilo Crustacea, classe Malacostraca) e 16 à classe Ophiuroidea (filo Echinodermata). No Golfo de Cádis, a maior concentração de espécies encontra-se a pouca profundidade (200 a 1200 m) e estão maioritariamente localizadas nos vulcões de lama. As espécies heterotróficas foram encontradas na maioria das estruturas em estudo, com exceção do vulcão de lama Semenovich. Este resultado está de acordo com o esperado, uma vez que os organismos heterotróficos apresentam uma distribuição global. O número de espécies heterotróficas diminui com o aumento da profundidade, possivelmente devido à escasses de alimento. A via nutricional dominante dentro dos organismos quimiotróficos é a *thiotrophy*, o que acontece devido à elevada disponibilidade de enxofre na forma de sulfureto ou enxofre nas áreas de infiltração de metano no Golfo de Cádis. As espécies metanotróficas apenas se encontram em dois vulcões, *Mercator* (351 m) e Captain Arutyunov (1324 m), o que indica que o sistema biogeoquímico no Golfo de Cádis é possivelmente dominado por enxofre. A elevada concentração de espécies quimiotróficas ocorre em vulcões de lama localizados nas falhas SWIM 1 e SWIM 2, a uma profundidade superior a 1220 metros, o que sugere que estas falhas agem preferencialmente como condutas de fluidos, alimentando essas espécies. De uma forma geral, as infiltrações de metano são especialmente comuns e ativas a profundidades entre os 500 e os 1000 metros, em que a temperatura e a pressão combinam para desestabilizar os hidratos de gás, mas no Golfo de Cádis esta profundidade pode aumentar devido à influência da água quente vinda do Mediterrâneo (*Mediterranean Outflow Water*). A maior limitação deste trabalho foi a diferença existente entre o esforço de amostragem, que se encontrava entre uma e 19 estações.

Palavras-Chave: Macrofauna, Espécies Quimiotróficas, Vulcões de Lama, falhas SWIM, Golfo de Cádis, distribuição geográfica.

ABSTRACT

The Gulf of Cadiz is located in a complex tectonic area of the North-East Atlantic Ocean, west of Gibraltar Strait, offshore SW Iberia and NW Morocco. It straddles across the Africa-Eurasia lithospheric plate boundary, defined by the SWIM strike-slip faults, where presently tectonic activity is occurring. This tectonic activity is reflected in fluid escape structures on the seabed: pockmarks, diapiric ridges, carbonate mud mounds and mud volcanoes. The exhalation of geological fluids allows for the existence of biological chemosynthetic communities on the mud volcanoes of the Gulf of Cadiz. The main goal of this work is to understand the influence of the SWIM faults and mud volcanoes on the distribution of macrofauna. This study was based on published records of 122 species of the Phyla Annelida, Mollusca, Arthropoda, and Echinodermata, spatial information extracted from detailed swath bathymetry and backscatter, geographic localization, distance to the SWIM faults and association to mud volcanoes and inspection of the local oceanographic currents.

The data used in this work was compiled from the most relevant bibliography on the fauna observed in the Gulf of Cadiz mud volcanoes, including several recently published articles (Dworschak and Cunha 2007; Génio *et al*. 2008, 2013; Hilário and Cunha 2008; Rodrigues *et al*. 2008; Blażewicz-Paszkowycz *et al*. 2011a, 2011b; Oliver *et al*. 2011; Rodrigues *et al*. 2011, 2013). The samples were obtained using different gears depending namely on the specific objectives of each campaign, on the geological nature of the sampled seafloor, and on the ship equipment availability.

Using the ArcMap, a comprehensive geodatabase was created using ArcCatalog to store all the spatial and tabular data. The data was organized in layers: Feature Classes land Raster Dataset, which allowed to create the final maps. In total 122 species were analysed from 105 stations, 18 belong to the Family Siboglinidae (Phylum Annelida, Class Polychaeta), 14 to the Class Bivalvia (Phylum Mollusca), 56 to the Class Gastropoda (Phylum Mollusca), 17 to the Order Tanaidacea (Phylum Arthropoda, Sub-Phylum Crustacea, Class Malacostraca), one to the Order Decapoda (Phylum Arthropoda, Sub-Phylum Crustacea, Class Malacostraca) and 16 to the Class Ophiuroidea (Phylum Echinodermata).

In general, the higher concentrations of species in the Gulf of Cadiz occur at low depths, from 200 to 1200 m and are mostly located in the mud volcanoes. The heterotrophic species were found in most of the studied features of the Gulf of Cadiz, except in Semenovich MV, as expected, since they occur globally. The number of these species decreases with depth probably because the available food also becomes scarcer. The thiotrophy is the dominant nutritional pathway of the chemotrophic species. It occurs due to the high availability of sulfur in the form of sulfide or sulfur in the methane seepage areas of the Gulf of Cadiz. Therefore these species only occur in mud volcanoes, except in Pen Duick Escarpment. The methanotrophic species are only located in two mud volcanoes, Mercator (351 m) and Captain Arutyunov (1324 m), which indicates that the biogeochemical system in the Gulf of Cadiz is probably dominated by sulfur. The highest concentration of chemotrophic species occur in mud volcanoes located on the SWIM 1 and SWIM 2 faults at water depths ≥ 1200 m. Thus suggesting that these faults act as preferential fluid conduits, feeding those species. In general, the methane seeps are especially common and active at water depths of 500–1000 m, where temperature and pressure combine to destabilize gas hydrates (Hester and Brewer, 2009), but in the Gulf of Cadiz this depth may be greater owing to the influence of the warmer Mediterranean Outflow Water (Niemann *et al.* 2006; Sommer *et al.* 2009).

Keywords: Macrofauna, Chemotrophic Species Mud Volcanoes, SWIM faults, Gulf of Cadiz, geographic distribution.

ACKNOWLEDGEMENTS

This research project would not be possible without the support of several people. They have helped and gave me hope to finish this stage of my life.

First of all, I would like to thank God, my mother Elisa Viola, my father Rui Cunha and my brothers Pedro Cunha and Jorge Cunha for making me strong and believing in me.

Secondly, I would like to express my deepest gratitude to my supervisors, Filipe Rosas, Marina Cunha and Pedro Terrinha, for their availability and professionalism. Thank you for your guidance, numerous suggestions and encouragement, which helped leading this project to its completion.

I´m very grateful to the Pedro Terrinha team, without them this project would not be possible. They were my family, one amazing family during these months. A big, big thank to Pedro Terrinha, Carlos Ribeiro (the sweet Calex), Victor Magalhães, João Noiva, Debora Duarte, Sara Rodrigues, Marta Neres, Pedro Brito, Luís Baptista, Rui Quartau, Marisa Borralho, João Silva, Sónia Silva, Rachid Omira, Manuel Teixeira and João Duarte. They are the best co-workers ever.

A big thanks to Professor Rui Taborda and this scientific team, in special to Mafalda Carapuço and Ivana Bosnic for all support with the program ArcGis.

I´m also very grateful to Luciana Génio and Fábio Matos of the CESAM, Biology department, Aveiro University for allowing me to use the Class Gastropoda images.

I would also like to thank João Sobral, Paulo Alves, Luís Antunes, André Gaspar, Vanessa Rodrigues, Telma Marques, Dário Lucas for their excellent work. Your friendship and affection was very important to me. Thank you to all for reading parts of my project.

I´m also very grateful to Alcina Sousa, António Osório, André Azinheiro, Ana Teresa Marques, Luís Leão, Nuno Orfão, Gonçalo Dias, Hugo Monteiro, Ariana Moutinho, Carlos Gomes (the fofinho) and my new friend Ricardo Maçãs for the motivation and support.

A very special thanks to Rúben Soares, because without him this wouldn´t have been possible. You gave me a home, friendship, food, and everything that I needed in Lisbon.

Last but not the least, a very special thanks to a special boy named Tiago Nascimento. He believed me, gave me strength in all moments in special when everything was confused in my head; he was a good friend. I´m grateful for all moments spent by your side, our conversations, your love, your friendship, our lovely dinners and for everything. I miss your kiss, your hugs, your smile and our conversations; in one word I miss you. Without you, the sun has some clouds in his eyes.

TABLE OF CONTENTS

LIST OF FIGURES

Figure 2.4 - Simplified tectonic map of the Gulf of Cadiz area. Dark grey outline - Gulf of Cadiz Accretionary Wedge (GCAW; White lines – SWIM wrench system according to Zitellini *et al*. 2009). Black dots correspond to the location of known mud volcanoes (e.g.: Duarte *et al*. 2011);

Figure 3.1 - Gulf of Cadiz showing the three study areas of this work. Pink area - Deep Field (1200 – 4000 m); Blue area – Carbonate Province (600 – 1200 m); Green area - El Arraiche Field (200 – 600 m). Black dashed lines – limit of Portuguese, Spanish and Moroccan Exclusive Economic Zones;

Figure 3.2 – Gulf of Cadiz showing all sampled features in this work (Green dots). White dots – The features discovered until now in the Gulf of Cadiz. A, B and C: Zoom of the areas located inside the black squares, detailing the morphology of the Anastasya MV, Pipoca MV and Tarsis MV, Shouen MV, Yuma MV, Darwin MV and Ginsburg MV and No Name MV, Kidd MV, Lazarillo de Tornes MV, Pen Duick Escarpment (PDE), Gemini MV, Fiúza MV, Mercator and Vernadsky Ridge (VR);

Figure 3.3 - Schematic representation (cross section) of the criteria established to consider if a MV is related or not with a SWIM fault;

Figure 3.4 - Morphology of the El Arraiche mud volcano field (from Van Rensbergen *et al.* 2005b). DQ – Don Quichote; LdT - Lazarillo de Tormes;

Figure 3.5 - Schematic representation of the Gulf of Cadiz showing the main mud volcano fields in their structural setting (from Van Rensbergen et al. 2005b). GDR - Guadalquivir Ridge; SPM - Spanish Morrocan margin;

Figure 3.6 – A: Detail of some features of the Gulf of the Cadiz. Localization of the seismic line observed in (B); B: General high-resolution seismic line (sparker source) over Al Idrissi, Fiúza and Gemini mud volcanoes and Pen Duick escarpment. The mud volcanoes are characterized by a reflection-free seismic facies that show stacked outflow lenses within a stratified series of hemi-pelagic sediments above a regional unconformity. The inset shows a detail of interfingering mud flows that accumulate in moats at the base of the Fiúza mud volcano cone (Van Rensbergen *et al.* 2005b);

Figure 3.7 – A: Schematic overview of the stratigraphic setting of the Vernardsky Ridge and Mercator MV showing the location of the salt diaper. B: Geological interpretation of the seismic section (C). C: High-resolution seismic line over the Mercator MV, the outcrop of the Vernadsky Ridge and the Buried MV (Haffert *et al.* 2013).

Figure 3.8 – Swath bathymetry at the exit of the Gibraltar Strait (modified from Hernández-Molina *et al*., 2014). Red Lines – Delimit Northern and Southern parts of the Channel;

Figure 3.9 - Swath bathymetry of the central sector of the middle slope of the Gulf of Cadiz Contourite System, showing the main contourite channels, furrows and main diapiric ridges, with a NNE trend. Red line – Cadiz Channel (from Hernández-Molina *et al*. 2006);

Figure 4.1 – Examples of gear used to collect the samples analysed in this work. Gravity Corer - Mooring Systems, inc. website: http://www.mooringsystems.com/; Box Corer - KC Denmark website: http://www.kc-denmark.dk/; BIGO Lander - Pfannkuche *et al*., 2006; TV-Grab - Pfannkuche *et al*., 2006; Geology Dredge - American Geophysical Union website: http://blogs.agu.org/; Kasten Corer -

Alfred Wegener Institut website: www.awi.de; Multi Corer - Alliance for Coastal Technologies website: http://www.act-us.info/;

Figure 4.2 – The main operation performed in ArcMap;

Figure 5.1 – Number of species per feature. A: Chemotrophic species (Class Bivalvia and Polychaeta); B: Heterotrophic species (Order Tanaidacea, Class Gastropoda, Bivalvia and Ophiuroidea). Red rectangles - MV located at less than 10 km to the SWIM faults. West of Gibraltar (WoG); Vernadsky Ridge (VR); Pen Duick Escarpment (PDE); Iberico (Ibe); Formosa Ridge (FR); Cadiz Channel (CC); Al Idrissi (AI); Fiúza (Fiú); Gemini (Gem); Mercator (Mer); Lazarillo de Tornes (LdT); kidd (kid); No Name (NN); Anastasya Area (off Tarsis; AA); Meknès (Mek); Student (Stu); Ginsburg (Gin); Yuma (Yum); Aveiro (Av); Jesus Baraza (JB); Shouen (Sho); Darwin (Dar); Captain Arutyunov (CA); Sagres (Sag); Carlos Ribeiro (CR); Bonjardim (Bom); Semenovich (Sem); Porto (Por);

Figure 5.2 – Distribution of polychaetes. Green dots – Specie *Polybrachia* sp.1; Blue dot – Specie *Polybrachia sp.2; Pink dot* – Specie *Polybrachia sp.3; Red dots* – Specie *Polybrachia Va; Dark grey dots* – Specie *Polybrachia Vb; Dark blue dot* – Specie *Polybrachia Vc;*

Figure 5.3 – Distribution of polychaetes. Green dots – Specie *Siboglinum* Ia; Pink dots - Specie *Siboglinum* Ib; Blue dots – Specie *Siboglinum* Ic; Red dots – Specie *Siboglinum* Id; Dark grey dot – Specie *Siboglinum* Ie; Drk blue dots – *Siboglinum* If; Dark green dots – *Siboglinum* cf. *poseidon*i; Black dot – *Siboglinum* sp.1; Grey dots – *Siboglinum* sp.2;

Figure 5.4 – Distribution of polychaetes. Blue dot - Specie *Bobmarleya gadensis*; Red dot – Specie *Lamellisabella denticulate;* Green dot - Specie *Spirobrachia tripeira;*

Figure 5.5 – Distribution of bivalves. Green dots - Specie *Acharax gadirae;* Blue dots - Specie *Solemya (Petrasma) elarraichensis;*

Figure 5.6 – Distribution of bivalves. Dark blue dot - Specie *Axinulus croulinensis*; Blue dot - Specie *Spinaxinus* cf. *sentosus*; Green dots - Specie *Thyasira (Parathyasira) granulosa*; Pink dot - Specie *Thyasira tortuosa*; Red dots - Specie *Thyasira vulcolutre*;

Figure 5.7 – Distribution of bivalves. Green dot - Specie "*Bathymodiolus" mauritanicus;* Blue dot - *Isorropodon megadesmus; Red dot - Isorropodon* sp. indeterminate; Purple dot - *Lucionoma asapheu*;

Figure 5.8 - Distribution of tanaids. Green dots – Suborder Apseudomorpha (family Apseudidae and Sphyrapodidae); Blue dots – Suborder Tanaidomorpha (family Colletteidae, Leptocheliidae, Paratanaoidea incertae sedis, Pseudotanaidae and Tanaellidae);

Figure 5.9 – Distribution of ophiuroids. Green dots - Family Amphilepididae; Dark blue dots - Family Amphiuridae; Blue dot - Family Ophiacanthidae; Yellow dots – Family Ophiactidae; Pink dot – Family Ophiolepididae; Red dot - Family Ophiuridae;

Figure 5.10 – Distribution of gastropods. Pink dots - Subclass Caenogastropoda;

Figure 5.11 – Distribution of gastropods. Blue dots - Subclass Vetigastropoda;

LIST OF TABLES

ABBREVIATIONS

GCAW:	Gulf of Cadiz Accretionary Wedge
SWIM:	South West Iberian Margin
NACW:	North Atlantic Central Water
ENACW:	Eastern North Atlantic Central Waters
ENACWt:	Eastern North Atlantic Central Waters subtropical
ENACWp:	Eastern North Atlantic Central Waters subpolar
MLD:	Mixed Layer Depth
NADW:	North Atlantic Deep Water
AIW:	Atlantic Inflow Water
MOW:	Mediterranean Outflow Water
MU:	Mediterranean Upper Water
ML:	Mediterranean Lower Water
SB:	Southern Branch
PB:	Principal Branch
IB:	Intermediate Branch
MV:	Mud Volcano
MVs:	Mud Volcanoes
TTR:	Training Through Research
AOM:	Anaerobic Oxidation of Methane
O_2:	Oxygen

H_2S: Hydrogen Sulfide

CO_2: Carbon Dioxide

WMF: Western Moroccan Field

MSM: Maria Sibylla Merian

Chapter 1

Introduction

1.1. Motivation and objectives

The Gulf of Cadiz has been studied extensively since the 1970ies from a geological, oceanographic and biological point of view for various reasons, such as:

- It straddles across the Africa-Eurasia lithospheric plate boundary, defined by the South West Iberia Margin (SWIM) strike-slip faults, where the Alpine orogeny terminate;
- It is the locus of important mega-seismicity, like the 1755 Lisbon earthquake;
- It is a gulf where various Atlantic currents come together and meet the Mediterranean Outflow Water;
- Biological chemosynthetic communities associated with the exhalation of geological fluids have been found in the last two decades, only.

The mud volcanoes in the Gulf the Cadiz have been studied for the past two decades and it has been found that they host chemosynthetic species associated with cold seeps that depend on methane and sulphate. The motivation for this work is trying to understand if there is a relationship between the geologic substrate, environmental conditions and the distribution of the macrofauna.

Thus, the main goal of this work is to understand the influence of the SWIM faults and the mud volcanoes on the distribution of macrofauna in the Gulf of Cadiz. This study was based on published records of 122 species of the Phyla Annelida, Mollusca, Arthropoda, and Echinodermata, spatial information extracted from detailed swath bathymetry and backscatter, geographic localization, distance to the SWIM faults and association to mud volcanoes and inspection of the local oceanographic currents.

In order to achieve this scientific goal the following technical tasks were carried out:

1. Construction of a database including the compilation of all biological information available in published scientific papers;

2. Using the ArcGIS software as a study tool in order to analyse the spatial distribution of macrofauna in the Gulf of Cadiz;

3. Analyse the macrofauna species distribution according to their metabolic strategy, geographic distribution and depth;

4. Analyse the distribution of the macrofauna as a function of the distance to the SWIM faults and to mud volcanoes.

1.2. Thesis Outline

This dissertation is organized in the following sixth chapters:

First Chapter - Introduction

The thesis presents an introduction (this chapter) about the fluid circulation and seepage in sedimentary basins, the geophysic data, the submarine mud volcanoes, the general context of the Gulf of Cadiz and the Trophic Status.

Second Chapter – Regional Setting

The second chapter describes the main environmental drivers of the biological assemblages studied in this work: the oceanographic circulation in the Gulf of Cadiz and the existence of major right-lateral strike-slip faults (the so called SWIM faults).

Third Chapter – Study Areas

The third chapter presents all study areas within the Gulf of Cadiz in which macrofauna species were reported to occur: the El Arraiche Field, the Carbonate Province. The geologic and biologic characteristics of these features are described, based on the information available from published scientific papers and cruise reports.

Fourth Chapter – Data and Methods

The fourth chapter addresses the employed methodological approach, including several aspects of the used software package, the ArcGis.

Fifth Chapter – Results

In the fifth chapter are presented the main results of the analyses performed, including mapping of taxa distribution.

Sixth and Seventh Chapters – Discussion and Conclusion

The sixth chapter concerns the discussion of the obtained results, and the seventh chapter the consequent main conclusions.

1.3. Fluid Circulation and Seepage in Sedimentary Basins

The chemoautotrophs, because of the absence of light, are the only autotrophic organisms in the deep sea (see **subchapter 1.7**). These organisms usually inhabit hydrothermal vents, cold seeps and other reducing environments and can be free-living or symbiotic. Since cold vents are so far the only source of crustal fluids exalted into the shallow sediments and to the seafloor in the study area, these

systems are have described in more detail as well as the origin of methane, the main energy source for chemotrophic species at these depths.

1.3.1. Hot Vents

The seafloor seepage can be distinguished in two categories, Hot Vents (Hydrothermal Vents) and Cold Seeps. Hot Vents, in its majority, are located along the ocean spreading centres where high temperature fluids escape from the seafloor (Damm, 1990). Asthenospheric upwelling brings the mantle rocks up to the surface. As a result, the lithostatic pressure decreases, allowing adiabatic fusion of part of the mantle rocks. The resulting magmatic fluid of this partial fusion (primary magma) feeds the oceanic ridges' typical volcanism. This volcanism, drastically, modifies the geothermal gradient. The geothermal gradient variation promotes water convention through the oceanic crust rocks (i.e.: Basalts). In contact with the oceanic crust rocks, the seawater heats up to 300-400°C and becomes extremely corrosive. This hot fluid dissolves the surrounding basaltic rock, leaching out metals and other elements. The fluid begins rising rapidly back to the surface due to increased pressure, being responsible for the occurrence of fluid seepage at the sea floor (Hot Vents). Two main types of hot venting systems, can be distinguish, the black or the white smokers (**Figure 1.1** and **1.2**). The black smokers emit hot plumes (~370ºC) loaded with fine, dark particles of sulphide material. This fluid is quickly mixed with the ambient oxic bottom water, resulting in the precipitation of bulk sulphide and silicate minerals, forming hydrothermal vent chimneys (Kelley, 2001; Gartman *et al.* 2014). The white smokers are, in general located on the margins of the mounds and discharge fluids exhibiting temperatures between 265 and 300 °C. Due to their relatively lower temperatures, when compared with the black smokers, the white smokers are typically encrusted with worm tubes and other organisms. Their venting fluids are white because the white barium and calcium sulphate ($BaSO_4$ + $CaSO_4$) minerals precipitates (Libes, 1992; Kelley, 2001).

1.3.2. Cold Seeps

Cold seeps form due to upward migration of hydrocarbons, dissolved and/or gaseous (Fischer *et al.* 2012; Sauer *et al.* 2015). These geologically and geochemically active systems (Omoregie *et al.* 2009) are found where reduced sulfur and methane emerge from seafloor sediments (Levin, 2005). They occur worldwide (**Figure 1.3)** at passive and active continental margins and show strong temporal and spatial variations in the flux (Fischer *et al.* 2012; Sauer *et al.* 2015). The cold seeps surface expressions include mud volcanoes, pockmarks, brine pools, oil and asphalt seeps, being the mud volcanoes and pockmarks the most common (Petersen and Dubilier, 2009). The Gulf of Mexico, the Gulf of Cadiz (the most extensive cold seepage area known along the different European margins; Dworschak and Cunha, 2007; Hilário and Cunha, 2008; Rodrigues *et al*. 2008), the continental margins of India, the western African margin and the Eastern Mediterranean, are examples of passive margins prone of cold seepage (Omoregie *et al.* 2009; Wenau, 2013). These active seafloor systems often host dense and diverse microbial and faunal communities fuelled by low temperature fluids (when compared with the hot vents) and by gas emissions to the sea floor (Omoregie *et al.* 2009; Petersen and Dubilier, 2009; Wenau, 2013). The typical temperatures of the cold seep are close to the temperature of the bottom sea water where they occur.

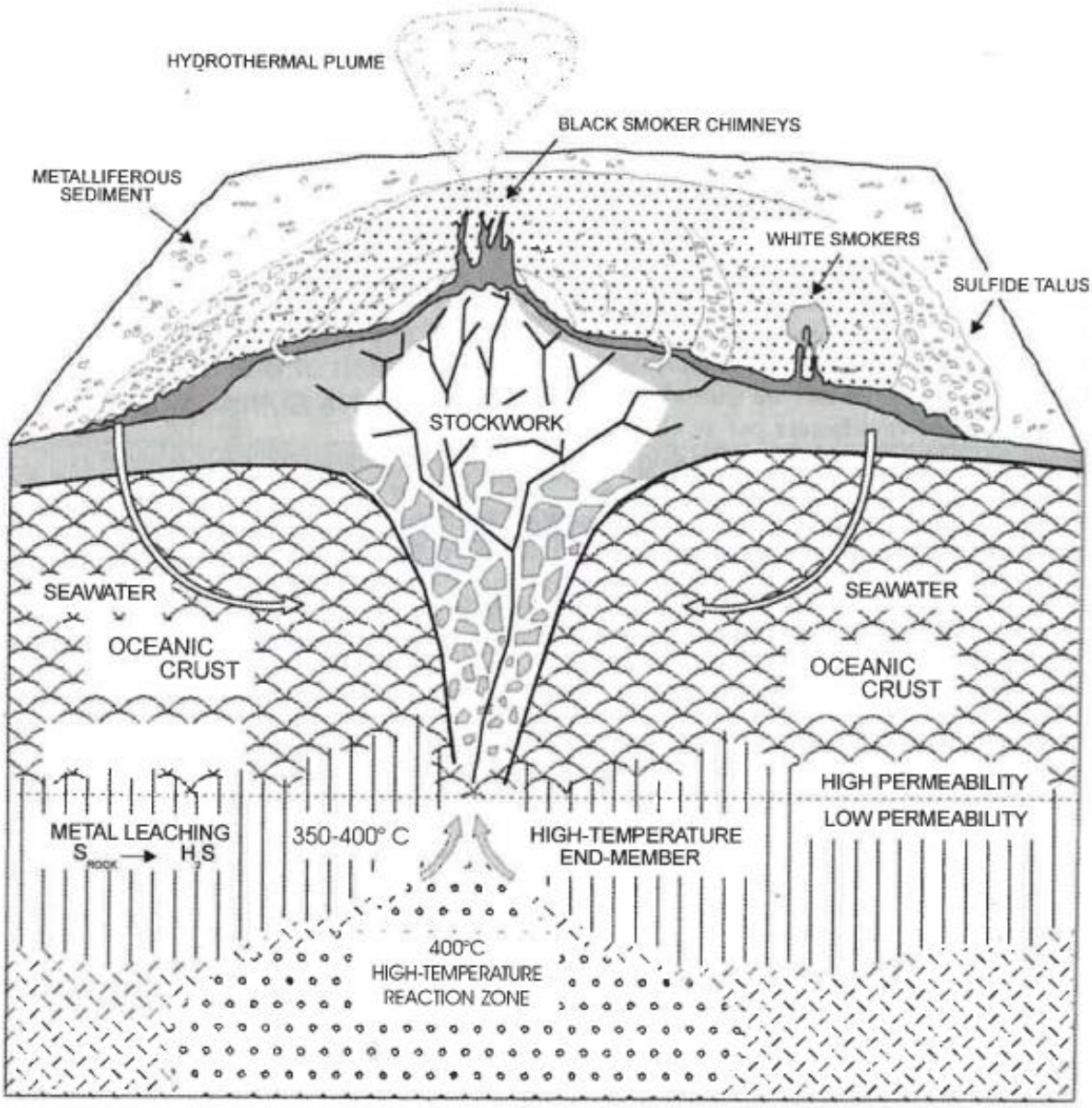

Figure 1.1 - Surface features and internal structures of an active hydrothermal mound and stockwork complex at an oceanic spreading centre (Schulz and Zabel, 2000).

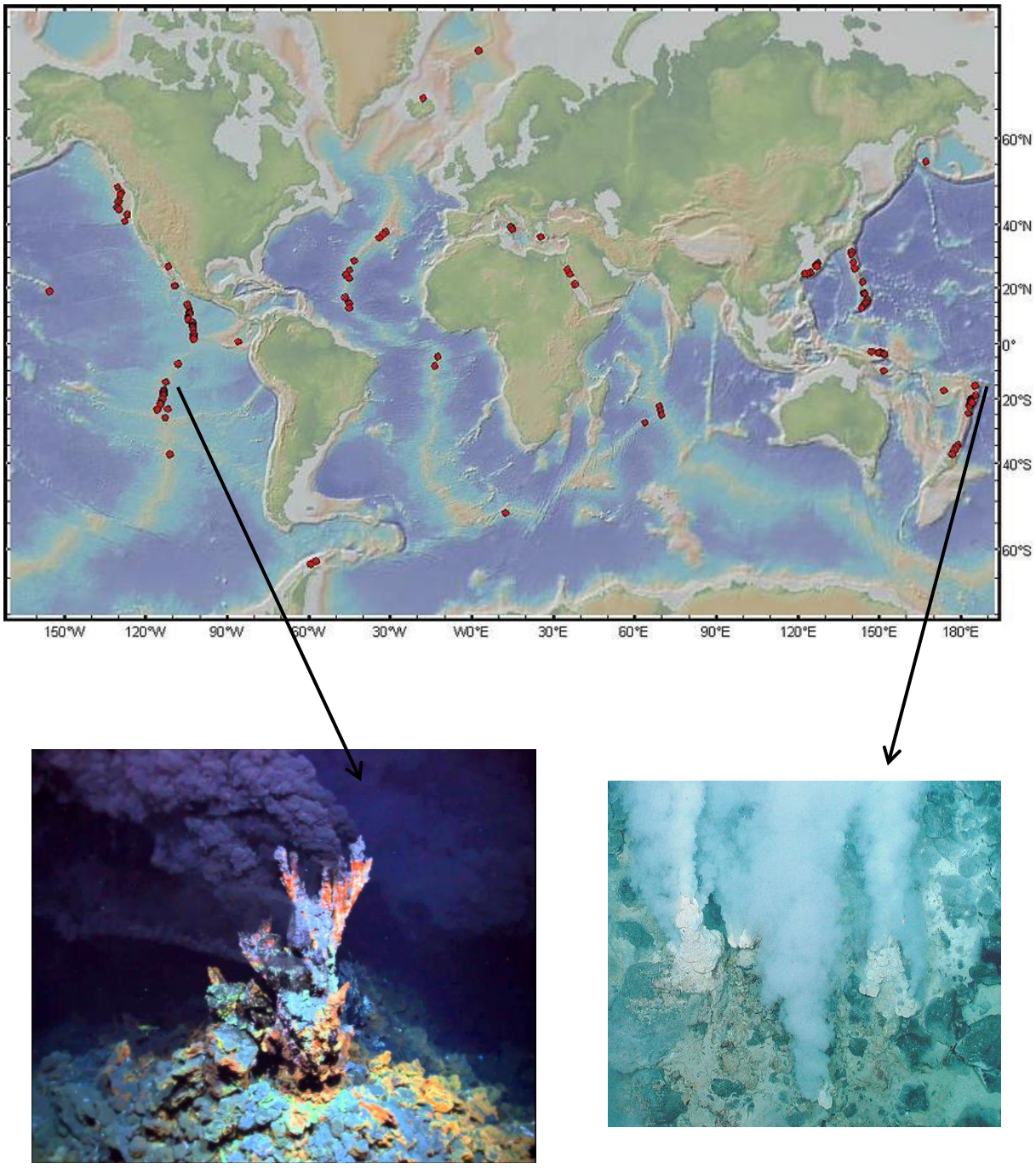

Figure 1.2 - A: Global distribution of the Hot Vents (Archive Website: http://archive.noc.ac.uk/). B: Black smokers located in the Pacific Ocean (Hydrothermal vents Sound Website: http://www.bio.miami.edu/); C: White smokers near to the Vanuatu Island from NW of Australia (Piccola Era Glaciale Website:http://PiccolaEraClaciale.com).

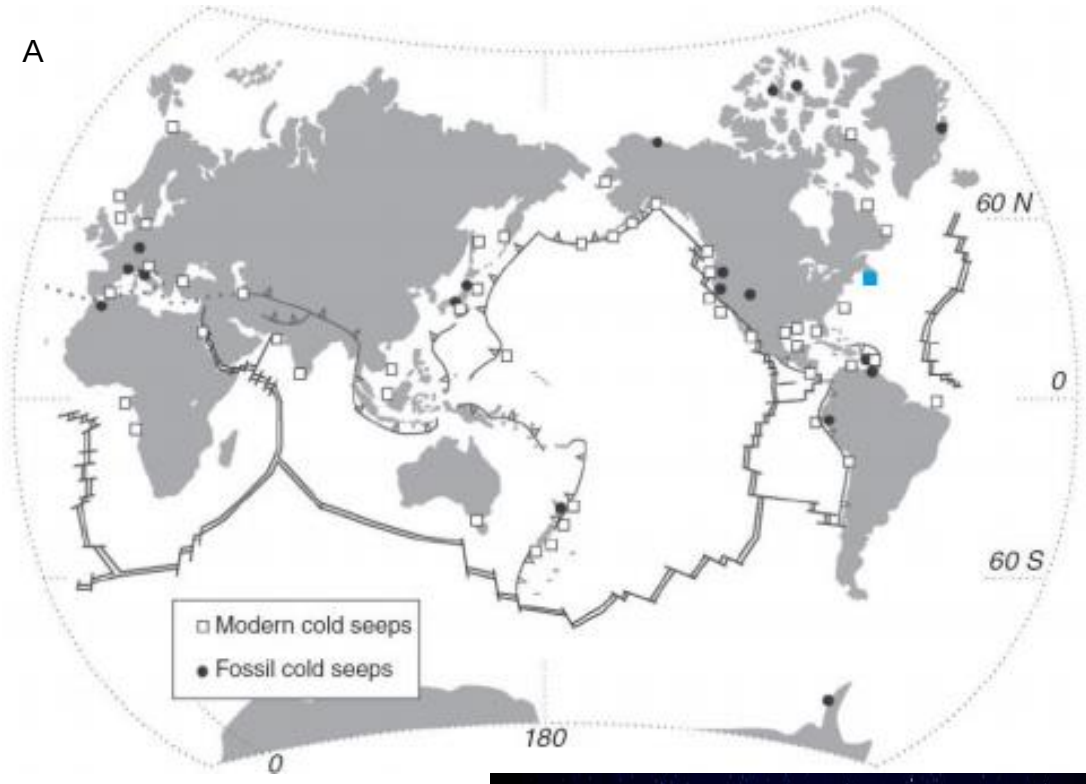

Figure 1.3 – A: World-wide distribution of modern and ancient cold seeps (adapted from Campbell *et al*. 2002). B: Methane bubbles (Gas Plumes) flow in small streams out of the sediment on an area of seafloor offshore Virginia north of Washington Canyon (Okeanos Explorer Website: http://oceanexplorer.noaa.gov/). The blue square shows the methane bubbles location, illustrated by Figure B.

1.3.3. Methane formation

In the earth´s crust, the methane is very abundant and it is often found to be related with fluid flow features and gas hydrate formation. In seabed sediments there are three possible sources of methane: thermogenic, abiogenic and microbial (as specified above).

Methane seepage occurs when the amount of organic matter contents in the sediments are sufficient to allow the generation of high volumes of methane within the sedimentary column and the features that facilitate the methane migration towards the seafloor are present. The escape of fluids, such as methane from the seafloor is a consistent feature throughout geologic time, as documented by both seismic surveys and seepage outcrops (Judd, 2003).

1.3.3.1. Thermogenic Methane

The thermogenic methane occurs when the organic matter that is not degraded by methanogenic microbes within the top 1000 m of the sedimentary column is buried and can be degraded by thermocatalystic processes. The organic matter that survives the burial is transformed into amorphous organic matter (kerogen), under the influence of increasing temperature and pressure. The kerogen undergoes thermal cracking, while burial increases, which leads to the formation of various hydrocarbons compounds with solid, liquid and gaseous fractions. The most abundant and mobile molecule formed is the methane, since it has the simplest and the smallest molecule size, therefore it is the most prone to migrate to the seabed (Judd, 2001).

1.3.3.2. Abiogenic Methane

Abiogenic methane (or abiotic) is formed by chemical reactions (carbon dioxide reduction; Lollar *et al.* 2002) that do not directly include organic matter (Etiope and Lollar, 2013). The most commonly invoked reaction for abiotic hydrocarbons generation is the Fischer–Tropsch type reaction that converts CO_2 to hydrocarbon gas by reacting it with H_2 (Potter *et al*., 2004; 2013; Cao *et al*., 2014):

$$nCO_2 + (3n + 1)_2 \rightarrow CnH2n+2 + 2nH_2O \qquad \text{Equation 1.1}$$

Methane (CH4) is produced when n = 1:

$$CO_2 + 4H_2 \rightarrow CH_4 + 2H_2O \qquad \text{Equation 1.2}$$

The hydrothermal alteration of Fe-rich minerals, at temperatures above 200ºC, is one of the possible origins of the H_2 required for the reaction (Potter *et al.* 2004; Tassi *et al*. 2012). This process occur during the magma cooling, during the serpentinizations of ultramafic rocks (e.g. the serpentinization of olivine in ultramafic rocks will generate magnetite and H_2, which contributed to the elevated CH_4 and H_2 concentrations in hydrothermal fluids venting from submarine ultramafic-hosted systems, fumarolic gases of volcanoes and in fluid inclusions in alkaline complexes; Lollar *et al.* 2002; Cao *et al*., 2014) and more commonly in hydrothermal systems during water-rocks interactions (Lollar *et al.* 2002).

1.3.3.3. Microbial Methane

The decomposition of organic matter, realized by microbial activity (e.g.: methanogenic archaea), at small burial depths under low temperature and pressure conditions, originated the microbial methane (Judd, 2001; Moore and Wade, 2013). In the oceans, the most of the organic matter available is generated through photosynthesis by primary producers (autotrophs organisms; see **subchapter 1.7**)

and after the dead of the organisms, settles through the water column. The organic matter is oxidized in the uppermost oxygen-rich layer of the sedimentary column (the top few millimetres or centimetres of the sediments) as long as oxygen is available. In the anoxic environment immediately below the oxygen rich zone, oxidation stops and the organic matter is buried and may be decomposed anaerobically. This is a very complex process and the final steps of it may be summarized by the following equation representing the formaldehyde decomposition into methane and carbon dioxide by the action of methanogenic microbes:

$$2CH2O \rightarrow CH4 + CO2 \qquad \text{Equation 1.3}$$

1.3.4. Gas Hydrates

Gas hydrates are crystalline solids formed from water and hydrocarbon gases under low temperature and high-pressure conditions (**Figure 1.4**; Léon *et al.* 2009). The water molecules form cages containing guest molecules such as methane and other light hydrocarbons (ethane, propane, butane and pentane; Grauls, 2001). They are common worldwide in sediments of continental margins at water depths exceeding 300 m (Léon *et al.* 2009). The methane hydrate is the most common hydrate form in the marine sediments (Schmidt *et al.* 2005) but clathrates of carbon dioxide or sulphide may also occur (Arvo, 2014). Gas hydrates are considered by the scientific community as the main hydrocarbon source for the coming century, as resources account for 50 % of the total organic carbon in the earth or twice the conventional fossil fuel energy (Grauls, 2001).

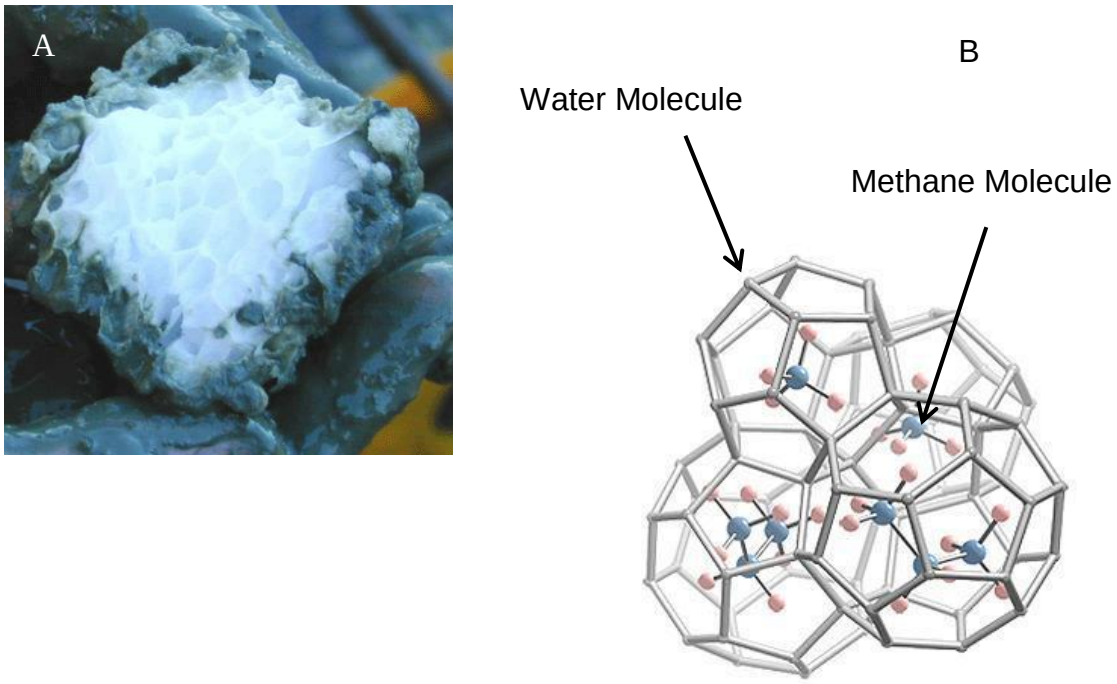

Figure 1.4 – Gas hydrates. A: Hand sample of the methane clathrate (Laboratório de Química no Estado Sólido Website: http://lqes.iqm.unicamp.br/); B: Crystalline Structure (MarieCuriesNews Website: https://mariecuriesnews.wordpress.com/).

1.4. Geophysical Data

To pursue the present study, it was mandatory to discuss the different geophysical data and methods, such as swath bathymetry, seismic reflection and backscatter, based on which the morphologic features of the Gulf of Cadiz were found and described.

1.4.1. Bathymetry

The swath bathymetry is an important acoustic tool to investigate the seafloor morphology. It characterizes the seafloor topography and allows the interpretation of the geomorphology of the seafloor. Therefore it is used to identify the mud volcanoes and define the settings where the macrofauna occurs.

1.4.2. Seismic Reflection

The seismic reflection method is based on the fact that the acoustic signals propagates in the water column and in the sub-seafloor, and are reflected by interfaces between media with different acoustic impedance resultant mainly from differences in density between the two rocks or sediments. Seismic reflection data corresponds therefore to an acoustic vertical 2D image of the structure and the stratigraphic layers under the seabed. This method depends on the generation and detection of acoustic waves that are mechanically generated. When the seismic reflection profiles are of very high resolution they may image fluid channels within faults and mud volcanoes allowing a better interpretation of the cold seeps systems.

1.4.3. Backscatter

The backscatter data consist of a measurement of the intensity and characteristics of the echoes returns from the sound pulses at the seafloor. The backscatter signal depends on the physical nature of the seafloor, the frequency and angle used and orientation of the illuminated surface. Acoustic backscatter data are used for classifying seafloor characteristics. A weak return signal (low intensity) indicates a soft bottom substrate, while a strong return signal (high intensity) indicates a hard bottom substrate.

Chemosynthetic cold seep communities and authigenic carbonate may cause an acoustic impedance and roughness clearly distinct than the surrounding normal seafloor. Therefore, acoustic backscatter data (high backscatter) can be used to identify the distribution of potential seeps sites. Acoustic anomalies at the sea-floor morphology can be detected with side-scan sonars mounted on submersibles, ROVs, or towed vehicles, which can mark the location of gas seeps (e.g.: mud volcanoes and pockmarks; Naudts *et al*. 2008; Orange *et al.* 2002).

1.5. Submarine Mud Volcanoes

Submarine Mud Volcanoes (MVs) are sedimentary structures on the seafloor created by the rapid advection of fluid and methane-saturated muds from over-pressured sediment layers deep beneath the seafloor (Vanneste *et al.* 2012). They are formed when a mud rich material with clasts and other fluids reaches the seafloor, where extrusive features (such as mud flows, craters, gryphons, mud pools or salses) are formed. The material extruded from the MVs is composed of a fluidized mixture of sediments dominated by clays, liquids and gases that, in general, incorporate rock fragments (e.g.: clasts) pulled up from the pierced sedimentary sections (Magalhães, 2007). Although marly clay and salt diapirism are considered important in the formation of the MVs, seismic profile analysis and geochemical data indicate that mud volcanism in the Gulf of Cadiz is fault-controlled (Nuzzo *et al.* 2009; Vanneste *et al*. 2013), since some of the MVs are located along major WNW-SE and ENE-SW trending faults (Pinheiro *et al.* 2003).

In general the MVs occur along the world´s oceans (**Figure 1.5**; Vanneste *et al.* 2011). Fifty of these were confirmed by coring (Medialdea *et al.* 2009) on the Iberian and Moroccan margins (Pinheiro *et al.* 2003; Vanneste *et al.* 2013), because on this area we have a relatively thick sedimentary succession in which the diagenetic and compaction processes generate significant amount of overpressure and fluids (water and hydrocarbons) and in which the tectonic setting with faults promotes the seepage of these fluids (Vanneste *et al.* 2012). They are defined as conical shape positive morphological features in relation to the regional morphology, with a central feeder chimney or conduit and extrusive features such as mud flows (Cordes *et al.* 2010; Vanneste *et al.* 2012). The MVs are in water depths ranging from 200 to 4000 m (Cunha *et al.* 2013), with a diameter between 800 to 4000 m and up to 200 m height (Vannest *et al.* 2011; Vanneste *et al.* 2013). These MVs show considerable variations in morphology, dimension and composition of erupted material and fluids (Pinheiro *et al.* 2003; Van Rensbergen *et al.* 2005b). The MVs situated in the deeper areas of the Gulf of Cadiz are under the influence of deep Atlantic water masses, in turn the shallower mud volcanoes are strongly influenced by the Mediterranean Outflow Water (Pinheiro *et al.* 2003; Van Rensbergen *et al.* 2005b).

The MVs usually occur in petroliferous regions. Their seepage fluids are mainly solutions enriched by hydrocarbon gases (particularly CH_4), hydrogen sulfide, carbon dioxide, and petroleum products and their escape is expressed in the sea floor by positive reliefs such as mounds or cones (Stadnitskaia *et al.* 2006). MVs are active during short periods of time (ranging from hours up to years) that intercalate with, in general, longer periods of dormancy that typically vary between hundreds to thousands of years (Vanneste *et al.* 2012). The study of authigenic carbonates is one way to evaluate the long-term variation in carbon fluxes, which precipitate from the ascending fluids and are generally well preserved in the geological record (Vanneste *et al.* 2012). In general, gas and fluid seepage activity at the MVs is considered to be moderate with advection velocities up to 15 cm yr^{-1}. However the presence of methane-derived authigenic carbonates throughout the Gulf of Cadiz suggests several episodes of extensive methane seepage in the past (Vanneste *et al.* 2012).

The first Mud Volcano was discovered and sampled in Gulf of Cadiz in 1999 (Pinheiro *et al.* 2003; Van Rensbergen *et al.* 2005b) during the Training Through Research (TTR) 9 cruise (Pinheiro *et al.* 2003), of Research Vessel (R/V) Professor Logachev which were carried out within the framework of the UNESCO/IOC 'Floating University' Programme (Stadnitskaia *et al.* 2006) and since then have been extensively investigated during several research cruises (e.g.: TTR 10, Anastasya, TTR 11, TTR 11A, Tasyo, Cadipor, TTR 12, GAP, TTR 14, Merian Cruise, Darwin Cruise, TTR 15, TTR 16, TTR

17, MvseisHespérides; Kenyon *et al.* 2001, 2002, 2003, 2006; Akhmetzhanov *et al.* 2007, 2008; Hensen *et al.* 2007; Ivanov *et al.* 2010).

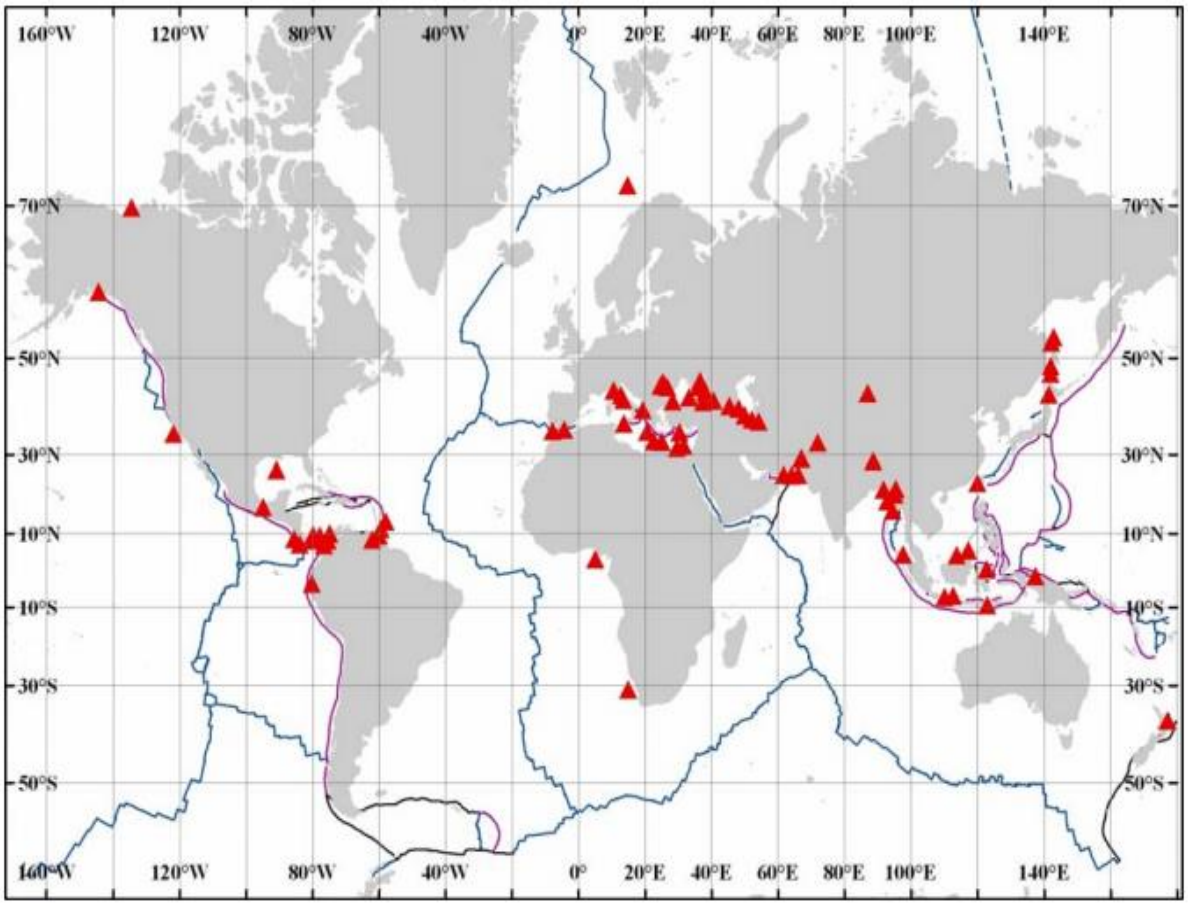

Figure 1.5 - Worldwide occurrence of mud volcanoes (Magalhães, 2007). Red triangles – Mud Volcanoes; Blue lines – Plates Boundaries.

1.6. The Gulf of Cadiz – General Context

The Gulf of Cadiz is a wide marine basin located in a complex tectonic area of the North-East Atlantic Ocean, west of Gibraltar Strait, offshore SW Iberia and NW Morocco (**Figure 1.6**; Navarro *et al*. 2006; Duarte *et al.* 2009; Rosas *et al.* 2009; Duarte, 2011; Vanneste *et al.* 2011). It is positioned on the transition area between the Gloria transform fault zone delineating the African-Eurasian plate boundary in the Atlantic, and the Western-most part of the Alpine-Mediterranean orogenic belt, marked by the Gibraltar (or Betic-Rif) Arc (León *et al.* 2006; Stadnitskaia *et al.* 2006; Vanneste *et al.* 2011). The region is seismically active and is thought to host the epicentre of the famous 8.5 to 8.7 (Johnston, 1996) magnitude 1755 Great Lisbon Earthquake that originated a devastating tsunami and decimated the city of Lisbon, Portugal (Hensen *et al.* 2007; Duarte, 2011). It was the largest tsunami ever experienced in Western Europe (Zitellini *et al.* 2009).

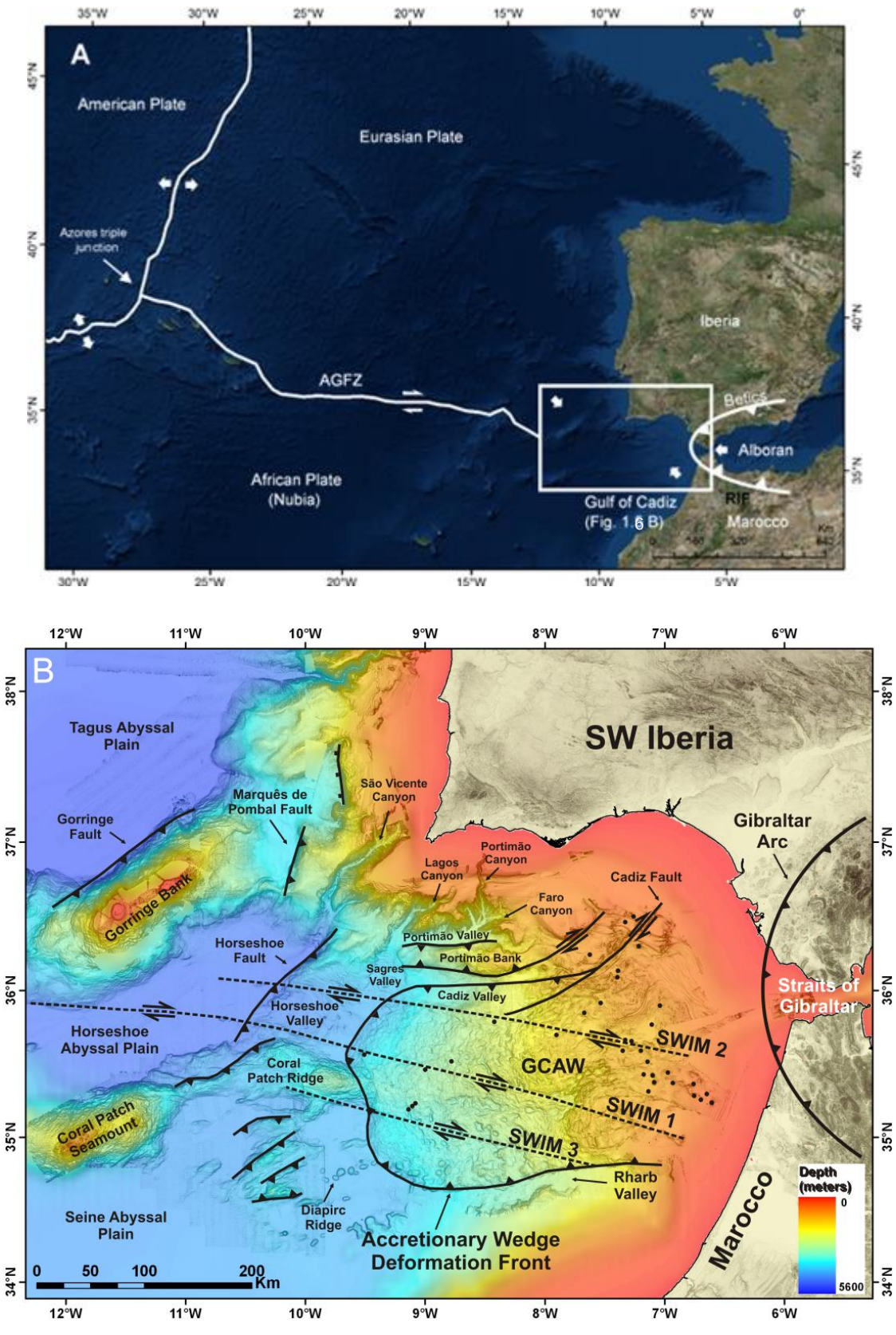

Figure 1.6 – A: Location of the Gulf of Cadiz area in the general tectonic setting of the Eurasia - Africa plate boundary. AGFZ - Azores-Gibraltar Fracture Zone (adapted from Rosas *et al*. 2009; Duarte, 2011 and Duarte *et al.* 2011); B: Simplified tectonic map of the Gulf of Cadiz area (from Duarte *et al.* 2011); Black dots – mud volcanoes; Black dashed line – SWIM faults.

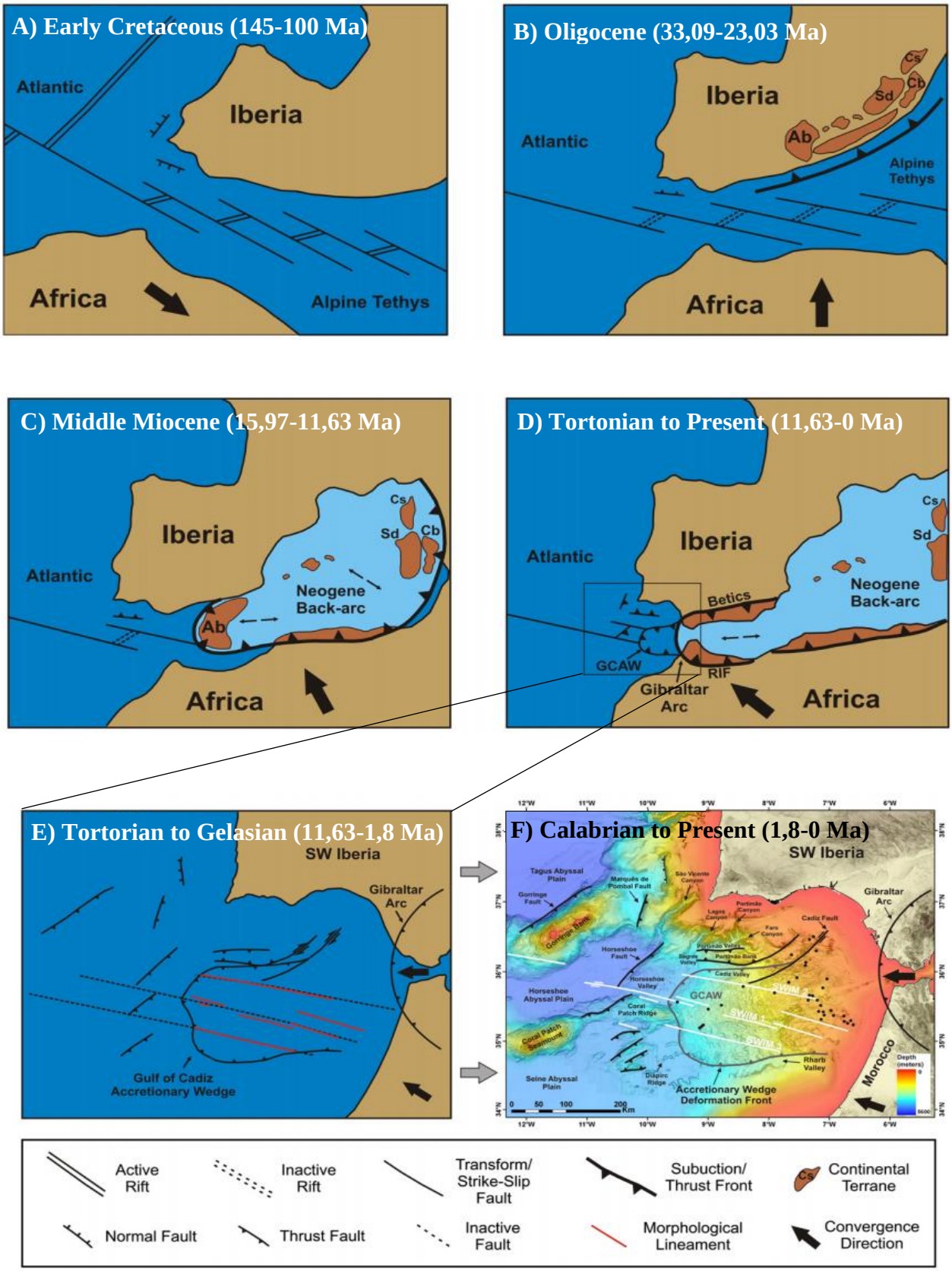

Figure 1.7 - The formation (Cretaceous to Present) of the Gulf of Cadiz Accretionary Wedge (adapted from Duarte *et al.* 2011). Ab - Alboran; Cb - Calabria; Cs - Corsica; Sd - Sardinia. The absolute ages in Ma correspond to the limits of the intervals.

During the Late Cretaceous and Tertiary, the opening of the North Atlantic Ocean induced the divergence of North America and Eurasia, in parallel with the convergence of Africa and Eurasia (**Figure 1.7**). The African continent was diverted to north causing the progressive closure of oceanic basins of the Tethys Ocean and the rapid propagation to west of the Alpine, Betic–Rif orogenic collision front in the Gulf of Cadiz, at the same time that the western Mediterranean basin development (Maldonado *et al.* 1999).

The Gibraltar Arc was formed due the convergence between Africa and Eurasia plates. The convergence caused the narrowing of the East-West oceanic corridor between Africa and Iberia and led to the collision of the Alboran terrane (that was migrating almost unimpeded towards the Atlantic Ocean, in the Middle Miocene) with the SE Iberia and NW Africa (see **Figure 1.7 - C**; Duarte, 2011). The Gibraltar Arc migrated west dragged by the roll back of the subducted Gibraltar oceanic slab. At the same time as the Gulf Cadiz Accretionary Wedge (GCAW; a high rugosity sedimentary slope with an undulating surface morphology; Gutscher *et al.* 2008) formed as a consequence of rollback subduction of the Tethyan slab beneath Gibraltar (Duarte, 2011; Duarte *et al.* 2011; see **Figure 1.7 - D**) on top of basement faults (nowadays the SWIM faults).

According to Duarte *et al.* 2011, the formation of the SWIM faults can be associated with the opening of the Tethys Ocean. The SWIM basement faults were probably inactive during Middle Miocene times, although capable of originating a linear-like perturbation in the GCAW surface morphology. At the same time, the convergence between Iberia and Africa gradually suffered a counterclockwise rotation, shifting from N–S (see **Figure 1.7 - B**) to near WNW–ESE (see **Figure 1.7 - E**). This rotation triggered a dextral strike-slip reactivation of the basement (SWIM) faults (see **Figure 1.7 - F**) during a period in which the subduction driving the GCAW growth was slowing down.

1.7. Trophic Status

The macrofauna species studied in this work were analysed according to their metabolic strategy (**chapter 5**). Given this criteria and the following detailed explanation such species can be classified as autotrophic or heterotrophic. A second level of classification considers the type of symbiotic relationship between the deep-sea invertebrate host and its methanotrophic and/or thiotrophic bacteria (see below).

Heterotrophs include all organisms that obtain the energy for their metabolism from organic carbon sources in their food (e.g.: all animals, including man, fungi, and many parasitic plants and saprophytic angiosperms as well as many microorganisms). In opposition autotrophs fix inorganic carbon using sunlight (photoautotrophs) or chemical energy (chemoautotrophs).

1.7.1. Thiotrophy and Methanotrophy

Symbiotic invertebrates in deep-sea environments derive all or part of their nutrition from microbial symbiont metabolism. The organisms that rely partly on chemotrophic nutrition but retain the ability to

feed heterotrophically are designated as mixotrophic. Symbiotic associations with thiotrophic or methanotrophic bacteria occur in a wide range of animal species that live in reducing environments (e.g.: hydrothermal vents, whale falls, sunken wood, cold seeps and sediments; Petersen and Dubilier, 2009). In rare cases species harbour both methanotrophic and thiotrophic symbionts, in which case they are designated as possessing a dual symbiosis.

Thiotrophic bacteria can exploit the chemical energy from the oxidation of sulfide or sulfur with oxygen or nitrate for their cell metabolism and growth (Grunke *et al.* 2012) while the methanotrophic bacteria utilize methane as a sole carbon and energy source (Hanson *et al.* 1996). The bivalves with sulfide-oxidizing gill symbionts are frequently found in environments that are inhospitable to other invertebrates due to a low oxygen (O_2) content and the presence of free hydrogen sulfide (H_2S). Sulfide-oxidizing bacteria are involved in symbioses with members of at least five bivalve families, occurring intracellularly in Vesicomyidae, Lucinidae, Mytilidae and Solemyidae, and mostly extracellularly in Thyasiridae (Rodrigues *et al.* 2010; Oliver *et al.* 2011). In addition to the bivalve, others important symbiotic seep organisms include siboglinidae polychaetes (vestimentiferan, frenulate and monoliferan tubeworms) and sponges (Cladorhizidae).

Chapter 2

Regional Setting

2.1. The oceanographic circulation in the Gulf of Cadiz

The Atlantic Ocean in Gulf of Cadiz is characterized by three main water masses (Eastern North Atlantic Central Water, North Atlantic Deep Water and Mediterranean Outflow Water; **Figure 2.1**) with different characteristics of salinity, temperature, oxygen content and current velocities. Hence, a combination of water circulation, chemically reduced habitat and trophic input will determine the benthic communities of this region (Blazewicz-Paszkowycz *et al.* 2011a).

2.1.1. Eastern North Atlantic Central Water

The North Atlantic Central Water (NACW) is located at the main thermocline of the North Atlantic Ocean (Pollard *et al.* 1996) and is characterized by an almost linear decrease of potential temperature (16.0˚C to 12.5˚C) and salinity (36.25 to 35.50 ‰; Alves *et al.* 2011) with depth. This body of water, in the upper 500 – 1000 m of the ocean (Pollard *et al.* 1996), is influenced by the mix of several waters (Cianca *et al.* 2009), the Mediterranean Water, the Antarctic Intermediate Water and the Labrador Sea Water (Mauritzen *et al.* 2001). The NACW, in the eastern North Atlantic, is more saline (usually by less than 0.1 ‰ at constant temperature) than in the western North Atlantic, due to the influence of Mediterranean Water (Pollard *et al*. 1996; Mauritzen *et al.* 2001). The Eastern North Atlantic Central Waters (ENACW) can be subdivided in two types as an exchange result of water and heat within the thermocline (Padin *et al.* 2011): the eastern North Atlantic central water subtropical (ENACWt) and the eastern North Atlantic central water subpolar (ENACWp). The ENACWt range from 12.2 to 18.5 °C and from 35.66 to 36.75 ‰ and its origin was located in a front near the Azores. The ENACWp is formed at the eastern flank of the North Atlantic Current, approximately north of Cape Finisterre (43ºN) and corresponds to water between 4 and 12 °C and between 34.96 and 35.66 ‰ (Bode *et al.* 2002; Padin *et al.* 2011). Besides the thermohaline differences, ENACWp and ENACWt also show different chemical properties due to changes in ventilation rates and remineralization of organic matter. In this way, the ENACWt is a nutrient-poor water whereas ENACWp is characterized by high nutrient levels mainly due to deep winter MLD (mixed layer depth) in the formation region (Padin *et al.* 2011).

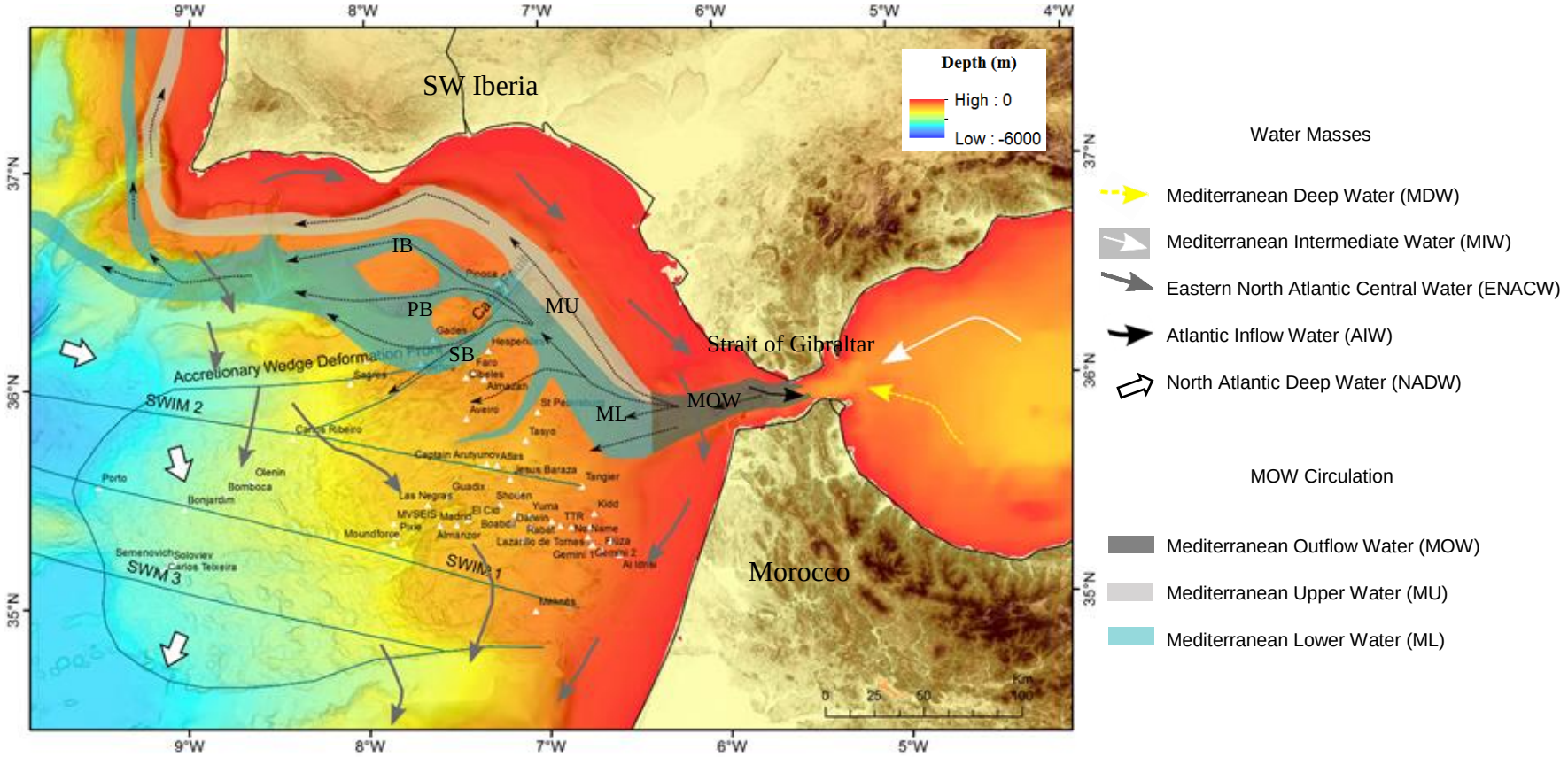

Figure 2.1 – Overview of the oceanographic patterns in the Gulf of Cadiz area, showing the three main water masses: ENACW (Dark grey arrow), MOW (Dark spot) and NADW (White fat arrow). The MOW current is split into two main currents, the MU and the ML, which is divided into the SB, the PB and the IB (modified from García *et al.* 2009; Wienberg *et al.* 2009).

2.1.2. Mediterranean Outflow Water

The Mediterranean Outflow Water (MOW), results from the exchange of water masses between the Mediterranean Sea and the Atlantic Ocean (Mulder *et al.* 2009), North Atlantic Surface Water (0 – 100 m) and North Atlantic Central Water (100 – 700 m; Toucanne *et al.* 2007; Singh *et al.* 2015). It is an energetic, saline (38 ‰) and warm (13 °C) water mass (**Figure 2.2**; Toucanne *et al.* 2007; Mulder *et al.* 2009; Bozec *et al.* 2011; Khélifi *et al.* 2014) moving from the SE to the NW along the middle slope (which is formed by four relatively flat terraces with gradients of less than 0.5°, at average depths of 500, 675, 750 and 850 m; **Figure 2.3**) between 500 and 1200 m water depth above the NADW (García *et al.* 2009). This independent strong contour current enters the Gulf of Cadiz at depths of 250 – 300 m with a western trend and velocities of up to 250 cm s^{-1} (García *et al.* 2009; Mulder *et al.* 2009). The main MOW current divides into two main currents that flow along the seabed at water depths of 300 – 1400 m, the Mediterranean Upper Water (MU) and the Mediterranean Lower Water (ML; see **Figure 2.1**; Mulder *et al.* 2009). The MU represents the upper, less dense (salinity is 37.07 ‰), warm (13.7 °C) core that flows at the base of the upper Spanish and Portuguese continental slopes at depths of 300 – 600 m. Its average velocity is 0.46 ms^{-1}. The ML constitutes the lower, more saline (salinity is 37.42 ‰) current that forms the main MOW. Its mean temperature is 13.6 °C, is centred between 600 – 1400 m and its velocity range between 0.2 and 0.3 m s^{-1} (Mulder *et al.* 2009). The ML, splits into three minor branches (Mulder *et al.* 2009), the Southern Branch (SB), the Principal Branch (PB) and the Intermediate Branch (IB; see **Figure 2.1**, Garcia *et al.* 2009), each one of which follows its own deep channel (Mulder *et al.* 2009). They return to join at 8,333º W and leave the Gulf of Cadiz towards the west Iberian margin and central north-Atlantic (Garcia *et al.* 2009).

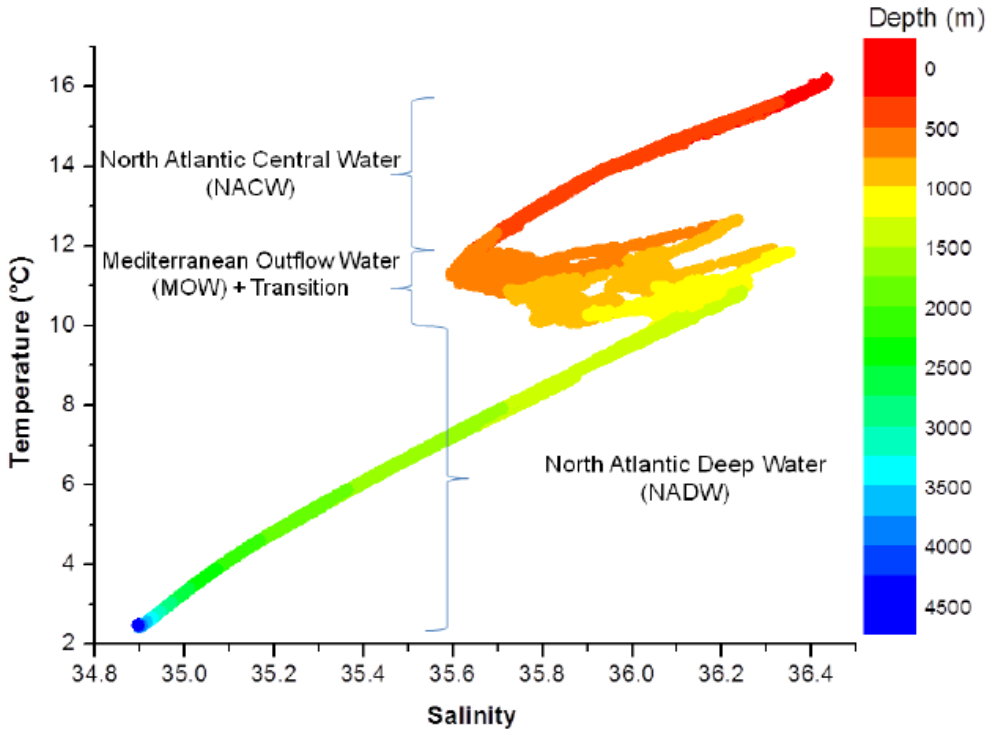

Figure 2.2 – The temperature and salinity of three masses of water, NACW, MOW and NADW. The presence of the MOW, carrying slightly warmer and saltier water is clearly evident in the 600 to 1200 m depth range (Hansen *et al.* 2012).

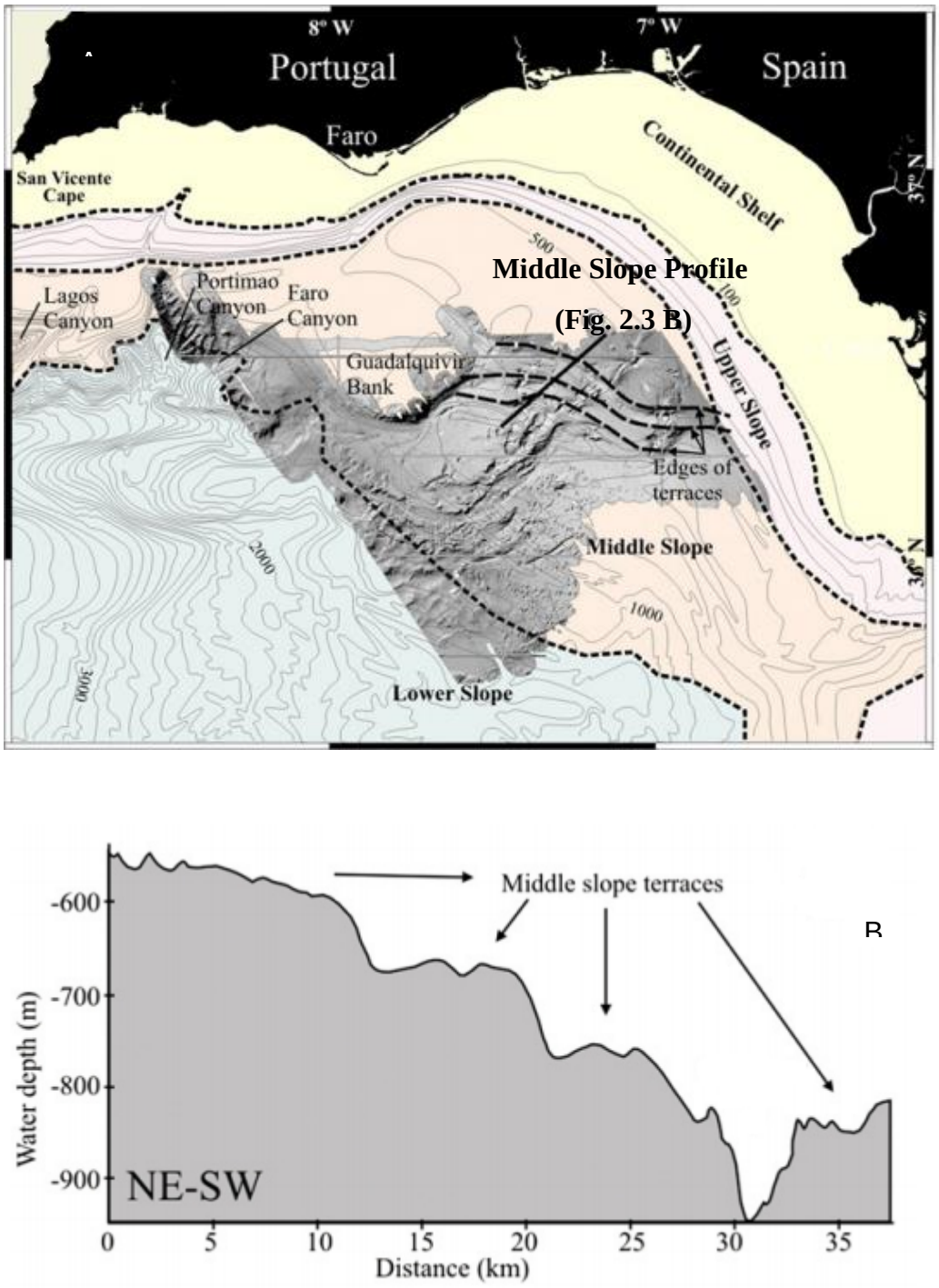

Figure 2.3 – The Gulf of Cadiz slopes. A: Physiography of the continental shelf, upper, lower and middle slope. Dashed lines - Limits of the middle slope terraces; B: Topographic profile along the middle slope terraces (from García *et al.* 2009).

2.1.3. North Atlantic Deep Water

The North Atlantic Deep Water (NADW) is formed in the high-latitude regions of the Atlantic Ocean and incorporates upper Labrador Sea Water (uLSW), classical Labrador Sea Water (cLSW),

Iceland-Scotland Overflow Water (ISOW), and Denmark Straits Overflow Water (DSOW; Van Sebille *et al.* 2011). It is a cold (3 – 8 ºC) and less saline (34.95 – 35.5 ‰) water mass that flows at depths > 1500 m from the Greenland–Norwegian Sea region towards the south. In the Gulf of Cadiz, the NADW is joined by part of the saltier but warmer MOW. This mixture flows southwards down the eastern part of the Atlantic Ocean (Knauss, 1978; see **Figure 2.1** and **2.2**).

2.2. SWIM Faults

The morphology of the Gulf of Cadiz is largely controlled by the main tectonic processes in the area, namely the thrust faults (reverse faults) accommodated in the Gulf of Cadiz Accretionary Wedge (GCAW) and the wrenching associated to the South West Iberian Margin (SWIM) fault system (Duarte *et al.* 2011). In addition to the accretionary wedge, the thrust faults are also accommodated in other structures as the Horseshoe Thrust Fault, the Marquês de Pombal Fault, Gorringe Bank and the Tagus Abyssal Plain (although this last one is out of the Gulf of Cadiz strict domain; see **Figure 2.4**; Rosas *et al.* 2012).

The SWIM lineaments are faults (the SWIM faults) corresponding to a set of WNW – ESE trending, vertical right-lateral strike–slip faults, in agreement to the observation and interpretation of several seismic profiles and swath bathymetry that cross cut these features (Rosas *et al.* 2009; Terrinha *et al.* 2009, Zitellini *et al.* 2009; Duarte *et al.* 2011). These lineaments are described by six a hundred-kilometer long linear bathymetric expression and extend from the easternmost part of the GCAW until the Horseshoe Abyssal Plain, south of the Gorringe submarine mountain (Gorringe Bank; see **Figure 2.4**; Duarte *et al.* 2009; Rosas *et al.* 2012).

The SWIM Fault Zone is located between the western and eastern ends of two well-established plate boundaries, the Gloria Fault and the Rif-Tell fault and forms the southern boundary of the main seismically and tectonically active area of the Gulf of Cadiz (Zitellini *et al.* 2009). The morphologic expression of the SWIM faults corresponds to a continuous alignment of seafloor crests and troughs (valleys), corresponding to fold crests and fault traces in the Holocene sediments (Zitellini *et al.* 2009), sometimes exhibiting an en echelon geometrical disposition, and commonly punctuated by active mud volcanoes within the domain of the Accretionary Wedge. This overall linear morphology is more salient both in the Horseshoe Valley and close to the northern part of the GCAW front, where lineaments can be followed almost continuously for more than 200 km (Duarte *et al.* 2011).

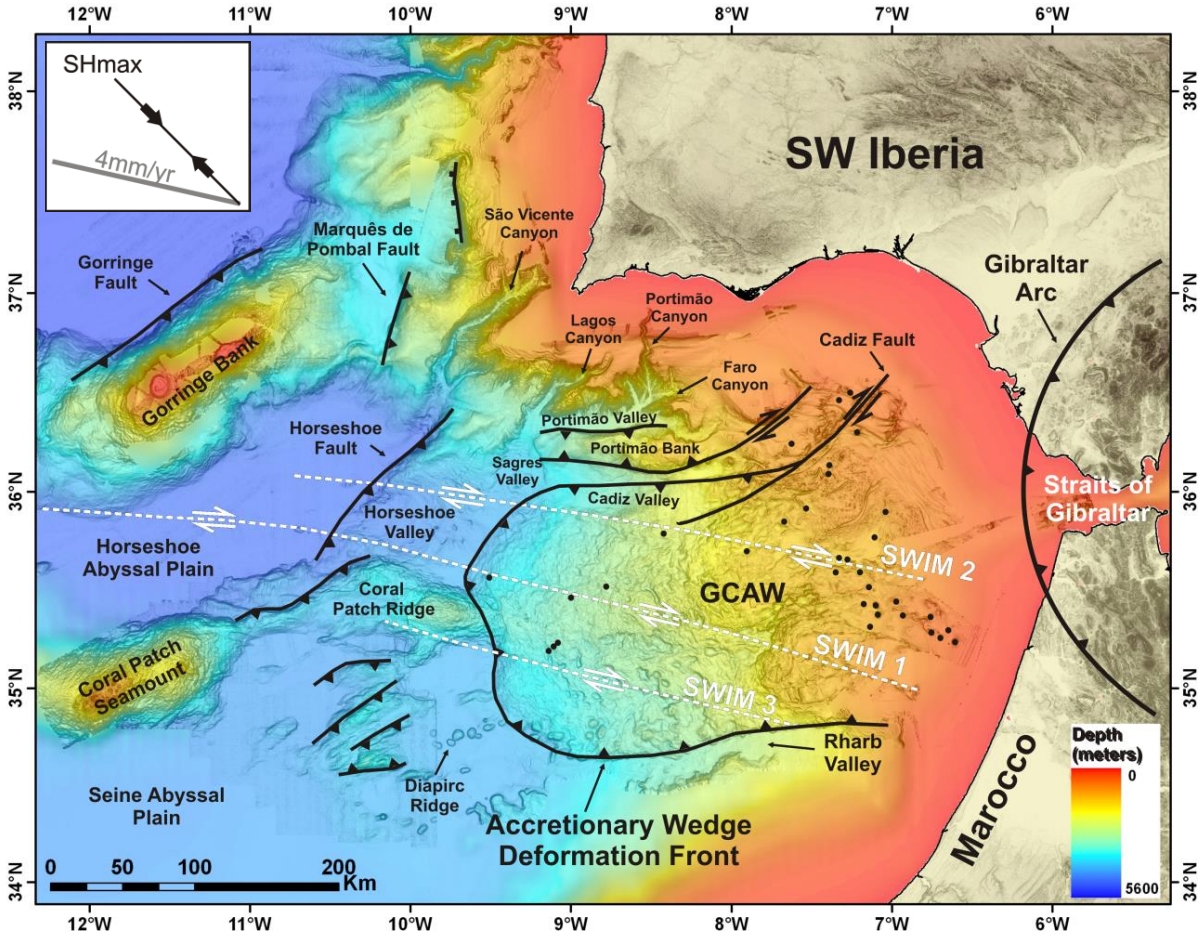

Figure 2.4 - Simplified tectonic map of the Gulf of Cadiz area. Dark grey outline - Gulf of Cadiz Accretionary Wedge (GCAW; White lines – SWIM wrench system according to Zitellini *et al*. 2009). Black dots correspond to the location of known mud volcanoes (e.g.: Duarte *et al*. 2011).

The SWIM 1 fault (see **Figure 2.4**) exhibits an evident morphological expression in the Horseshoe Valley and intersects the wedge deformation front to the north of the Coral Patch Ridge. Its continuation to the east is less visible, although punctuated by mud volcanoes (Duarte *et al*. 2011). This fault exceeds 600 km, corresponds to a strike-slip fault and can be followed from the Gorringe bank southern flank to the Morocco shelf. In some fault segments to the North of the Coral Patch Ridge is possible to identify E-W-striking undulations with maximum lengths of about 8 km. These features show an en échelon pattern, which corresponds to oriented folds of the recent sedimentary cover, thus allowing the establishing of a dextral strike-slip movement (Rosas *et al*. 2009).

The SWIM 2 fault (see **Figure 2.4**), intercepts a northern segment of the GCAW front in the proximity of the Sagres Valley. The morphological expression of the SWIM 2, within the thrust wedge to the east, is well marked by a slightly arched trough that splays in the same direction (Duarte *et al*. 2011).

The SWIM 3 fault (see **Figure 2.4**), characterized by several elongated WNW–ESE ridges, troughs and slope breaks, cuts along the southern flank of the Coral Patch Ridge, crosses a small portion of the Seine Abyssal Plain to the east and intersects the GCAW deformation front (Duarte *et al*. 2011).

Chapter 3

Study Areas

The mud volcanoes described in this work are organized in three main areas, according to their depth and to their geographic settings: the El Arraiche Mud Volcano Field, the Carbonate Province and Deep Mud Volcano Field (**Figure 3.1**). Within the Carbonate Province several morphological features, here designated as "Other Features" and that are not mud volcanoes, are described and discussed because they host, or have hosted in the past, seepage-related processes. The geologic and biologic characteristics of the described features (mud volcanoes and other morphological features) was based solely on the information available from published scientific papers and cruise reports.

The El Arraiche field encompasses several mud volcanoes (Al Idrissi, Fiúza, Gemini, Mercator, Lazarillo de Tornes and Kidd) in the shallow Moroccan margin (200 – 600 m). The Carbonate Province, pierced by several mud volcanoes (No Name, Anastasya, Pipoca, Tarsis, Meknès, Student, Ginsburg, Yuma, Aveiro, Jesus Baraza, Shouen and Darwin) and other features (Channel West of Gibraltar Strait, Vernadsky Ridge, Pen Duick Escarpment, Iberico, Formosa Ridge and Cadiz Channel), corresponds to an extensive bathymetric strip (600 – 1200 m) along the Moroccan and Spanish margins. The deep-water field (1200 – 4000 m), mostly within the Portuguese margin, includes several of the most active mud volcanoes in the region (Captain Arutyunov, Sagres, Carlos Ribeiro, Bonjardim, Semenovich and Porto; Génio *et al*. 2013; **Figure 3.1** and **3.2**).

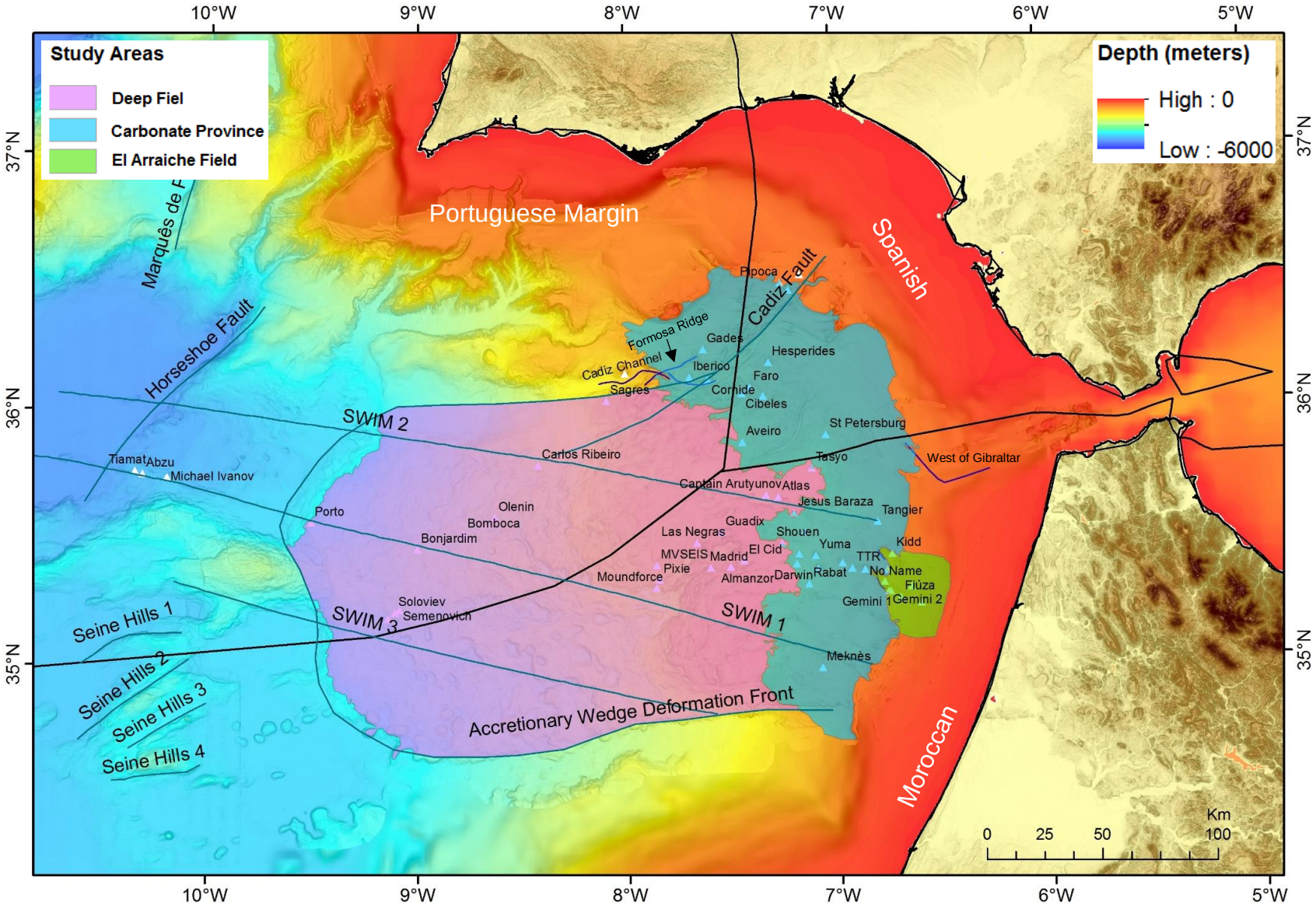

Figure 3.1 - Gulf of Cadiz showing the three study areas of this work. Pink area - Deep Field (1200 – 4000 m); Blue area – Carbonate Province (600 – 1200 m); Green area - El Arraiche Field (200 – 600 m). Black dashed lines – limit of Portuguese, Spanish and Moroccan Exclusive Economic Zones.

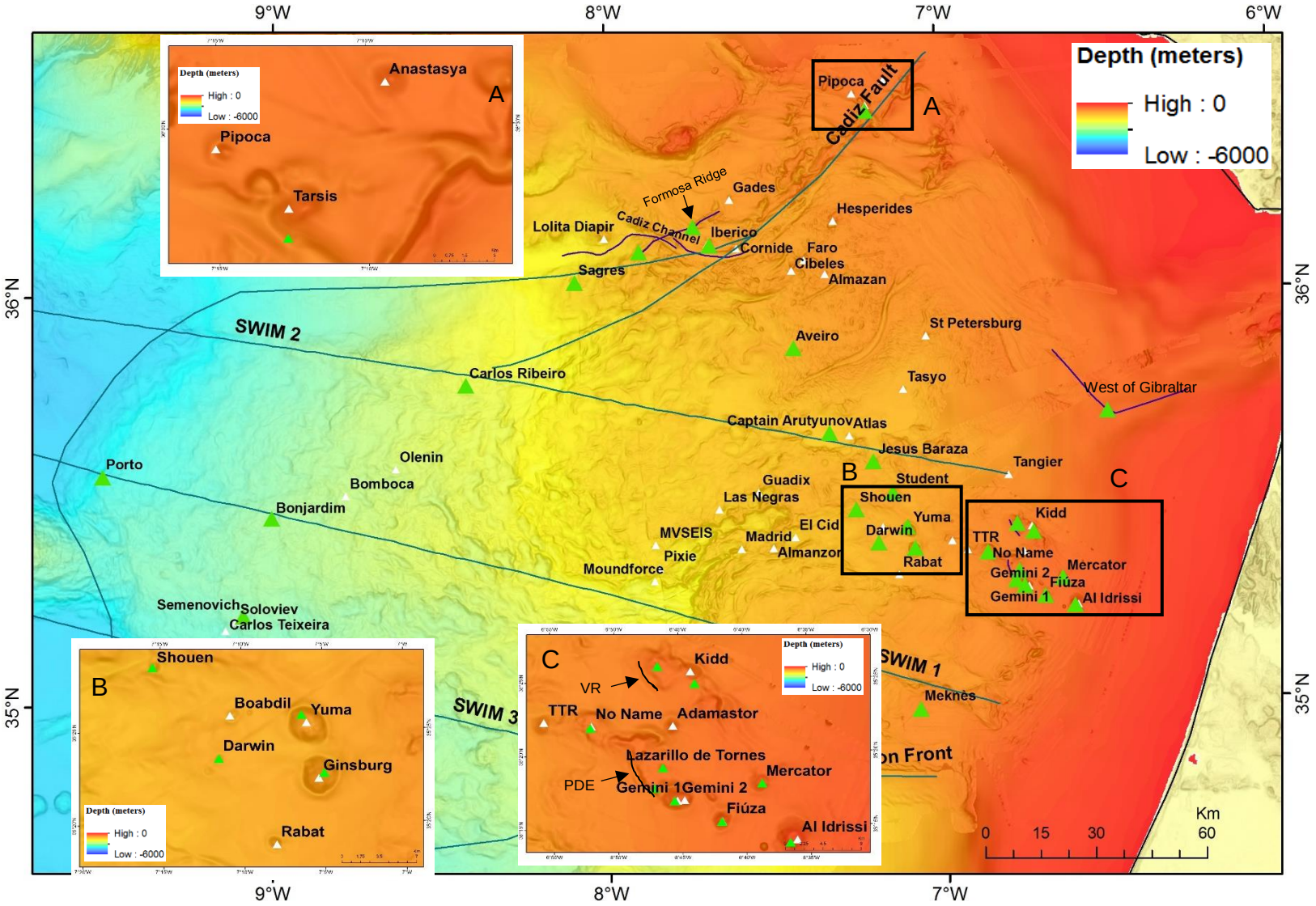

Figure 3.2 – Gulf of Cadiz showing all sampled features in this work (Green dots). White dots – The features discovered until now in the Gulf of Cadiz. A, B and C: Zoom of the areas located inside the black squares, detailing the morphology of the Anastasya MV, Pipoca MV and Tarsis MV, Shouen MV, Yuma MV, Darwin MV and Ginsburg MV and No Name MV, Kidd MV, Lazarillo de Tornes MV, Pen Duick Escarpment (PDE), Gemini MV, Fiúza MV, Mercator and Vernadsky Ridge (VR).

The average thickness of the sedimentary pile in the study areas is, for the purpose of this work, assumed to be of about 10 km. Based on reflection seismic data it is also assumed that the SWIM faults are, most probably, sub-vertical faults, however in this work it is considered that the they can have a minimum dip angle of 45º. Therefore, any MV located at more than 10 km from the fault surface trace will not considered as being related with the fault, and the MVs located at less than 10 km from the fault are considered as probably being related or controlled by this fault (**Figure 3.3**). The SWIM 3 fault was not studied here in detail since the Semenovich mud volcano is the only one in the vicinity of this fault with reported macrofauna data available. Nevertheless, this MV is at a distance greater than 10 km from the SWIM 3 fault, while the other two (so far) known nearby mud volcanoes (e.g.: Soloviev and Carlos Teixeira; see **Figure 3.1**), which are at distances < 10 km, lack relevant available macrofauna information.

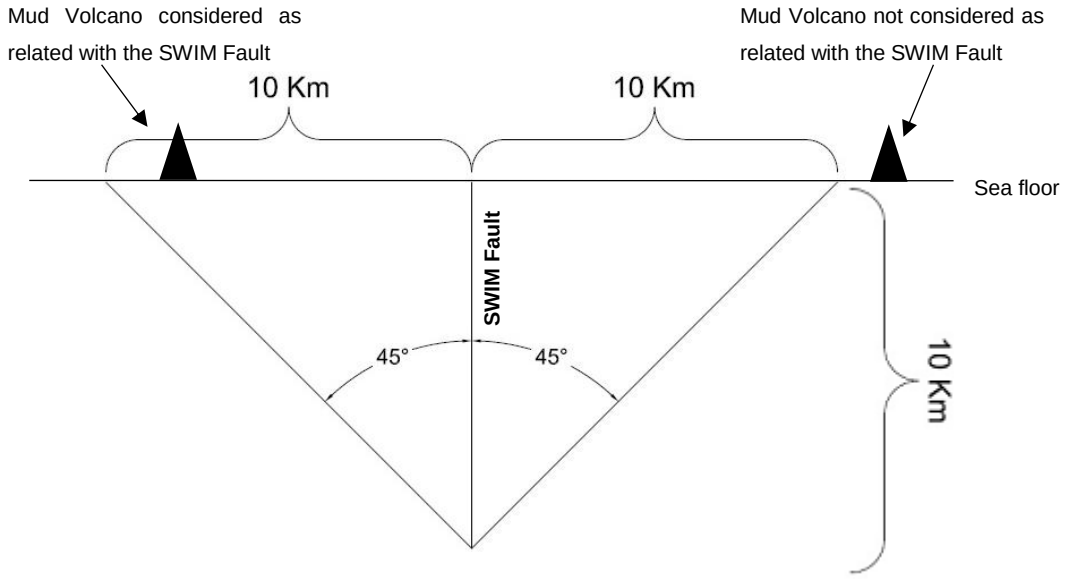

Figure 3.3 - Schematic representation (cross section) of the criteria established to consider if a MV is related or not with a SWIM fault.

3.1. El Arraiche Field

In May 2002 the El Arraiche Mud Volcano field was discovered during the TTR 12 cruise in the Moroccan Atlantic margin in the Gulf of Cadiz. It is constituted by eight mud volcanoes (Kidd, Mercator, Al Idrissi, Fiúza, Don Quichote, Lazarillo de Tornes, Gemini and Adamastor), six of them are studied in this project (**Figure 3.4**). The mud volcanoes have variable size and shape just below the shelf edge, at a water depth from 200 to 700 m. Al Idrissi is the largest mud volcano, 255 m high and 5400 m in diameter. Don Quichote and Lazarillo de Tornes, are the smallest mud volcanoes, only about 25 m high (Van Rensbergen *et al.* 2005a; Van Rensbergen *et al.* 2005b). The mud volcanoes are situated around the ridges on top of normal faults, which constrain the rotated blocks (**Figure 3.5**; Van Rensbergen *et al*. 2005b; Wehrman *et al.* 2011), bound by lystric faults (concave normal fault; Vandorpe *et al*. 2014).

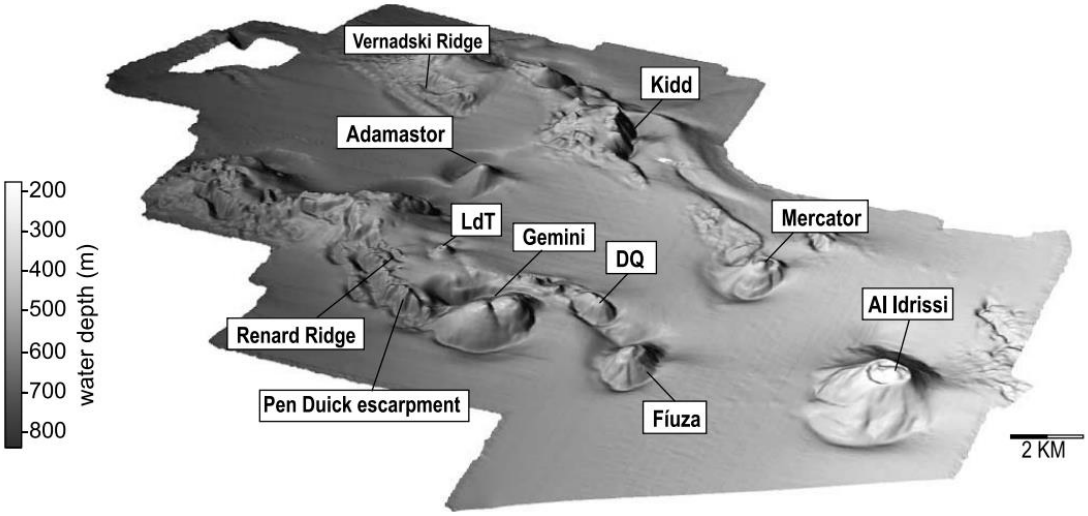

Figure 3.4 - Morphology of the El Arraiche mud volcano field (from Van Rensbergen *et al.* 2005b). DQ – Don Quichote; LdT - Lazarillo de Tormes.

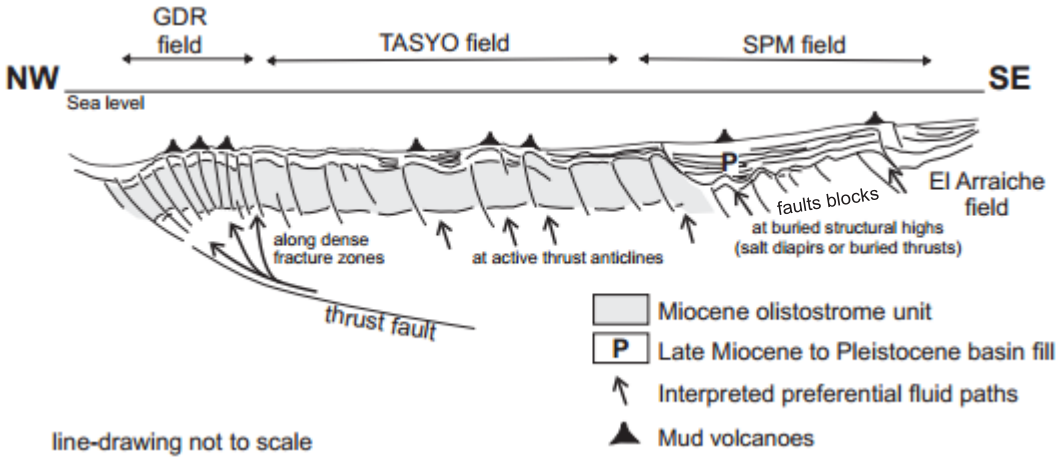

Figure 3.5 - Schematic representation of the Accretionary Wedge showing the main mud volcano fields in their structural setting (from Van Rensbergen *et al.* 2005b). GDR – Guadalquivir Ridge; SPM - Spanish Morrocan margin.

The El Arraiche field is part of a larger cluster of mud volcanoes that lie within the GCAW. On regional seismic lines this distinction is clear (Van Rensbergen *et al.* 2005b). The El Arraiche mud volcanoes, as other mud volcanoes in the Gulf of Cadiz, are long-lived structures thought to be related to the episodic migration of hydrocarbons. Its mud volcanic activity is estimated to have started 2.4 Ma ago (Van Rensbergen *et al.* 2005b; Wehrman *et al.* 2011) and occurred in several phases (Vandorpe *et al*. 2014).

3.1.1. Al Idrissi

The Al Idrissi Mud Volcano (see **Figure 3.2** and **3.4**) discovered during the Cadipor cruise in 2002 is the largest and the shallowest mud volcano in El Arraiche mud volcano field, situated just below the shelf edge in water depths of about 420 m. It appears to be located on a westward plunging anticline flank, visible in the bathymetry and on the seismic data (see **Figure 3.6**; Van Rensbergen *et al.* 2005a, 2005b). The MV is 225 m high, up to 5400 m wide at its base and 1500 m wide at the top, with 197 m water depth at the top (**Table 3.1**; Van Rensbergen *et al.* 2005a, 2005b). It is almost circular at the base and has an eye-shaped crater at the top. The crater is up to 17 m deep at the western side, the eastern part is occupied by a central dome-shaped elevation; maximum 42 m above the crater floor and the flanks of the mud volcano are dominated by down slope mud flows (Van Rensbergen *et al.* 2005b).

3.1.2. Mercator

The Mercator Mud Volcano (see **Figure 3.2**) is an asymmetric mud volcano, about 141 m high at the southern side, 90 m high on the northern side and only 51 m high on the eastern side, discovered during the Cadipor cruise in 2002. It has a maximum diameter of 2450 m at the base and 1100 m at its top, at a water depth of 351 m at the top (see **Table 3.1**). In this case, the slope is characterized by concentric steps rather than radial sediment flow deposits. The crater is very shallow, < 2 m, but the central dome is large, 38 m and forms the caldera of the mud volcano (Van Rensbergen *et al.* 2005a, 2005b; Haffert *et al.* 2013). The MV is situated on the Moroccan continental margin, on an anticline (an antiform fold with oldest rocks at its core) formed by the halokinesis of a salt diapir (**Figure 37**; Haffert *et al.* 2013).

The MV is one of the shallowest mud volcanoes and differs significantly from the other mud volcanoes by the high chloride enrichment of its pore water (Blazewicz-Paszkowycz *et al.* 2011a; Oliver *et al.* 2011; Rodrigues *et al.* 2011). The top of Mercator contains patches of disturbed sediments from which gas-venting is occasionally observed. Solitary corals (*Caryophyllia* sp.), accompanied by Cidaridae echinoids and Onuphidae polychaetes (*Hyalinoecia tubicola)* are abundant at the central area of the crater (Blazewicz-Paszkowycz *et al.* 2011a; Oliver *et al.* 2011; Rodrigues *et al.* 2011). *Lucinoma asapheus* was found live only at Mercator MV at a water depth of 358 m (Oliver *et al.* 2011). The widespread presence of authigenic carbonates and also extensive Neptunea and Bathymodiolus graveyards, usually within the crater of the mud volcanoes, suggest that this was a very active seepage area in the past (Oliver *et al.* 2011).

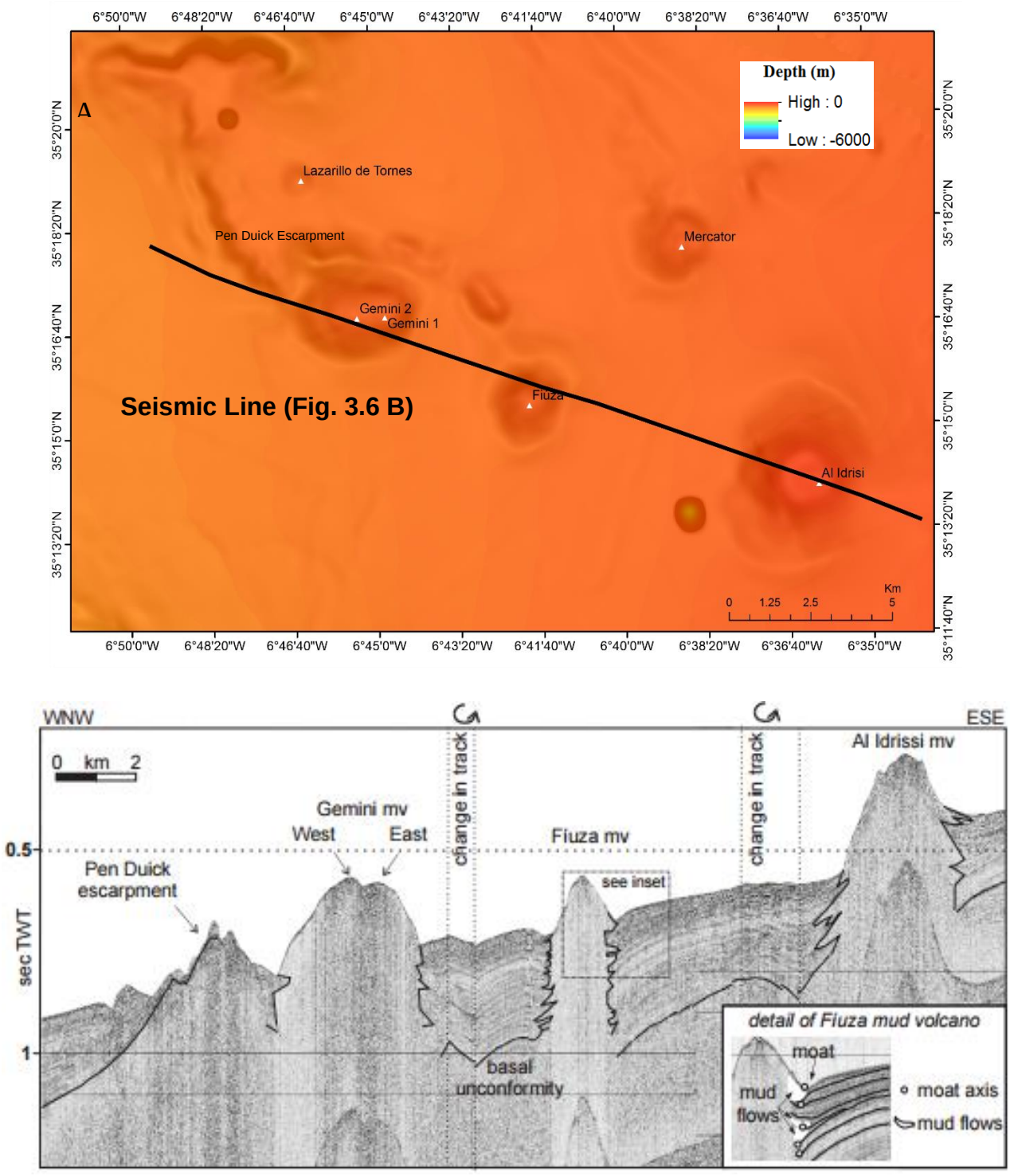

Figure 3.6 – A: Detail of some features of the Gulf of the Cadiz. Localization of the seismic line observed in (B); B: General high-resolution seismic line (sparker source) over Al Idrissi, Fiúza and Gemini mud volcanoes and Pen Duick escarpment. The mud volcanoes are characterized by a reflection-free seismic facies that show stacked outflow lenses within a stratified series of hemi-pelagic sediments above a regional unconformity. The inset shows a detail of interfingering mud flows that accumulate in moats at the base of the Fiúza mud volcano cone (Van Rensbergen *et al.* 2005b).

Table 3.1 – General characteristics of the mud volcanoes from the three study areas: El Arraiche Field, Carbonate Province and Deep Field.

Name	Mud Volcano Elevation (m)	Width at the base (m)	Width at the top (m)	Water depth (m)	Cruise	Year of Discovery
Al Idrissi	225 m	5400 m	1500 m	197 m	Cadipor	2002
Mercator	141 m southern side, 90 m northern side, 51 m eastern side	2450 m	1100 m	351 m	Cadipor	2002
Fiúza	143 m	2200 m	750 m	393 m	Cadipor	2002
Gemini East	252 m	2300 - 4100 m	1300 m	423 m	Cadipor	2002
Gemini West	252 m	2300 - 4100 m	900 m	423 m	Cadipor	2002
Lazarillo de Tornes	25 m	500 m	-	494 m *	Cadipor	2002
Kidd	60 - 160 m	500 m	420 m	502 m *	TTR 09	1999
No Name	-	-	-	598 m *	TTR 09	2000
Meknès	60 m	1000 m	-	650 m	TTR 14	2004
Student	200 m	1700 m	200 m	955 m *	TTR 10	2000
Ginsburg	250 m	3800 m	400 m	911 m *	TTR 09	1999
Yuma	250 m	4500 m	2000 m	964 m *	TTR 09	1999
Aveiro	80 m	1500 m	-	1065 m *	TTR 12	2002
Jesus Baraza	150 m	-	600 - 1600 m	1091 m *	TTR 10	2000
Shouen	150 m	1100 m	700 m	1180 m *	TTR 16	2006
Darwin	50 m	-	-	1105 m	TTR 16	2006
Captain Arutyunov	100 m	2000 m	300 m	1324 m	TTR 12	2002
Sagres	110 m	2700 m	-	1554 m *	TTR 17	2008
Carlos Ribeiro	80 m	-	-	2173 m	TTR 10	2000
Bonjardim	150 m	2000 m	-	3060 m	TTR 10	2000
Semenovich	70 m	-	-	3200 m	TTR 15	2005
Porto	-	-	-	3900 m	TTR 15	2005

* Depth values from SWIM bathymetry (Zitellini *et al.* 2009).

3.1.3. Fiúza

The Fiúza is a conic shaped Mud Volcano (Kenyon *et al.* 2003) discovered during the Cadipor cruise in 2002. It is located at the western termination of the Renard Ridge (see **Figure 3.4)** and possibly at the southern continuation of the collapsed depression that hosts the Mercator mud volcano, but no faults could be traced in either direction to its location; in agreement with Van Rensbergen *et al.* 2005a, 2005b). The MV has a maximum height of 143 m, 2200 m wide at the base and has a flat top 750 m wide with a 27 m high central dome of and maximum 700 m wide, with 393 m water depth at the top of the mud volcano (see **Table 3.1**; Kenyon *et al.* 2003; Van Rensbergen *et al.* 2005a, 2005b). It is

characterized by a series of concentric rims with high backscatter mud flows extending down the flanks, and up to 1300 m from the crater (**Figure 3.6**; Kenyon *et al.* 2003).

3.1.4. Gemini

The Gemini Mud Volcano (see **Figure 3.2**) discovered during the Cadipor cruise in 2002, occurs south of the large fault escarpments at the sea floor that bound the southern flank of the Renard Ridge (see **Figure 3.4**), at a water depth of about 423 m at the top. It consists of two mud volcanoes in one large oval-shaped mud cone, separated by an almost NS trending faults (see **Figure 3.4**; Kenyon *et al.* 2003; Van Rensbergen *et al.* 2005b). The entire mud volcano is up to 252 m high, 4100 m long to 2300 m wide at the base, the maximum diameter at the top of the eastern part (Gemini East) is 1300 m and the maximum diameter of the western part (Gemini West) is 900 m (see **Table 3.1**). The summits of both Gemini East and Gemini West consist of a flat crater area with a central dome of respectively 23 and 27 m above the flat crater area (Van Rensbergen *et al.* 2005b). The differentiation between the two summits is visible, from about 80 m below the top of the mud volcano, as 400 m long and 20 m deep creases (Van Rensbergen *et al.* 2005a). The MV is also characterized by typical concentric rims and mud flows. Mud flows are especially large at the western side where they extend about 1800 m down the slope (Kenyon *et al.* 2003).

3.1.5. Lazarillo de Tornes

The Lazarillo de Tornes Mud Volcano (see **Figure 3.2**) discovered during the Cadipor cruise in 2002, is located at the crest of fault blocks on top of the Renard Ridge, and together with Don Quichote Mud Volcano constitutes the smallest mud volcanoes of the field. It is only 500 m wide and 25 m high, at a water depth of about 494 m (Van Rensbergen *et al.* 2005b; see **Table 3.1**).

3.1.6. Kidd

The Kidd Mud Volcano (see **Figure 3.2**) discovered during the TTR 09 cruise in 1999, is situated on top of the Vernadsky Ridge with the top of the volcano at a water depth of 502 m. The MV is approximately 4000 m in diameter and shows an asymmetrically shaped volcanic edifice, with a steep SE slope and a gently sloping NW flank. The base of the MV is at a depth of ca. 500 m and its top is at ca. 420 m. It is approximately 4000 m wide and its height is situated between 60 and 160 m. The central crater has an approximate diameter of 350 m with several concentric rings, defining its central part (Van Rensbergen *et al.* 2005b; Kenyon *et al.* 2006; see **Table 3.1**).

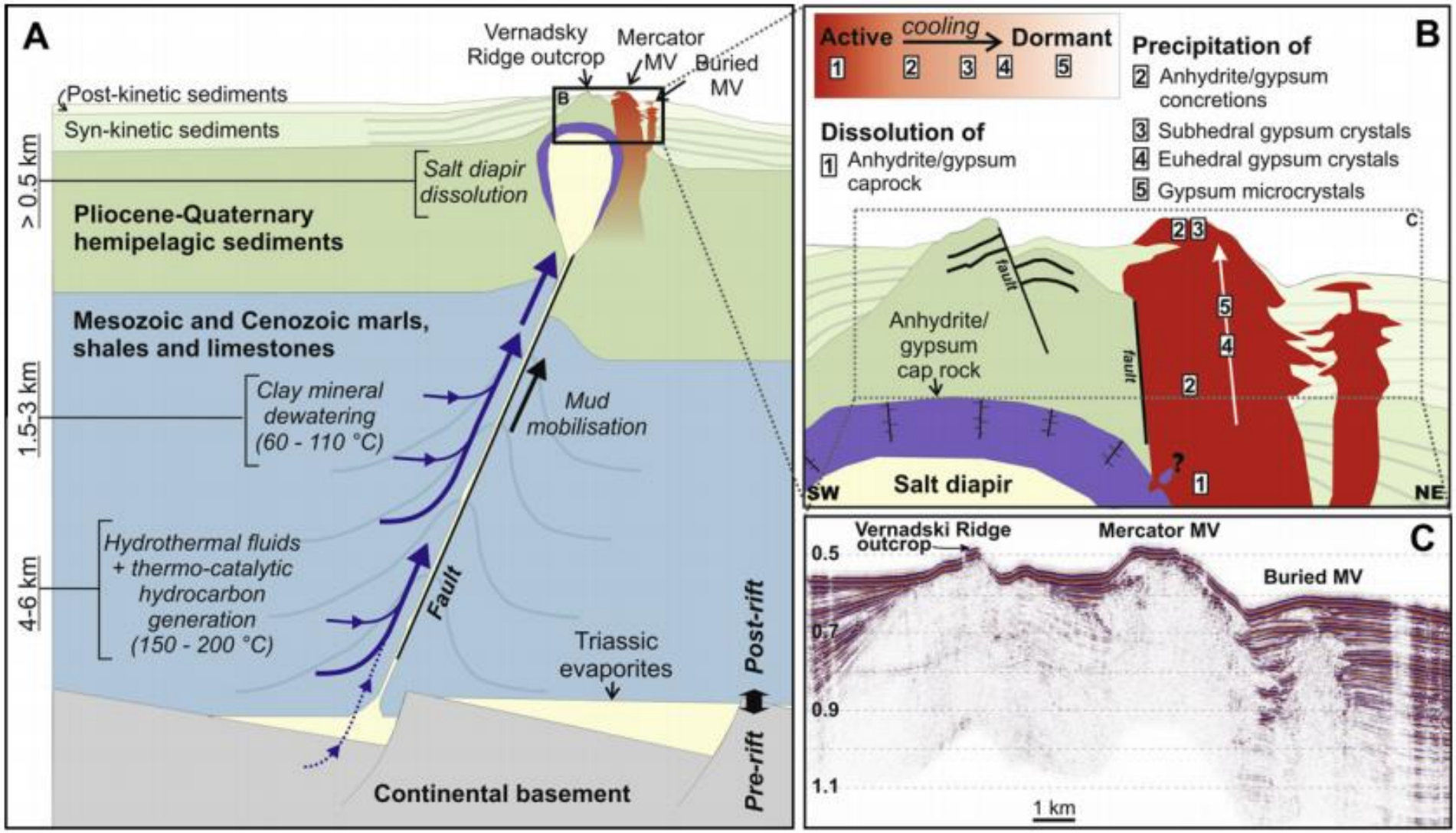

Figure 3.7 – A: Schematic overview of the stratigraphic setting of the Vernardsky Ridge and Mercator MV showing the location of the salt diaper. B: Geological interpretation of the seismic section (C). C: High-resolution seismic line over the Mercator MV, the outcrop of the Vernadsky Ridge and the Buried MV (Haffert *et al.* 2013).

3.2. Carbonate Province

3.2.1. Mud Volcanoes

3.2.1.1. No Name

The No Name mud volcano discovered during the TTR 09 cruise in 1999, is located between TTR MV and the Pen Duick Escapment area (see Figure 3.2), at a water depth of 598 m. This MV is approximately 5000 m in diameter, with 598 m water depth at the top of the mud volcano (Table 3.1; Kenyon *et al.* 2000).

3.2.1.2. Anastasya Area (off Tarsis)

The Anastasya area is constituted by three mud volcanoes: Anastasya, Pipoca and Tarsis (see **Figure 3.2 - A**).

The Anastasya mud volcano is the most prominent structure, an 80 m cone-shaped mound, 1500 m in diameter with its top at 452 m water depth. The regular cone shape of this mud volcano is symmetrical with respect to its slopes. In the centre of the volcano is a small flat-topped, dome-like feature (about 350 m in diameter) with steep slopes. The Pipoca mud volcano is morphologically similar to Anastasya, it presents a sub-rounded cone shaped feature with a maximum diameter of 2100 m, a relief of 97 m and the summit occurs at 536 m water depth. On the southwestern slope of this mud volcano can be identified several lobes formed by successive mud flows. The Tarsis mud volcano, NW of Pipoca, occurs at 762 m water depth and is a low-relief mound surrounded by a ring-shaped moat. Its diameter at the seabed is 900 m and its height is 60 m (Somoza *et al*. 2003).

3.2.1.3. Meknès

The Meknès Mud Volcano has a high backscatter central pear shaped crater at a water depth of about 650 m and the base is at 710 m. The MV discovered during the TTR 14 cruise in 2004, is located on the SWIM 1 fault (see **Figure 3.1**). It is 60 m high and its width is about 1000 m (see **Table 3.1**; Kenyon *et al*. 2006; Mhammedi *et al.* 2008, 2010). According with Mhammedi *et al.* 2010 the main minerals of the MV are carbonates, calcite, dolomite and aragonite. (Kenyon *et al*. 2006). The crater of the Meknès MV is formed by a large number of empty shells of the gastropod *Neptunea* and green mud breccia with scattered clasts (Oliver *et al.* 2011).

3.2.1.4. Student

The student mud volcano was discovery during the TTR 10 cruise in 2000 (Kenyon *et al.* 2001; see **Figure 3.2**). It is 200 m high and it has a very sharp morphology, with a diameter of about 1700 m at its base and 200 m at the top, at a water depth at the top of about 955 m (see **Table 3.1**). This mud volcano is delimited by a well-defined moat, particularly on the westernmost flank, where there are small features that are probably carbonate mounds (Akhmetzhanov *et al*. 2008).

3.2.1.5. Ginsburg

The Ginsburg Mud Volcano discovered in TTR 09 cruise in 1999 (Kenyon *et al.* 2000; Kenyon *et al.* 2010; see **Figure 3.2 - B**), is located in the Western Moroccan Field in the Eastern domain of the Olistostrome and is probably one of the largest mud volcanoes in this area (Van Rensbergen *et al.* 2005b; Stadnitskaia *et al.* 2008). This conical shaped MV is over 250 m high, with a diameter of about 3800 m at the base and 400 m at the top, (see **Table 3.1**; Van Rensbergen *et al.* 2005b; Akhmetzhanov *et al.* 2008), at a water depth of about 911 m.

3.2.1.6. Yuma

The Yuma Mud Volcano (see **Figure 3.2**) discovered during the TTR 09 in 1999 (Kenyon *et al.* 2000) is constituted by a large, approximately 4000 m in diameter, gently domed summit upon which a smaller dome is located. It is a conical shaped mud volcano with approximately 250 m high, about 4500 m wide at the base and 2000 m at the top (Akhmetzhanov *et al.* 2008). This mud volcano is located in the southeastern part of the Gulf of Cadiz, with a bathymetric relief of more than 200 m (Gardner, 2001; Murton and Biggs, 2003; Ovsyannikov *et al.* 2003) at a water depth of about 964 m (see **Table 3.1).**

3.2.1.7. Aveiro

The Aveiro Mud Volcano (see **Figure 3.2**) discovered during the TTR 12 cruise in 2002, is 1500 m wide and about 80 m high (Kenyon *et al*. 2003; Ivanov *et al.* 2010), at a water depth of 1065 m (see **Table 3.1**). Sediment samples were collected and subdivided into three intervals during the TTR 12: the upper interval, the middle interval and the lower interval. The upper one, 0 to 4 cm presents brown marl with foraminifera. The middle interval, 4 to 91 cm is light gray homogeneous, bioturbated marl with foraminifera. The mud breccia is present in the lower interval, up to 0.5 – 1 cm diameter with a clayey matrix and a large number of sedimentary rock fragments (Kenyon *et al.* 2003).

3.2.1.8. Jesus Baraza

The Jesus Baraza Mud Volcano (see **Figure 3.2**) discovered during the TTR 10 cruise in 2010 (Kenyon *et al.* 2001) is an asymmetrical hill with an ellipsoidal top (Kenyon, 2003), located on the SWIM 2 fault in the Western Moroccan Field (WMF) at a water depth of about 1091 m. The asymmetry of the crater area results from the presence of another crater developing about 300 m to the south (Kenyon, 2003). The Eastern domain is characterized by mud volcanism and mud diapirism, which are structurally controlled (inverse structures within a chaotic body - GCAW) and likely triggered by the tectonic forces related to the convergence of the African and the Eurasian plates (Stadnitskaia *et al.* 2008). The MV is about 150 m high, the crater is 1600 m long and about 600 m wide (see **Table 3.1**; Kenyon, 2003).

3.2.1.9. Shouen

Shouen MV is a conical shaped mud volcano located approximately 16 km to the WNW of the Yuma MV and about 11 Km to the north of Darwin MV (see **Figure 3.2 - B**), with water depths at the top of 1180 m and high backscatter. It was discovered during the TTR 16 cruise in 2006, and it is approximately 150 m high, with a diameter of about 1100 m at its base and 700 m at the top (see **Table 3.1**). This crater shows scattered crusts, clasts, small dead colonies of scleractinean coral and numerous life traces. During the TTR 16 cruise was observed a few soft corals and pandalidae shrimps, and were collected samples that contained some worms (Siboglinidae and other polychaetes), cnidarians (Hydrozoa and Scyphozoa) and one bivalve. The Shouen MV has a similar morphology to Darwin MV and is also a site of active seepage (Akhmetzhanov *et al.* 2008).

3.2.1.10. Darwin

The Darwin Mud Volcano (see **Figure 3.2**) discovered during the TTR 16 in 2006 (Akhmetzhanov *et al.* 2008), is situated on the Moroccan continental margin, at a water depth of 1105 m. The MV is cone shaped and approximately 50 m in height. In the centre of the crater a patch of seafloor approximately 80 m in diameter is covered with a carbonate crust pavement that is broken up by a network of fissures. The individual carbonate slabs are up to 10 m in diameter and are often tilted creating local escarpments of up to 0.5 m high (see **Table 3.1**; Vanneste *et al.* 2012).

Darwin MV differs from the others in the Carbonate Province area because its crater is completely covered by large carbonate slabs and crusts. The fissures among the slabs and depressions with scattered crust are filled with abundant shell hash of *Bathymodiolus* and *Neptunea contraria* (Génio *et al.* 2008; Blazewicz-Paszkowycz *et al.* 2011a) and occasionally small clumps of living Bathymodiolus mauritanicus (Von Cosel, 2002; Blazewicz-Paszkowycz *et al.* 2011a; Oliver *et al.* 2011; Rodrigues *et al.* 2011). Soft corals and other epifauna are occasionally present on the rocks and sediment surface (Genio *et al.* 2008). Discrete AOM hotspots have been observed at the rim of the crater, suggesting a relocation of seep activity (Vanreusel *et al.* 2009).

3.2.2. Other Features

In this work besides the mud volcanoes, other morphologic features of tectonic origin were also studied (e.g.: the Vernadsky Ridge, the Pen Duick Escarpment, the Formosa Ridge). In addition to these, whitin and in the vicinity of the MOW channels, abundant macrofauna was observed and also sampled. These features include the Iberico mud mound, the Cadiz Channel and the Channel west of Gibraltar.

3.2.2.1. Channel West of Gibraltar Strait

A large erosive channel is located west of the Camarinal Sill along the Gibraltar Strait exit. This channel may be divided into two main zones in agreement with Hernández-Molina *et al*. 2012: The eastern zone (**Figure 3.8**) is approximately 3000 to 4000 m wide and has a relatively linear WSW trend until reaching basement highs. The western zone (see **Figure 3.8**) of the channel is about 6000 m wide and has a sinusoidal shape with a SW trend until 35.770º N and 6.717º W, where it changes its trend towards the NW and narrows to approximately 4000 m (Hernández-Molina *et al*. 2012; 2014). The channel changes to a small depression towards NW being delimited by a contourite terrace to the NE and an associated huge contourite levee to the SW. In the middle to distal part of the terrace there are other minor channels, erosional scour alignments, valleys and depositional features (Hernández-Molina *et al*. 2012). The MOW circulates along this channel being partially responsible for its morphological characteristics (see **Figure 2.1**).

3.2.2.2. Vernadsky Ridge

The Vernadsky Ridge is a sea floor ridge located in the El Arraiche mud volcano field, sub-parallel to the Renard ridge and has a steep fault escarpmentat their S flank (see **Figure 34 and 37**; Van Rensbergen *et al.* 2005b; Wehrmann *et al.* 2011). It is located in water depths of about 700 m and stretches to the shelf edge (Van Rensbergen *et al.* 2005b).

The total amount of mounds and cold-water coral patches on this northern edge of the Vernadsky Ridge can be estimated at 130. The central part of the Vernadsky Ridge consists also of a topographic height, providing substrate for the settlement of benthic organisms. At the edges, mound like structures are recognized, which can be interpreted as small NW-SE orientated mound patches. They have a similar acoustic signature on seismic and sidescan sonar imagery as the mound-like structures at the northern edge of the Vernadsky Ridge (Foubert *et al*. 2008).

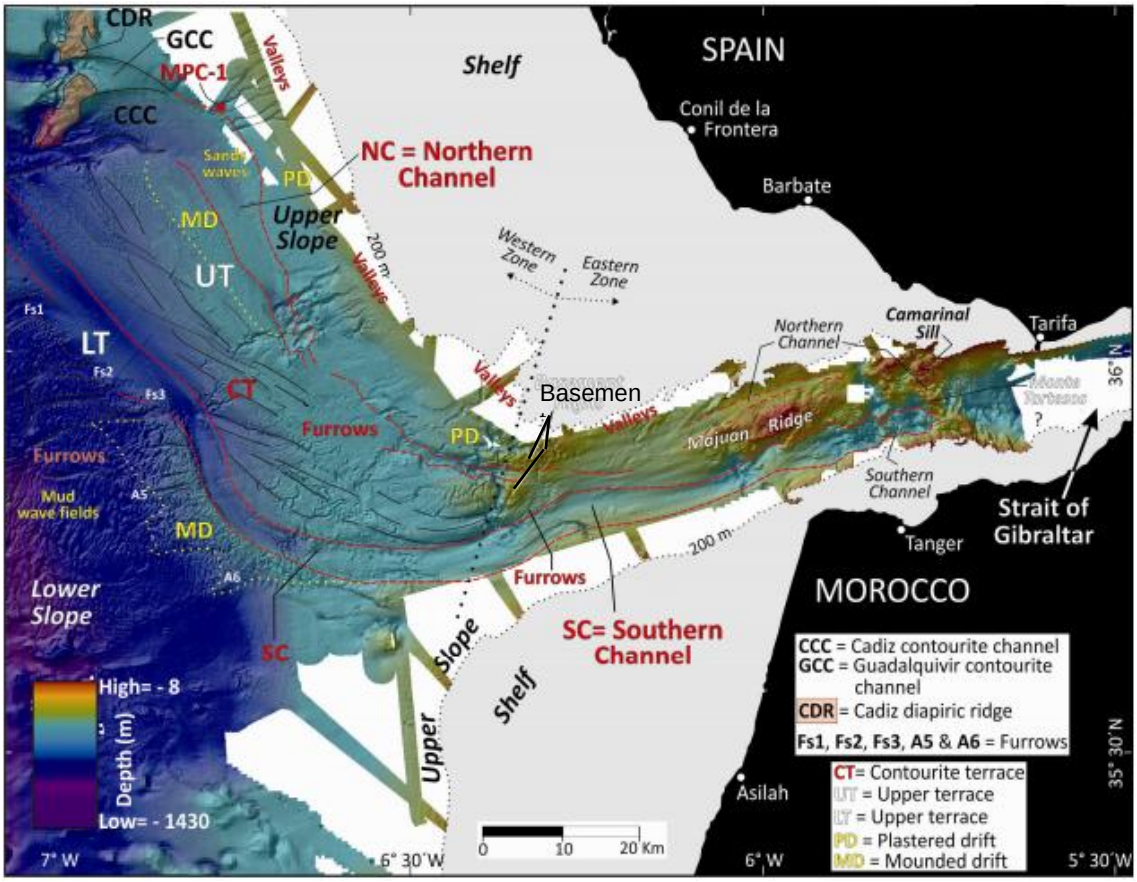

Figure 3.8 – Swath bathymetry at the exit of the Gibraltar Strait (modified from Hernández-Molina *et al.*, 2014). Red Lines – Delimit Northern and Southern parts of the Channel.

3.2.2.3. Pen Duick Escarpment Area

The Pen Duick Escarpment located within the El Arraiche mud volcano field, represents the southeastern branch of the Renard Ridge (Kenyon *et al*. 2003; Van Rooij *et al*. 2011; Wehrmann *et al.* 2011; Mol *et al.* 2012) and it is separated from Gemini MV, by 1000 m wide moat feature (see **Figure 3.4**; Wehrmann *et al.* 2011). It represents a NE-SW oriented fault-bounded (normal fault) cliff of 6 km length and 80 to 125 m height (Van Rensbergen *et al.* 2005a; Van Rooij et al. 2011; Wehrmann *et al.* 2011) at a water depth of 525 m (Kenyon *et al.* 2003). Some studies using seismic profiles provide evidence for gas accumulation and features related to hydrocarbon (gas) seepage, across the Pen Duick Escarpment (Wehrmann *et al.* 2011).

On top of the Pen Duick Escarpment 15 cold-water coral mounds were recognized. These mounds are conical to elongated features with an average elevation of 15 m above the surrounding seabed (e.g.: mound C; Cunha personal communication). The mounds are distributed in a water depth of 500 – 600 m and reach up to 60 m in height and about 500 m in diameter at the mound base. The corals and the macrofauna located in the mounds are under the influence of the North Atlantic Central Water, with a bottom current speed of 10 cm s^{-1} at 1 m off the seafloor (Mol *et al*. 2012) and with

seabottom water temperatures ranging from 10.7 up to 11.8 °C and a salinity range of 35.55 – 35.65 (Van Rooij *et al*. 2011; Wehrmann *et al.* 2011).

3.2.2.4. Iberico

The Iberico (see **Figure 3.2**) is an 870 m deep and 165 m tall cone-shaped mud mound. This feature is defined by an asymmetric profile with steep slopes of 22º-25º and 12º-15º at its southward and northward flank, respectively (Somoza *et al*. 2003; see Figure 3.2).

3.2.2.5. Formosa Ridge

The Formosa Ridge (see **Figure 3.2**) is a diapiric ridge formed by the ascending movement of salt/shale deposits of the olistostrome masses or deeper plastic units. The movement of these less dense units is likely triggered by the tectonic transpressional setting related to the convergence of the African and the Eurasian plates (Magalhães *et al.* 2012).

3.2.2.6. Cadiz Channel

The Cadiz Channel is the largest and most important contourite channel. It has a total length of 110 km and an orientation that varies from SE-NW to NE-SW. This submarine channel is subject to high current speeds and erosional processes (Hernández-Molina *et al*. 2006; see **Figure 3.2** and **3.9**).

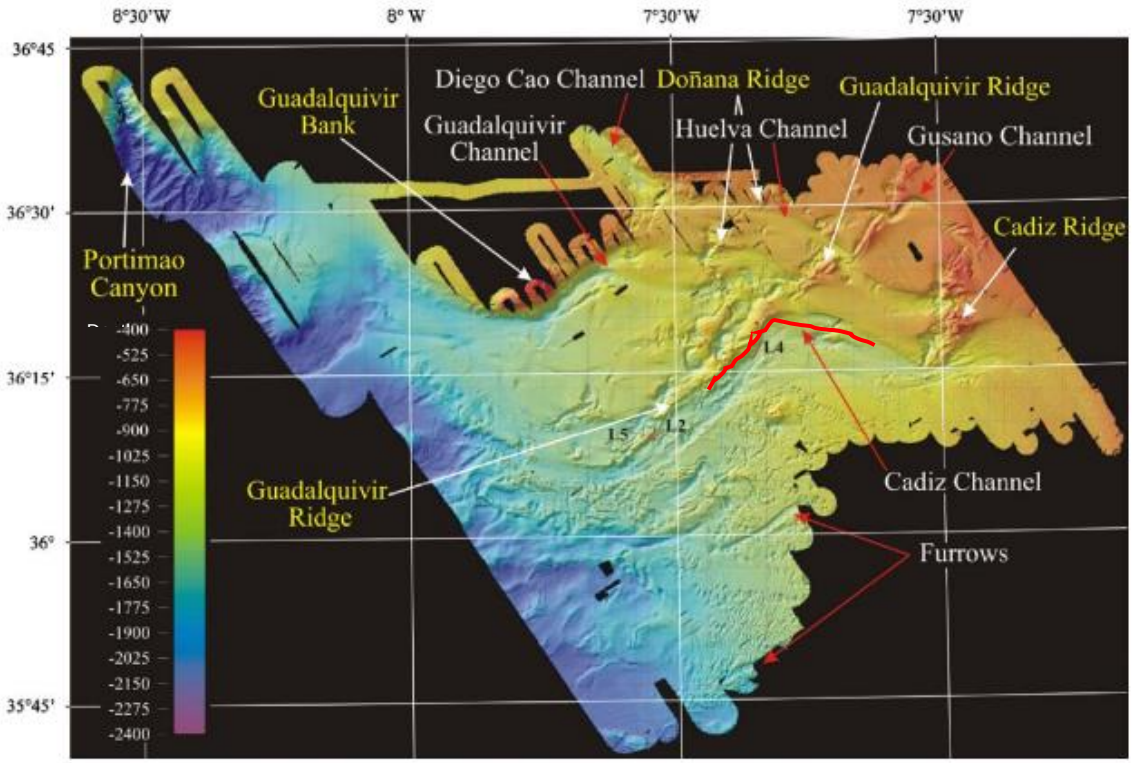

Figure 3.9 - Swath bathymetry of the central sector of the middle slope of the Gulf of Cadiz Contourite System, showing the main contourite channels, furrows and main diapiric ridges, with a NNE trend. Red line – Cadiz Channel (from Hernández-Molina *et al*. 2006).

3.3. Deep Field

3.3.1. Captain Arutyunov

Captain Arutyunov is a cone-shaped Mud Volcano on a flat basin floor, discovered during the TTR 12 cruise in 2002 (Kenyon *et al.* 2003) at a water depth of 1324 m. This Mud Volcano is about 100 m high, 2000 m in diameter and has a 300 m wide circular crater at the top (see **Table 3.1**; Kenyon *et al.* 2003). It is located on one of the major SWIM lineaments (SWIM 2; see **Figure 3.2**), where the thickness of the accretionary prism is greatest (Thiebot and Gutscher, 2006). The Captain Arutynov is one of the most active mud volcanos in the Gulf of Cadiz (Niemann *et al.* 2006; Sommer *et al.* 2009), is categorized as an example of extensive generation and transport of fluids, petroleum and hydrocarbon gases from deeply buried sediments (Nuzzo *et al.* 2009) and is the place where an unusual member of the Callianassidae has been found (Dworschak and Cunha, 2007). The most conspicuous animals were cidarid echinoids clustered at the centre of the crater. Several samples taken at the top showed that the central area is rich in gas hydrates and is densely covered by aggregations of *Siboglinum* accompanied by buried thyasiridae bivalves and patches of abundant polychaetes and tanaidaceans (Dworschak and Cunha, 2007).

3.3.2. Sagres

Sagres Mud Volcano is the shallowest mud volcano discovered on the Portuguese margin (see **Figure 3.2**) during the TTR 17 cruise in 2008, at a water depth of 1554 m. It presents an asymmetric structure with a steep flank on the SE and its crater, at a 1630 m water depth, coincides with an area of high backscattering. The MV is about 110 m high and 2700 m wide at its base (see **Table 3.1**), and based on the seismic profile it appears to have been controlled by faulting (Ivanov *et al.* 2010).

3.3.3. Carlos Ribeiro

The Carlos Ribeiro Mud Volcano discovered during the TTR 10 cruise in 2000 (Kenyon *et al.* 2001), is located on the deep Portuguese margin on the lower slope of the accretionary wedge at less than 10 km of the SWIM 2 fault, at 2173 m below sea level (Vanneste *et al.* 2011, 2013; see **Figure 3.2**). The MV is circular with a flat-top summit, extending approximately to 80 m in height and 1500 m in diameter (see **Table 3.1;** Pinheiro *et al.* 2003; Vanneste *et al.* 2011, 2013). The focus of activity (the eye) of the Mud Volcano lies slightly to the north of its centre, and is surrounded by a series of concentric ridges which build up the MV (Vanneste *et al.* 2011, 2013).

Gas hydrates recovered from the sediment and methane concentrations measured on the Carlos Ribeiro mud volcano are some of the highest from the Gulf of Cadiz (Hilário and Cunha, 2008). In spite of this, the methane emissions, into the overlying water column, are relatively low (0 – 806 mmol m^{-2} yr^{-1}), which has been attributed to low fluid flow velocities (0.4 – 4 cm yr^{-1}) coupled with efficient microbial methanotrophy (Vanneste *et al.* 2013) and as result of the retention of methane in the form of hydrates. Fluid flow activity focused at the eye of the MV, gradually decreases towards its periphery and shows only modest fluid expulsion activity, when compared to other MVs (Vanneste *et al.* 2011, 2013). In the Carlos Ribeiro Mud Volcano the macrofauna is diverse on the flanks, and by contrast, the top (2200 m) is almost devoid of macrofauna with the exception of scattered ophiuroids and *Bobmarleya gadensis*, which inhabit small depressions of the seafloor (Hilário and Cunha, 2008).

3.3.4. Bonjardim

The Bonjardim Mud Volcano is located on the deep Portuguese margin (see **Figure 3.2**; Pinheiro *et al.* 2003), on SWIM 1 lineament in a water depth of about 3060 m (Pinheiro *et al.* 2003; Van Rensbergen *et al.* 2005b). This Mud Volcano was discovered during the TTR 10 cruise in 2000 (see **Table 3.1**; Kenyon *et al.* 2001; Pinheiro *et al.* 2003) and has approximately 2000 m in diameter and 150 m in high (Akhmetzhanov *et al.* 2008) with a sea floor depression at the rim of the cone (Pinheiro *et al.* 2003). The crater rim is well developed, enclosing the 800 m wide, very high backscatter crater domain. On the southeastern end of the crater there is a small, elevated area about 150 m in diameter. The western flank of the Bonjardim mud volcano is cut by a NE-SW slope failure, over 1000 m long that appears to be related to a particularly large mud flow (Akhmetzhanov *et al.* 2008). The characteristic feature of the mud breccias from the Bonjardim MV is the presence of very thin cover of pelagic sediments which indicates that the sampling sites were located on relatively recent mud flows (Stadnitskaia *et al.* 2006).

3.3.5. Semenovich

The Semenovich Mud Volcano, located on the deep Portuguese margin (still in the accretionary wedge; see **Figure 3.1**) was discovered during the TTR 15 cruise in 2005 at a water depth of 3200 m approximately (Akhmetzhanov *et al.* 2007; **Table 3.1**). It is one of the deepest mud volcanoes found in the Deep Portuguese Mud Volcano field together with Porto, Bonjardim, Olenin and Carlos Ribeiro. This MV is 70 m high, has two craters with high backscatter and sharp rims, and well defined mudflows that are more developed to the northwest (Akhmetzhanov *et al.* 2008).

3.3.6. Porto

The Porto Mud Volcano is located at the deep Portuguese margin (see **Figure 3.1**; Blazewicz-Paszkowycz *et al.* 2011a), on SWIM 1 lineament, at the rim of the accretionary prism, in a water depth of about 3900 m (see **Table 3.1**; IFM-Geomar, 2006; Cunha *et al.* 2013). It was discovered during the TTR 15 cruise in 2005 (Akhmetzhanov *et al.* 2007) and has been until now, the deepest mud volcano known so far from the Gulf of Cadiz (IFM-Geomar, 2006). The top of the Porto mud volcano is covered by a continuous field of clumps of 20 to 50 individuals of *Spirobrachia tripeira* and an undetermined number of adult and juvenile specimens of *Polybrachia* sp. These clumps are accompanied mainly by the frenulate *Lamellisabella denticulata*, stalked hexactinellid sponges and crinoids (Hilário and Cunha, 2008).

Chapter 4

Data and Methods

The data used in this work was compiled from the most relevant bibliography on the fauna observed in the Gulf of Cadiz mud volcanoes, including several recently published articles (Dworschak and Cunha 2007; Génio *et al*. 2008, 2013; Hilário and Cunha 2008; Rodrigues *et al*. 2008; Blażewicz-Paszkowycz *et al*. 2011a, 2011b; Oliver *et al*. 2011; Rodrigues *et al*. 2011, 2013), which are presented in the main matrix of Appendix I – Table 1. The samples were obtained using different gears (e.g.: Gravity Corer - GC, FLUFO Lander - FLUFO, USNEL Box Corer - USNEL, Multi Corer - MUC, Geology Dredge - GD, Kasten Corer - KC, BIGO Lander - BIGO, TV-Grab - Gr, Suction Sampler ROV - SUS, Push Corer ROV - PUC, NIOZ Box Corer – NIOZ; examples shown in **Figure 4.1**), depending namely on the specific objectives of each campaign, on the geological nature of the sampled seafloor, and on the ship equipment availability.

Using the ArcMap, the main component of the ArcGis (Geographic Information System) software, a comprehensive geodatabase was created using ArcCatalog to store all the spatial and tabular data (e.g.: biological data, geographic coordinates, depths, cruises, stations, gear, structures and SWIM bathymetry). The data was organized in layers: Feature Classes and Raster Dataset, which allowed to create the final maps. All maps produced were projected using UTM Zone 29N coordinated system and World Geodetic System 1984 (WGS84) Datum.

4.1. Spatial analysis with ArcGIS

ArcGis is a geographic information system software with the ArcMap as the main component. The ArcMap is used primarily to view, edit, create, and analyse geospatial data. In this project, the ArcMap is used as a geospatial data tool in order to find spatial relationships between geological and biological data (as specified above), namely concerning the SWIM faults, the mud volcanoes and the bathymetry versus the macrofauna found in the study area, the Gulf of the Cadiz.

Figure 4.1 – Examples of gear used to collect the samples analysed in this work. Gravity Corer - Mooring Systems, inc. website: http://www.mooringsystems.com/; Box Corer - KC Denmark website: http://www.kc-denmark.dk/; BIGO Lander - Pfannkuche *et al*., 2006; TV-Grab - Pfannkuche *et al*., 2006; Geology Dredge - American Geophysical Union website: http://blogs.agu.org/; Kasten Corer - Alfred Wegener Institut website: www.awi.de; Multi Corer - Alliance for Coastal Technologies website: http://www.act-us.info/.

4.1.1. Workflow of the ArcMap

4.1.1.1. Geodatabase

A personal geodatabase, named BioData, is created using ArcCatalog to store all the spatial and tabular data (e.g.: biological data, geographic coordinates, depths, cruises, stations, gear, structures, SWIM bathymetry; **Figure 4.2**). The integration of all data in this format, allows tables correlations and several spatial analyses in a very simple and efficient way.

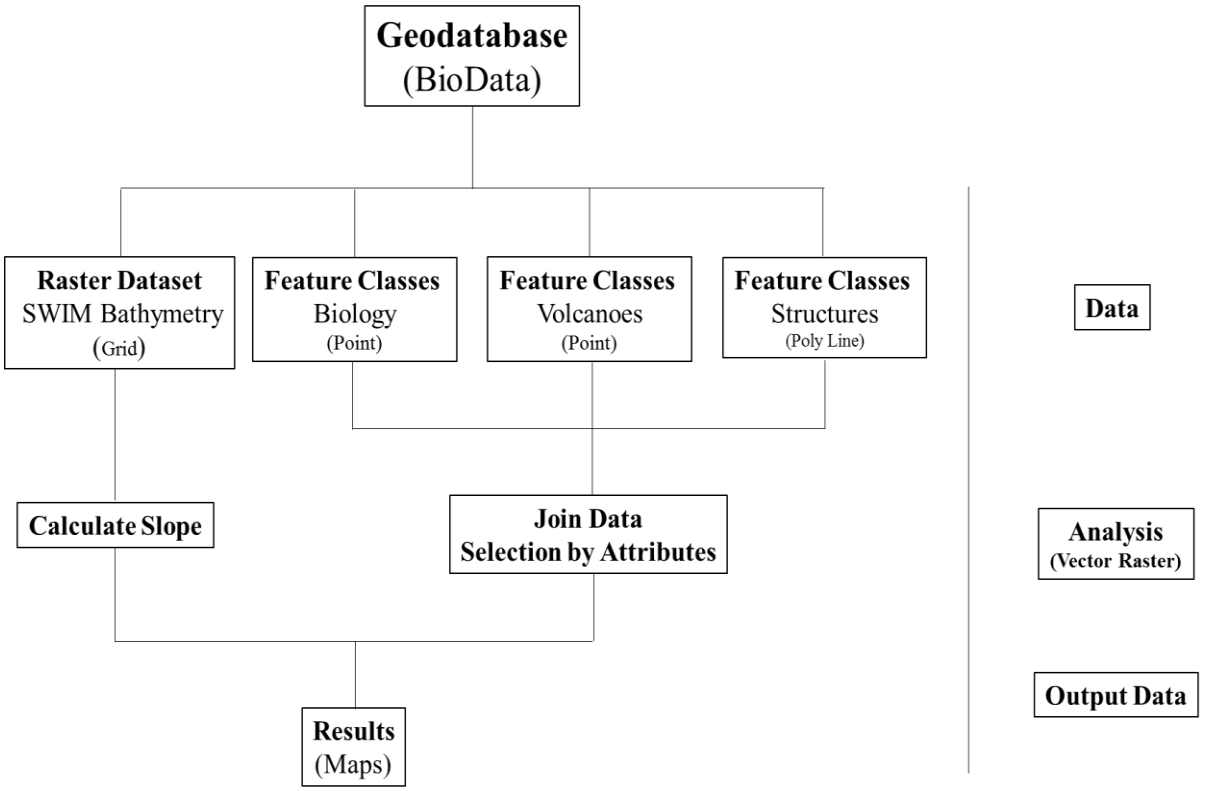

Figure 4.2 – The main operation performed in ArcMap.

4.1.1.2. Feature Classes and Raster Dataset

The Feature Classes (a collection of geographic features with the same geometry type (such as point, line, or polygon), attributes, and spatial reference, see ESRI website: http://www.esri.com/) can be created through four primary ways, using ArcCatalog or the Catalog window, using the Create Feature Class geoprocessing tool (the method used in this project), saving the contents of a map layer in ArcMap and converting an external data source into a geodatabase feature class. When creating a

feature class, it is possible to choose whether to create one that stores polygons, lines, points, annotation, multipoint, multipatch or dimension features. All feature classes in a feature dataset must use the same spatial reference, which is defined when the feature dataset is created. The Raster Dataset represents geographic features by dividing the geographical space into discrete square or rectangular cells laid out in a grid (e.g.: the SWIM bathymetry used to delimiter the SWIM lineaments). Each cell has a value that is used to represent some characteristic of that location (ESRI website: http://www.esri.com/).

4.1.1.3. Join Data and Final Maps

When the feature classes are defined, it is necessary to compile the data in the same table to create the maps. "Join Data" is a very important step to join all data in the same table (e.g.: heterotrophic and chemotrophic species, gears, and stations in the Biology feature class). This allows the selection and display of the necessary attributes in the different maps. After the necessary attributes are selected, the software superimposes the different layers (Feature Classes and Raster Dataset) and creates the final maps (e.g.: **Figure 3.1** and **3.2**).

Chapter 5

Results

The biological samples studied in this work were taken from 22 mud volcanoes, six from the El Arraiche Mud Volcano field, ten from the Carbonate Province and six from the Deep Field, and another six features (not mud volcanoes) in the Carbonate Province (see **Chapter 3**). The features with a high level of sampling effort (**Table 5.1**) are Captain Arutyunov MV (19 stations), Mercator MV (12 stations) and Pen Duick Escarpment (ten stations). The type of gear more frequently used to collect the biological samples were the TV-Grab (Gr) in thirty stations and the USNEL Box Corer (UB) in sixteen stations (see **Table 5.1**).

In total 122 species were analysed from 105 stations (**Annex I - Table 1**), 18 belong to the Family Siboglinidae (Phylum Annelida, Class Polychaeta), 14 to the Class Bivalvia (Phylum Mollusca), 56 to the Class Gastropoda (Phylum Mollusca), 17 to the Order Tanaidacea (Phylum Arthropoda, Sub-Phylum Crustacea, Class Malacostraca), one to the Order Decapoda (Phylum Arthropoda, Sub-Phylum Crustacea, Class Malacostraca) and 16 to the Class Ophiuroidea (Phylum Echinodermata; **Table 5.2**). The Order Decapoda was not analysed like the other taxa since the available published data reports one family only (Callianassidae, Genus *Vulcanocalliax*, Species *V. arutyunovi*; **Annex II** – **Figure 1**) found in Captain Arutyunov MV at depths between 1327 and 1339 m.

The interpretation of the number of species per feature distribution shows that the number of chemotrophic species increases with the depth increment (**Figure 5.1 - A**). Two exceptions can be observed, in the El Arraiche Field and in the "Other Features" from the Carbonate Province. Although the Mercator MV is located at only 351 m depth, a high number of chemotrophic species (eight species) was observed, when compared with other features from the El Arraiche Field, located at the same depth. In the "Other Features" no chemotrophic species are observed, with the exception of the Pen Duick Escarpment (between 445 and 1275 m), where two thiotrophic species were found. The mud volcanoes (red rectangles in the **Figure 5.1**) that show a higher number of chemotrophic species are located at less than 10 km relatively to the SWIM faults, with the exception of the Jesus Baraza MV where only one specie was found. The predominant metabolic strategy in all analysed areas ("Other Features", El Arraiche Field, Carbonate Province and Deep Field) is the thiotrophic nutrition. On the other hand, the less utilized metabolic strategy is the Dual Symbiosis, only observed in species localized in Darwin MV.

The distribution of the heterotrophic species (**Figure 5.1 - B**) shows that the number of taxa tends to decrease with depth (76 species in the El Arraiche Field, 60 species in the Carbonate Province, 36 species in the "Other Features" and 47 species in the Deep Field). Thus, a higher number of these species is observed in the El Arraiche Field than in the Deep Field. In both cases the majority of species belong to the Class Gastropoda. In the "Other Features" the number of species is lower than expected for these depths and also lower than in the Deep Field. In three of the six MV situated at less than 10 km of the SWIM faults, a high number of heterotrophic organisms can be observed (Meknès, Captain Arutyunov and Porto MV).

Table 5.1 - Number of samples taken with different types of gear in each feature. NIOZ Box Corer (NIOZ); USNEL Box Corer (UB); Multi Corer (MUC); Kasten Corer (KC); TV-Grab (Gr); Gravity Corer (GC); Geology Dredge (GD); BIGO Lander (BIGO); FLUFO Lander (FLUFO); Push Corer ROV (PUC); Suction Sampler ROV (SUS); Rov Arm (ARM).

	Quantitative				Qualitative			Lander		ROV			Frequency
Features	NIOZ	UB	MUC	KC	Gr	GC	GD	BIGO	FLUFO	PUC	SUS	ARM	(Number of stations)
Al Idrissi	1	0	0	0	0	0	1	0	0	0	0	0	2
Fiúza	0	0	0	0	1	1	0	0	0	0	0	0	2
Gemini	3	0	0	0	0	0	0	0	0	0	0	0	3
W of Gibraltar	0	0	0	0	1	0	1	0	0	0	0	0	2
Mercator	0	4	3	0	1	1	0	0	0	0	0	3	12
Lazarillo de Tornes	1	0	0	0	0	0	0	0	0	0	0	0	1
Vernadsky Ridge	0	0	0	0	0	0	1	0	0	0	0	0	1
Kidd	0	3	0	0	1	1	0	0	0	0	0	0	5
Pen Duick Escarp.	5	0	0	0	5	0	0	0	0	0	0	0	10
No Name	0	0	0	0	1	0	0	0	0	0	0	0	1
Anastasya Area	1	0	0	0	0	0	0	0	0	0	0	0	1
Meknès	0	3	0	1	3	1	0	0	0	0	0	0	8
Iberico	0	0	0	0	0	0	1	0	0	0	0	0	1
Student	0	0	0	0	1	0	0	0	0	0	0	0	1
Ginsburg	0	0	0	0	1	0	0	0	0	0	0	0	1
Yuma	0	0	0	0	3	0	0	0	0	0	0	0	3
Formosa Ridge	0	0	0	0	1	1	2	0	0	0	0	0	4
Aveiro	0	0	0	0	1	1	0	0	0	0	0	0	2
Jesus Baraza	0	0	0	0	1	0	0	0	0	0	0	0	1
Shouen	0	0	0	0	1	0	0	0	0	0	0	0	1
Darwin	0	0	0	0	1	1	0	0	0	0	2	1	5
Cadiz Channel	0	0	0	0	0	0	1	0	0	0	0	0	1
Captain Arutyunov	0	3	2	1	6	3	0	3	1	0	0	0	19
Sagres	0	0	0	0	1	0	0	0	0	0	0	0	1
Carlos Ribeiro	0	1	3	1	1	1	0	0	0	1	0	0	8
Bonjardim	0	1	0	0	2	0	0	0	0	0	0	0	3
Semenovich	0	0	0	0	1	0	0	0	0	0	0	0	1
Porto	0	1	0	0	3	0	0	0	1	0	0	0	5
Total	11	16	8	3	37	11	7	3	2	1	2	4	105

Table 5.2 - Number of Families, Genera and Species of the different taxa.

Taxa	Family	Genus	Species
Polychaeta	1	5	18
Bivalvia	5	10	14
Gastropoda	31	49	56
Tanaidacea	8	13	17
Decapoda	1	1	1
Ophiuroidea	7	10	16
Total	53	88	122

5.1. Chemotrophic Organisms

5.1.1. Class Polychaeta

The Class Polychaeta is represented by 18 species (one family, five genera; see **Table 5.2**); ten of these species occurred in this study only once (singletons), *Bobmarleya gadensis* (**Annex II** – **Figure 2**, *Lamellisabella denticulata*, *Spirobrachia tripeira* (Annex II – Figure 2), *Polybrachia* sp.2, *Polybrachia* sp.3, *Polybrachia* Vb, *Polybrachia* Vc, *Siboglinum* Ie, *Siboglinum* sp.1 and *Siboglinum* sp.2.

Figures 5.2, **5.3** and **5.4** show the distribution of the Class Polychaeta in the study area. In **Figures 5.2** and **5.3** are mapped the distribution of the two genera that are represented by several species: - *Polybrachia* (six species) and *Siboglinum* (nine species). **Figure 5.4** shows the distribution of the remaining species of this taxon: *Bobmarleya gadensis*, *Lamellisabella denticulata* and *Spirobrachia tripeira*. The majority of species belonging to the genus *Polybrachia* are located in mud volcanoes from the Deep Field (Carlos Ribeiro, Captain Arutyun, Sagres, Bonjardim, Porto and Semenovich). The only specie of the Genus *Polybrachia* found outside the Deep Field is *Polybrachia* sp.1 (see **Figure 5.2**) that occurs in the Mercator MV. The species belonging to the Genus *Siboglinum* widespread throughout the study area (see **Figure 5.3**). Finally, the species *Bobmarleya gadensis*, *Lamellisabella denticulata* and *Spirobrachia tripeira* are observed only in the Deep Field, being restricted to the Carlos MV (*Bobmarleya gadensis)* and Porto MV (*Lamellisabella denticulata* and *Spirobrachia tripeira*), at less than 10 km to the SWIM faults (see **Figure 5.4**).

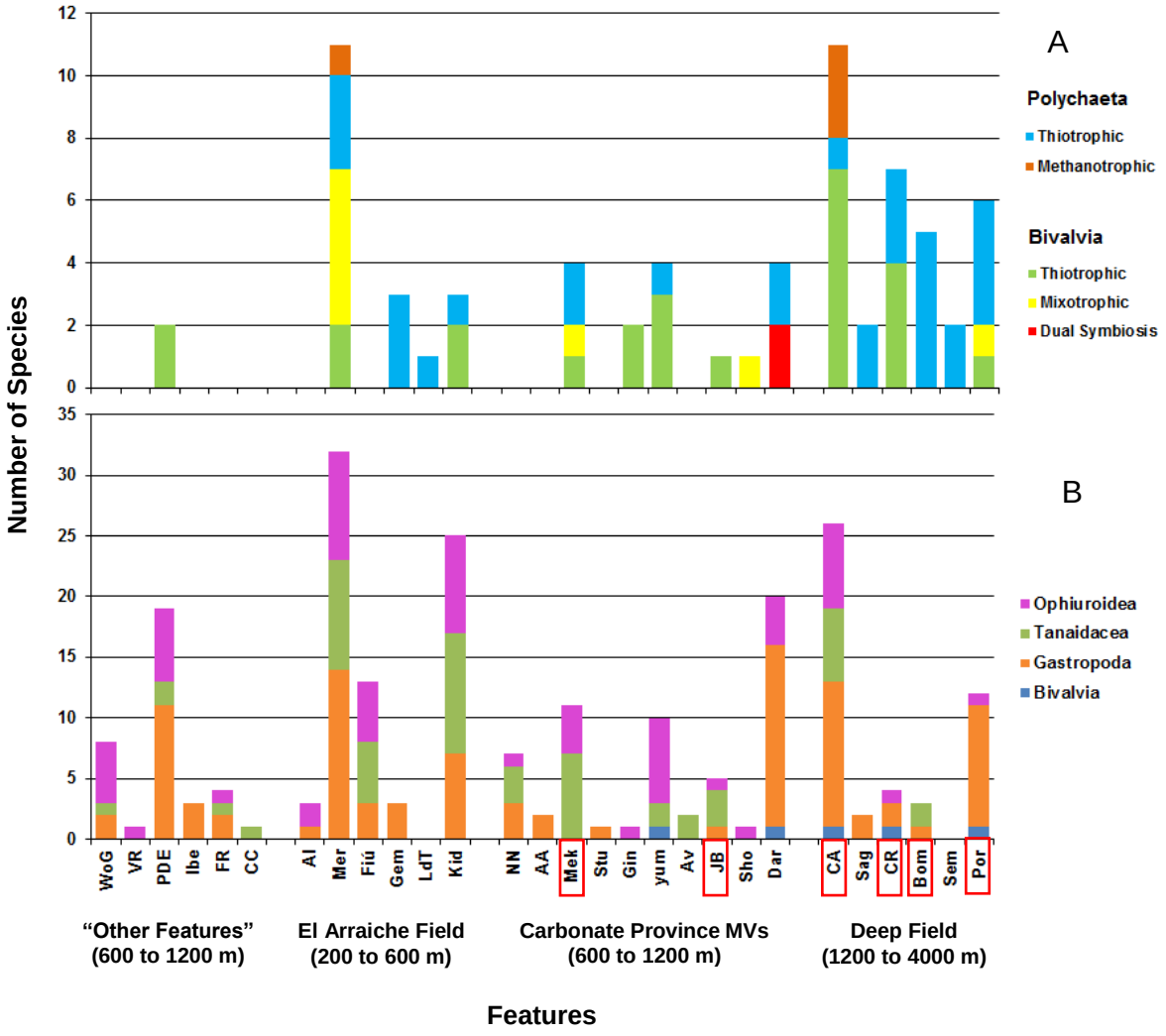

Figure 5.1 – Number of species per feature. A: Chemotrophic species (Class Bivalvia and Polychaeta); B: Heterotrophic species (Order Tanaidacea, Class Gastropoda, Bivalvia and Ophiuroidea). Red rectangles - MV located at less than 10 km to the SWIM faults. West of Gibraltar (WoG); Vernadsky Ridge (VR); Pen Duick Escarpment (PDE); Iberico (Ibe); Formosa Ridge (FR); Cadiz Channel (CC); Al Idrissi (Al); Fiúza (Fiú); Gemini (Gem); Mercator (Mer); Lazarillo de Tornes (LdT); kidd (kid); No Name (NN); Anastasya Area (off Tarsis; AA); Meknès (Mek); Student (Stu); Ginsburg (Gin); Yuma (Yum); Aveiro (Av); Jesus Baraza (JB); Shouen (Sho); Darwin (Dar); Captain Arutyunov (CA); Sagres (Sag); Carlos Ribeiro (CR); Bonjardim (Bom); Semenovich (Sem); Porto (Por). For the geographic location of the areas of occurrence see **Figure 3.1**.

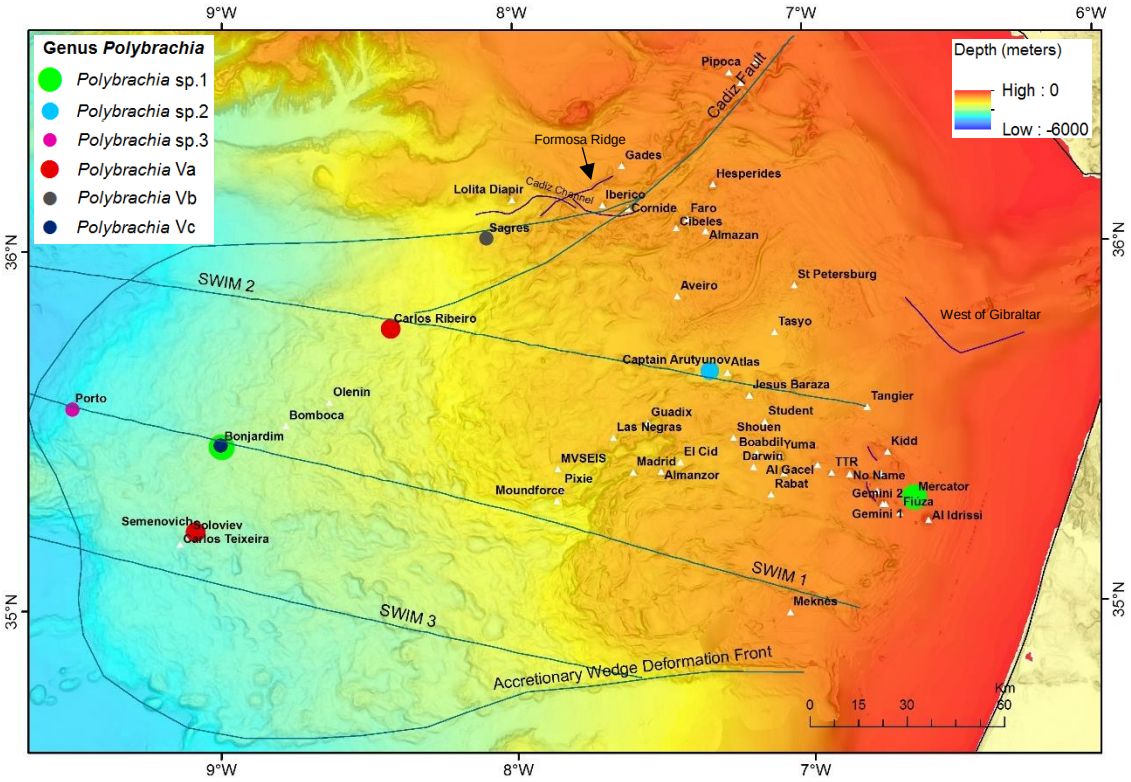

Figure 5.2 – Distribution of polychaetes. Green dots – Specie *Polybrachia* sp.1; Blue dot – Specie *Polybrachia sp.2; Pink dot* – Specie *Polybrachia sp.3; Red dots* – Specie *Polybrachia Va; Dark grey dots* – Specie *Polybrachia Vb; Dark blue dot* – Specie *Polybrachia Vc.*

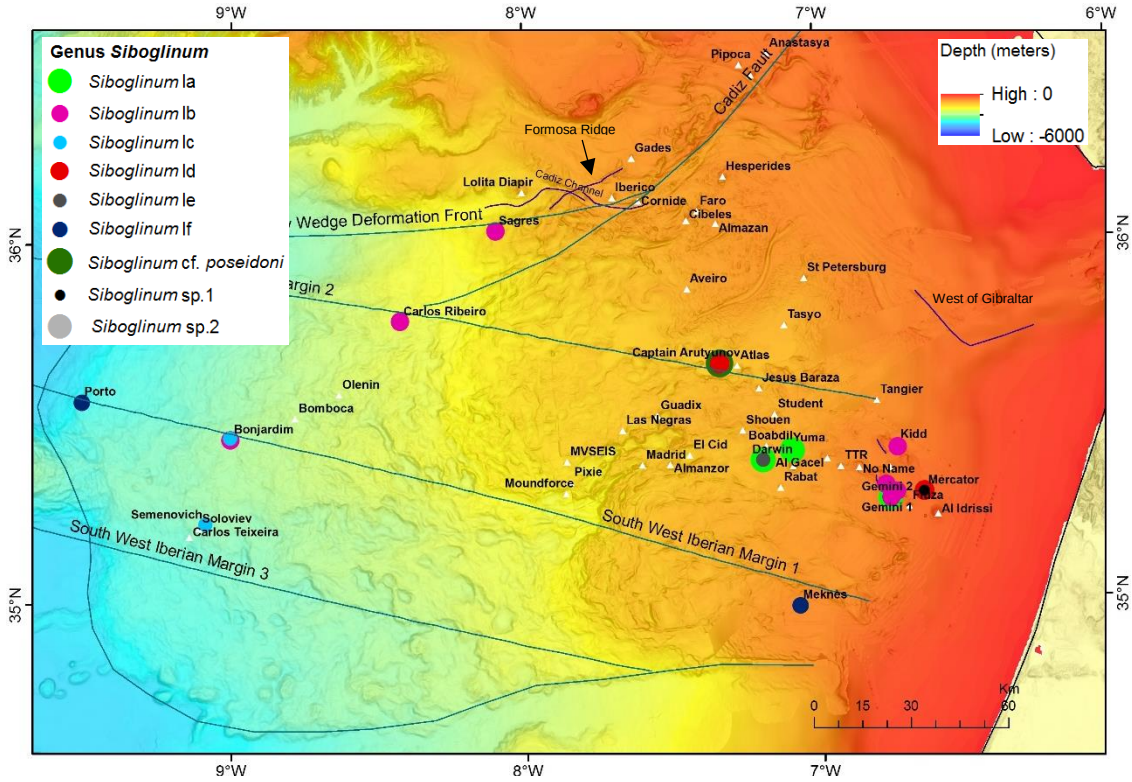

Figure 5.3 – Distribution of polychaetes. Green dots – Specie *Siboglinum* Ia; Pink dots - Specie *Siboglinum* Ib; Blue dots – Specie *Siboglinum* Ic; Red dots – Specie *Siboglinum* Id; Dark grey dot – Specie *Siboglinum* Ie; Drk blue dots – *Siboglinum* If; Dark green dots – *Siboglinum* cf. *poseidon*i; Black dot – *Siboglinum* sp.1; Grey dots – *Siboglinum* sp.2.

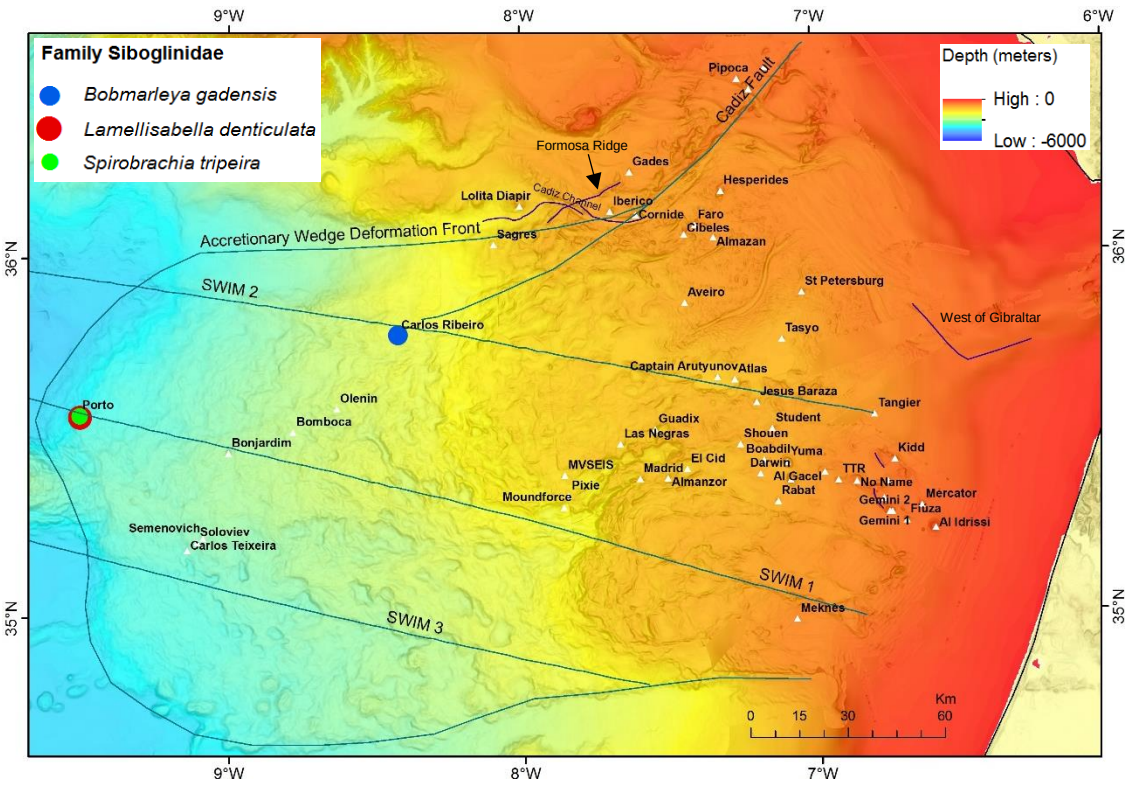

Figure 5.4 – Distribution of polychaetes. Blue dot - Specie *Bobmarleya gadensis*; Red dot – Specie *Lamellisabella denticulate;* Green dot - Specie *Spirobrachia tripeira.*

5.1.2. Class Bivalvia

The Class Bivalvia is represented by 14 species (ten genera in five families: Mytilidae, Solemyidae, Thyasiridae and Vesicomyidae; see **Table 5.2**; examples shown in **Annex II - Figure 3** to **8**), three of these are heterotrophic (**Figure 5.13**, **subchapter 5.2**) and 11 chemotrophic (**Figure 5.5**, **5.6** and **5.7**). Five of these species are singletons, *Isorropodon* sp. indeterminate, *Spinaxinus* cf. *sentosus, Lucinoma asapheus, Mendicula ferruginosa* and *Thyasira tortuosa*. **Figures 5.5** and **5.6** show the distribution of the two families with more species (Solemyidae and Thyasiridae) and **Figure 5.7** shows the distribution of the remaining species. The species *Acharax gadirae* (**Annex II** – **Figure 4**) occurs in a wide range of depths, 556 to 3860 m, contrasting with the species *Solemya (Petrasma) elarraichensis* (**Annex II** – **Figure 4**) that is restricted to lower depths, 358 to 1030 m, in the El Arriche Field, and Carbonate Province (see **Figure 5.5**). The species *Spinaxinus* cf. *sentosus* (blue dot; **Annex II** – **Figure 5**) and *Thyasira tortuosa* (pink dot) only appear once and are both located in the Deep Field. *Thyasira (Parathyasira) granulosa* (green dots) appears in three different features, Shouen MV, Meknès MV (Carbonate Province) and Mercator MV (El Arraiche Field) at depths between 350 and 1177 m. The specie *Thyasira vulcolutre* (red dots; **Annex II** – **Figure 3**) is located in the Depp Field (Carlos Ribeiro MV and Captain Arutyunov) at depths between 1221 and 2200 m. The last specie, *Axinulus croulinensis* was found only in the Mercator Mud Volcano in El Arraiche Field (see **Figure 5.6**). Finally, the species *"Bathymodiolus" mauritanicus*, *Isorropodon megadesmus* (**Annex II** – **Figure 6**), I*sorropodon* sp. indeterminate (**Annex II** – **Figure 7**) and *Lucinoma asapheus* (**Annex II** – **Figure 5**) are present in all areas at depths between 358 to 1323 m (see **Figure 5.7**).

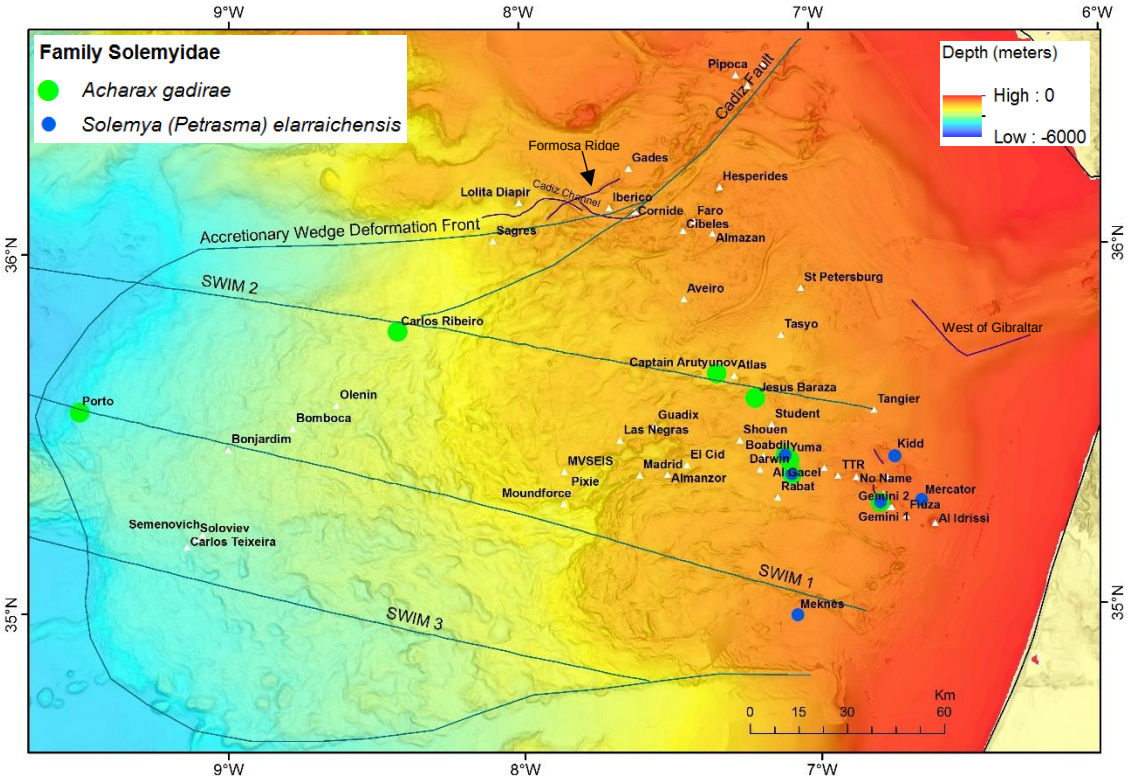

Figure 5.5 – Distribution of bivalves. Green dots - Specie *Acharax gadirae;* Blue dots - Specie *Solemya (Petrasma) elarraichensis.*

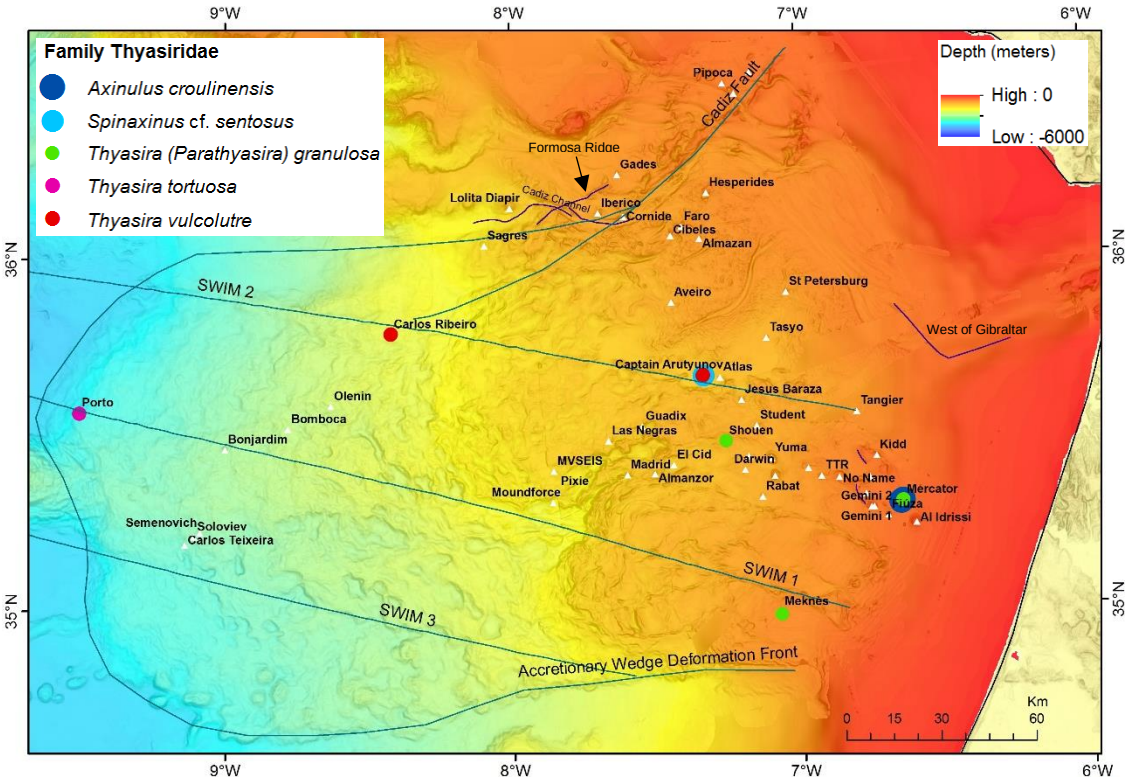

Figure 5.6 – Distribution of bivalves. Dark blue dot - Specie *Axinulus croulinensis*; Blue dot - Specie *Spinaxinus* cf. *sentosus*; Green dots - Specie *Thyasira (Parathyasira) granulosa*; Pink dot - Specie *Thyasira tortuosa*; Red dots - Specie *Thyasira vulcolutre*.

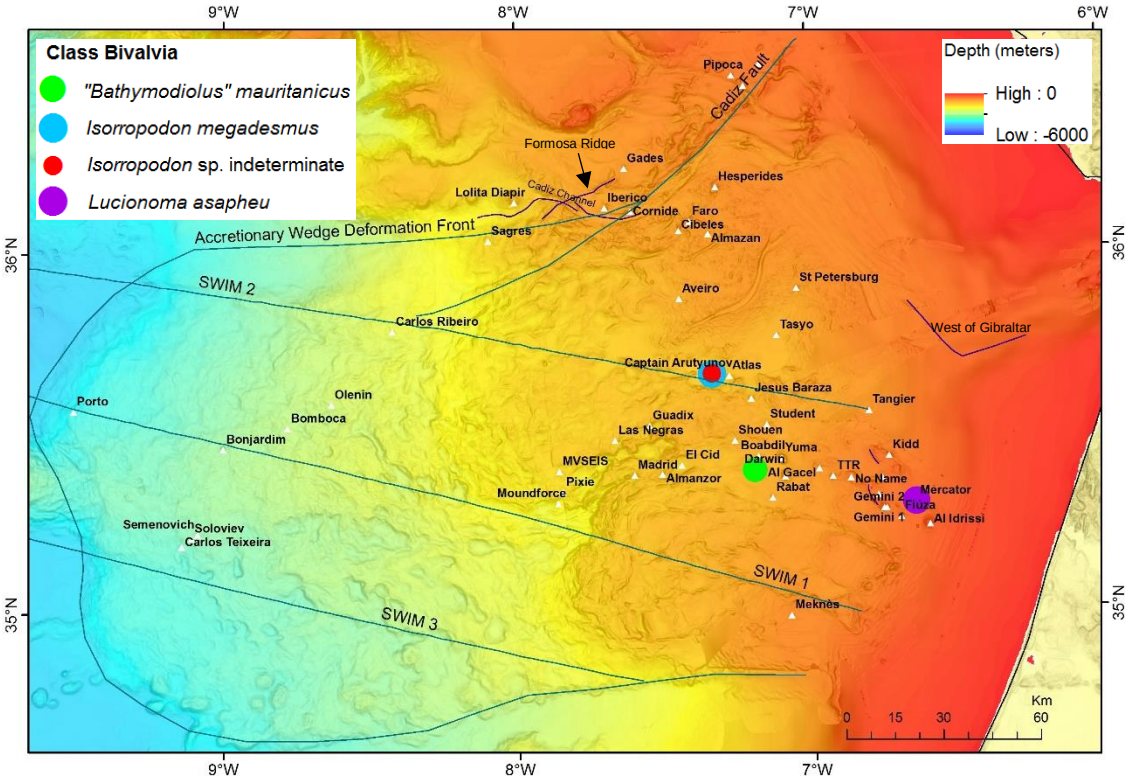

Figure 5.7 – Distribution of bivalves. Green dot - Specie "*Bathymodiolus" mauritanicus;* Blue dot - *Isorropodon megadesmus; Red dot - Isorropodon* sp. indeterminate; Purple dot - *Lucionoma asapheu*.

5.2. Heterotrophic Organisms

5.2.1. Order Tanaidacea

The Order Tanaidacea is represented by 17 species (13 genera in eight families; see **Table 5.2**; examples shown in **Annex II** – **Figure 9** to **16**); four of them are singletons: *Pseudosphyrapus*, *Pseudosphyrapus* sp. A (**Annex II** – **Figure 16**), *Sphyrapus meknes* (**Annex II** – **Figure 16**) and *Torquella ibérica* (**Annex II** – **Figure 11**). **Figure 5.8** shows the distribution of two Suborders, Apseudomorpha and Tanaidomorpha. The Suborder Apseudomorpha (green dots) occurs in a wide range of depths, 355 to 3061 m and it is present in all regions of the study area. On the other hand, the Suborder Tanaidomorpha (dark blue dots) only occurs in a lower range of depths, 355 to 1345 m, except for one specie, *Pseudotanais (Pseudotanais) tympanobaculum* (**Annex II** – **Figure 13**) belonging to the family Pseudotanaidae that also occurs deeper (3061 m).

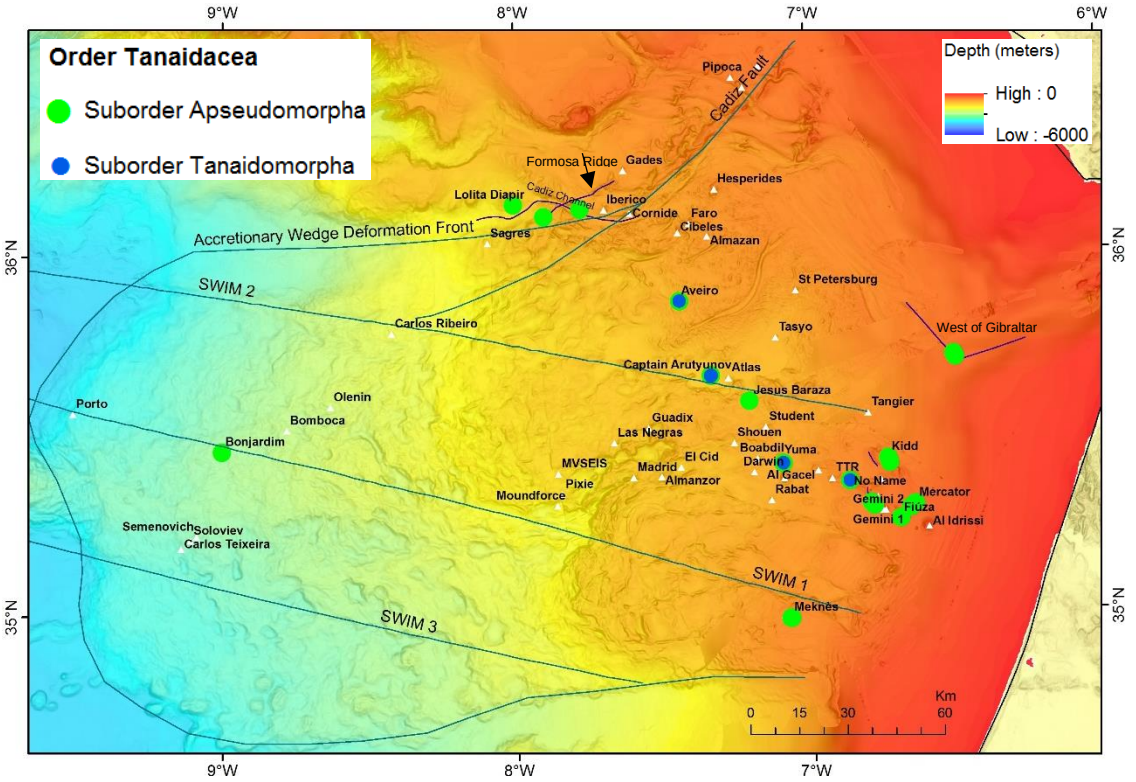

Figure 5.8 - Distribution of tanaids. Green dots – Suborder Apseudomorpha (family Apseudidae and Sphyrapodidae); Blue dots – Suborder Tanaidomorpha (family Colletteidae, Leptocheliidae, Paratanaoidea incertae sedis, Pseudotanaidae and Tanaellidae).

5.2.2. Class Ophiuroidea

The Class Ophiuroidea is represented by 16 species (ten genera in seven families; see **Table 5.2**; examples shown in **Annex II** – **Figure 17** to **21**); five of them are singletones, *Ophiacantha aristata* (**Annex II** – **Figure 17**), *Ophiopristis gadensis* (**Annex II** – **Figure 18**), *Ophiactis abyssicola* (**Annex II** – **Figure 19**), *Ophiomusium lymani*, and *Ophiura (Dictenophiura) carnea*. **Figure 5.9** shows the distribution of the six families, Amphilepididae, Amphiuridae, Ophiacanthidae, Ophiactidae, Ophiolepididae and Ophiuridae. These families are located at depths between 230 and 1390 m. The family Amphiuridae (blue dots) has a broader distribution, when compared with the other families and is present in 15 features (11 mud volcanoes).

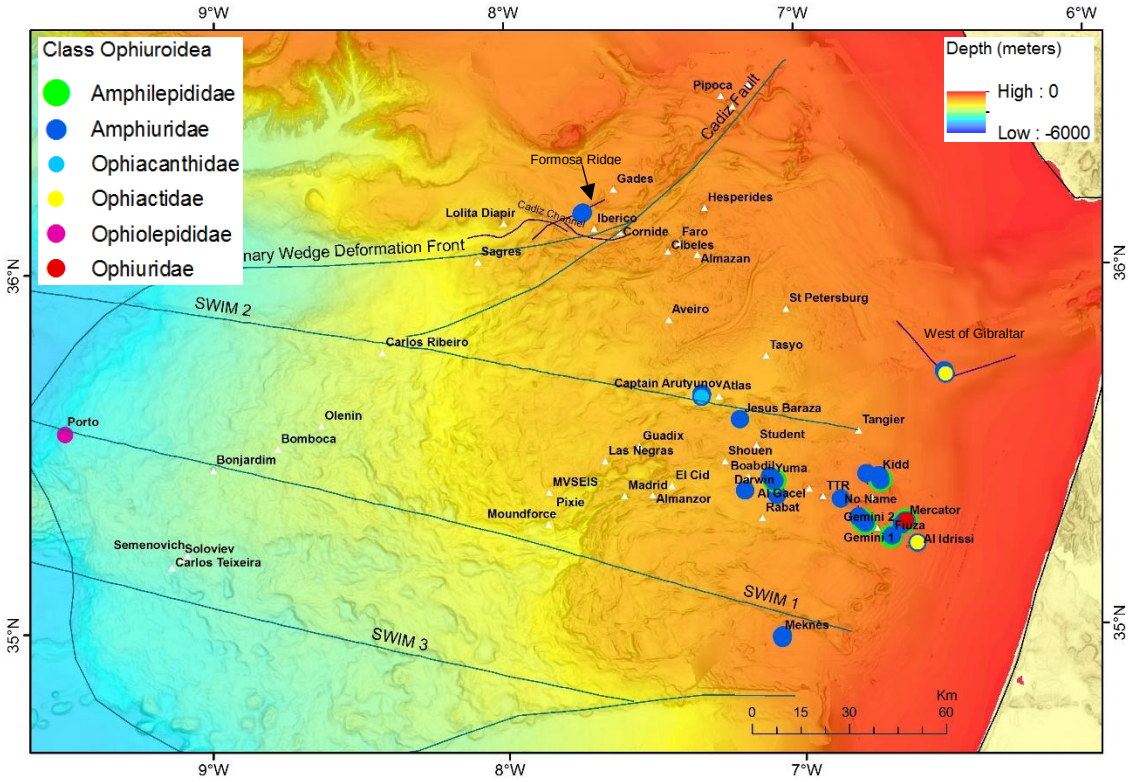

Figure 5.9 – Distribution of ophiuroids. Green dots - Family Amphilepididae; Dark blue dots - Family Amphiuridae; Blue dot - Family Ophiacanthidae; Yellow dots – Family Ophiactidae; Pink dot – Family Ophiolepididae; Red dot - Family Ophiuridae.

5.2.3. Class Gastropoda

The Class Gastropoda is represented by 56 species (49 genera in 31 families; see **Table 5.2**; examples shown in **Annex II - Figure 22**); 28 of them are singletons, *Alvania electa*, *Akritogyra* sp. A, *Benthomangelia macra*, *Cirsonella* aff. *romettensis*, *Cerithiopsidae* sp. A, cf. *Odostomia* sp., cf. *Sahlingia* sp. A, *Claviscala* sp. A, *Conoidea* sp. A, *Drilliola loprestiana*, *Danilia tinei*, *Emarginula multistriata*, *Eulimella* sp. A, *Fusceulima minuta*, *Graphis gracilis*, *Iphitus marshalli*, *Iothia* sp. A, *Lepetella* sp. A, *Lissotesta* sp. A, *Neptunea contraria*, *Pseudosetia* sp. A, *Puncturella* sp. A, *Pyramidellidae* sp. A, *Solariella amabilis*, *Strobiligera brychia*, *Sahlingia* sp. A, *Syrnola* sp. A and *Turbonilla* sp. A. **Figures 5.10** and **5.11** show the distribution of two subclasses, Caenogastropoda and Vetigastropoda, that are represented by several species and **Figure 5.12** shows the distribution of the remaining subclasses: Heterobrachia, Neomphalina and Patellogastropoda. The subclass Caenogastropoda (**Figure 5.10**) has a heterogeneous distribution, it is present in all regions (El Arraiche Field, Carbonate Province and Deep Field) and occurs in a wide range of depths, 350 to 3902 m. Although the subclass Vetigastropoda (**Figure 5.11**) is also present in all regions, it is mostly restricted to lower depths, 227 to 1390 m, occurring punctually also in Porto MV (3887 to 3902 m). The final map shows three subclasses in a lower range of depths, 379 to 1321 m. The subclass Heterobrachia (purple dots) has a wider distribution when compared with the other two subclasses, Neomphalina and Patellogastropoda.

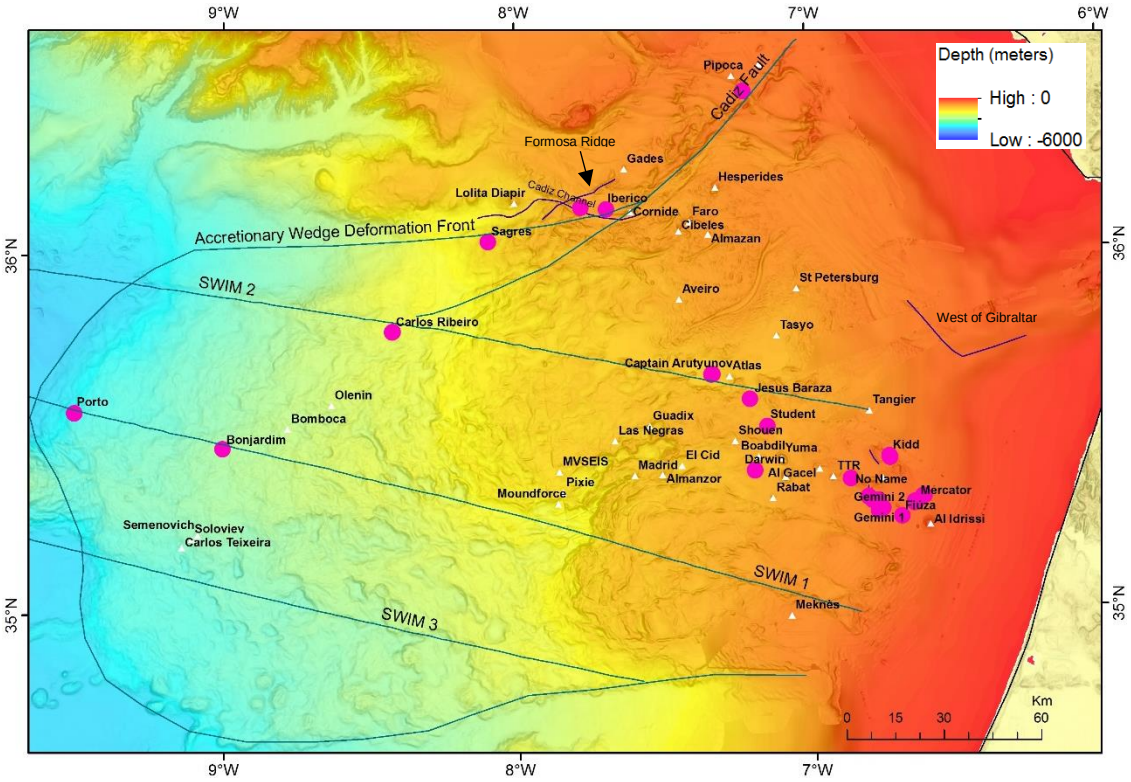

Figure 5.10 – Distribution of gastropods. Pink dots - Subclass Caenogastropoda.

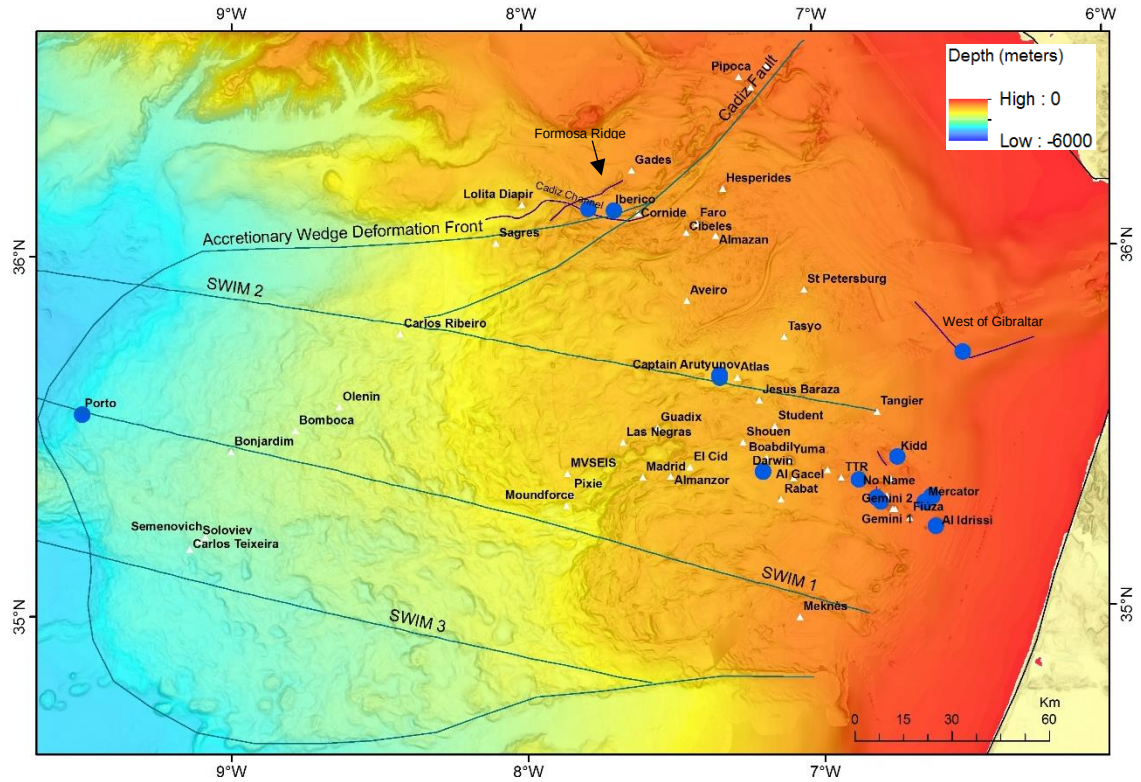

Figure 5.11 – Distribution of gastropods. Blue dots - Subclass Vetigastropoda.

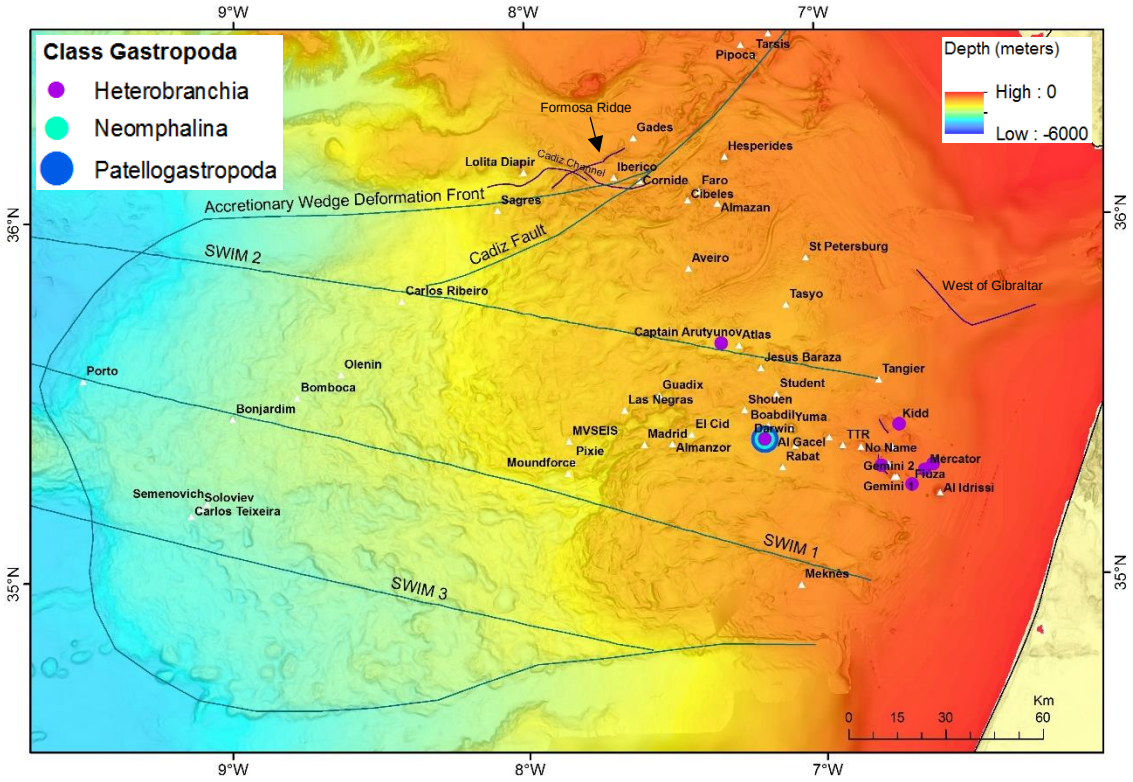

Figure 5.12 – Distribution of gastropods. Purple dots - Subclass Heterobranchia; Blue dot - Subclass Neomphalina; Dark blue dot -.Subclasse Patellogastropoda.

5.2.4. Class Bivalvia

The three heterotrophic species belonging to the Class Bivalvia have different distributions (**Figure 5.13**). The specie *Leptaxinus minutus* (green dots) is reported from three mud volcanoes, two in the Cabonate Province (Darwin and Yuma) and one in the El Arraiche Field (Mercator), while the specie *Mendicula ferruginosa* (dark blue dot) only appears in one mud volcano (Mercator). The specie *Thyasira obsoleta* (red dots) is reported, mostly from sites located at less than 10 km to the SWIM faults in the Deep Field. The exception is the occurrence of *Thyasira obsoleta* in the Mercator MV. This is the specie with the widest range of depths, 353 to 3860 m.

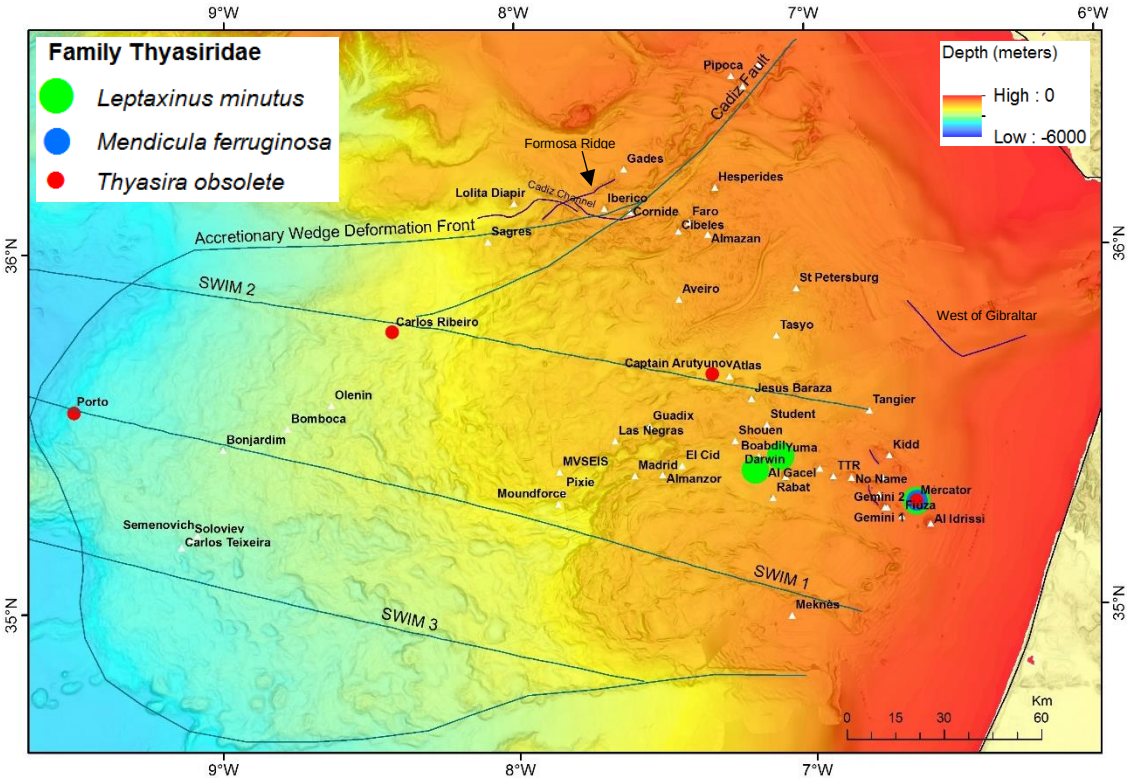

Figure 5.13 – Distribution of bivalves. Green dots - Specie *Leptaxinus minutus*; Blue dot - Specie *Mendicula ferruginosa*; Red dots - Specie *Thyasira obsolete*.

Chapter 6

Discussion

6.1. Strengths and Limitations of the data

The biological samples studied in this work were collected during several campaigns in the Gulf of Cadiz. The areas were sampled in accordance with the scientific objectives of these campaigns and ship operation capabilities, and therefore some features have a higher level of sampling effort (Captain Arutyunov MV - 19 stations, Mercator MV - 12 stations and Pen Duick Escarpment - ten stations) and others are represented by just one station (e.g.: Lazarillo de Tornes, Vernadsky Ridge, Iberico, Student; **Table 5.1**). The Captain Arutyunov MV has a high level of sampling effort, since it is one of the most active mud volcanoes in the Gulf of Cadiz (Niemann *et al.* 2006; Dworschak and Cunha, 2007; Sommer *et al.* 2009; Cunha *et al*., 2013). On the other hand, the Pen Duick Escarpment area was extensively sampled during the study of corals in the framework of Microsystems and Moundforce projects led by Belgian and Dutch teams (e.g.: Foubert *et al*. 2008; Van Rooij *et al*. 2011; Wehrmann *et al*. 2011). The Mercator MV is one of the largest mud volcanoes in the Gulf of Cadiz, located at shallow depths, which facilitates accessibility and time spent to collect samples. The marked differences between the sampling (1 to 19 stations) makes it difficult to proper compare the different sites. The number of species increases with the number of stations (see **Figure 5.1** and **Table 5.1**). Only in the ideal situation corresponding to a much similar sampling between the different sites, and to a similar identified number of specimens of all species, would it be possible to do a thorough detailed analysis of the species distribution.

In the collection of biological samples different gears were used (**Chapter 4**), which allows collecting diversified information, since the different equipment will harvest different types of organisms. Again, only in a situation in which the same type of equipment was to be used across the whole Gulf of Cadiz, would it be possible and easier to statistically analyse the distribution of species collected, and to do a more accurate study. However, on the other hand, this would probably signify a considerable lost of information regarding the detected marked diversity of species.

The species analysed in this work (122 species) are represented by chemotrophic organisms, 18 belong to the Class Polychaeta (see **Figure 5.2**, **5.3** and **5.4**) and 11 to the Class Bivalvia (see **Figure 5.5**, **5.6** and **5.7**), and heterotrophic organisms, 17 species belong to the Order Tanaidacea (see **Figure 5.8**), 16 to the Class Ophiuroidea (see **Figure 5.9**), 56 to the Class Gastropoda (see **Figure 5.10**, **5.11** and **5.12**) and three to the Class Bivalvia (**Figure 5.13**). Despite the high level of sampling effort and the still in progress analysis of all collected organisms in campaigns, the discovery of 52 singletons species (43% of the total studied species, mostly in the Class Gastropoda) indicates the necessity of a higher level of sampling effort in the future.

6.2. Spatial and Bathymetric Distribution

The mud volcanoes described in this work were organized in three main areas (see **Figure 3.1**): the El Arraiche Mud Volcano Field (200 - 600 m), the Carbonate Province (600 - 1200 m) and Deep

Mud Volcano Field (1200 - 4000 m). Within the Carbonate Province several morphological features, here designated by "Other Features" and that are not mud volcanoes, were analysed.

The El Arraiche Field encompasses a high number of heterotrophic species and a lower number of chemotrophic species when compared with the other studied areas in the Gulf of Cadiz (see **Figure 5.1**). On the other hand, the Deep Field has a lower number of heterotrophic species and a high number of chemotrophic species that rely on the more active fluid emission in this region. It has been found that the number of the chemotrophic species increases with depth and the number of the heterotrophic species decreases with depth. The exception is the Mercator MV located in the El Arraiche Field, since it has a high number of both heterotrophic and chemotrophic organisms. This can express some degree of bias due to the high level of sampling effort in this mud volcano as mentioned above. In fact, the level of sampling effort was very important for the assessment of biodiversity: the features that were well sampled also show a good representation of heterotrophic species but this are not well represented in features that were insufficiently sampled.

Observing the "Other Features" species distribution (see **Figure 5.1**) the chemotrophic species were only found in the Pen Duick Escarpment. In this case however, this is not due to different sampling efforts. As a matter of fact the Pen Duic Escarpment is a tectonic feature accommodating fluid and gas escape and accumulation in sediments (see decription in **subchapter. 3.2.2.3**), whereas the remaining "Other features" correspond to sedimentary and erosive features, or diapirs, where no methane migration and seepage is expected to occur.

The Deep Field includes several of the most active mud volcanoes in the Gulf of Cadiz (Pinheiro *et al*. 2003; Rodrigues *et al*. 2011; Cunha *et al.* 2013) and several of them (Captain Arutyunov, Carlos Ribeiro, Bonjardim e Porto) are aligned along major crustal strike–slip faults (SWIM faults) associated with the African-Eurasian plate boundary (Duarte *et al*. 2011). As said before this is a place with a high number of chemotrophic species and this majority was found in Captain Arutyunov MV, Carlos Ribeiro MV, Bonjardim MV and Porto MV (see **Figure 5.1**).

In general, the higher concentrations of species in the Gulf of Cadiz occurs at low depths, 200 to 1200 m (see **Figure 5.1**, **6.1** and **6.2**) and these are mostly located in the mud volcanoes (see **Figure 5.1**). Comparing the deepest mud volcanoes: Porto (3900 m), Seemenovich (3200 m), Bonjardim (3060 m) and Carlos Ribeiro (2173 m) with the shallowest mud volcanoes: Al Idrissi (197 m), Fiúza (393 m), Mercator (351 m) and Gemini (423 m), we see that the number of species found in the four deepest and four shallowest mud volcanoes is similarly low (except in Mercator MV), suggesting there is not a significant influence of the water depth on the number of species (see **Figure 5.1).** Nevertheless, this can also be due to the different sampling effort in the mud volcanoes, since some mud volcanoes have a higher sampling effort than others (1 to 12 stations; see **Table 5.1**). The highest number of heterotrophic and chemotrophic species was found in two mud volcanoes, Mercator and Captain Arutyunov. Again this can be due to the higher level of sampling effort in these mud volcanoes (12 and 19 stations, respectively) relatively to the sampling of the remaining mud volcanoes. The highest number of chemotrophic species can be also due the location of the Mercator MV, on an anticline formed by the halokinesis of a salt diapir. According to Haffert *et al.* 2013, a direct relation between halokinesis and seepage of fluids and gases exists, which has also been frequently documented in other regions (e.g.: Gulf of Mexico). The rising diapir fractures the overburden, thereby creating preferential pathways for the fluid and gas to escape. The pathways reach very deep and lead along the flanks of the diaper, which allows fluids and gases to rise to the surface (Haffert *et al.* 2013). In turn, the highest number of chemotrophic species in the Captain Arutyunov MV can be due to the high concentration of methane

near de surface (Hensen *et al.* 2007), which in Gulf of Cadiz normally occurs between 30 and 80 cm (or more) below the seafloor (Niemann *et al.* 2006; Hensen *et al.* 2007).

6.3. Metabolic Strategy

The heterotrophic species were found in most of the studied features of the Gulf of Cadiz (except in Semenovich MV; see **Figure 5.1**), as expected since they occur globally. In this work, the heterotrophic species are represented mainly by the Class Gastropoda (see **Figure 5.1**), although the Polychaetes and the Crustaceans are in general the best represented taxonomic groups, in accordance to Cunha *et al.* 2013. The number of these species decreases with depth (see **Figure 6.1**) probably because the available food also becomes scarcer. In relation to the chemotrophic species, the dominant nutritional pathway is the thiotrophy (see **Figure 5.1**), with mixotrophy, methanotrophy emerging as secondary strategies (Rodrigues *et al.* 2013). The thiotrophic species are in symbiosis with thiotrophic bacteria whose metabolism depends on the oxidation of sulfide or sulfur with oxygen or nitrate (**subchapter 1.7**). It occurs due to the high availability of sulfur in the form of sulfide or sulfur in the methane seepage areas of the Gulf of Cadiz. Therefore these species only occur in mud volcanoes (except Pen Duick Escarpment; see **Figure 5.1**). The methanotrophic species are only located in two mud volcanoes, Mercator (351 m) and Captain Arutyunov (1324 m), which indicates that the biogeochemical system in the Gulf of Cadiz is probably dominated by sulfur (see **Figure 5.1**).

The Gulf of Cadiz has a higher number of chemotrophic species when compared with other seep locations in the Eastern Mediterranean Sea and the Gulf of Guinea (e.g.: Warén and Bouchet, 2009; Oliver *et al.* 2008, 2011), which suggests the Gulf of Cadiz has a favourable nutritional condition for chemotrophic species.

6.4. Proximity to the SWIM Faults

The highest concentration of chemotrophic species occurs in mud volcanoes located on the SWIM 1 and SWIM 2 faults at water depths ≥ 1200 m (see **Figure 5.1**). This is suggestive of these faults acting as preferential fluid conduits, feeding those species. In general, the methane seeps are especially common and active at water depths of 500–1000 m, where temperature and pressure combine to destabilize gas hydrates (Hester and Brewer, 2009), but in the Gulf of Cadiz this depth may be greater due to the influence of the warmer Mediterranean Outflow Water (Niemann *et al.* 2006; Sommer *et al.* 2009).

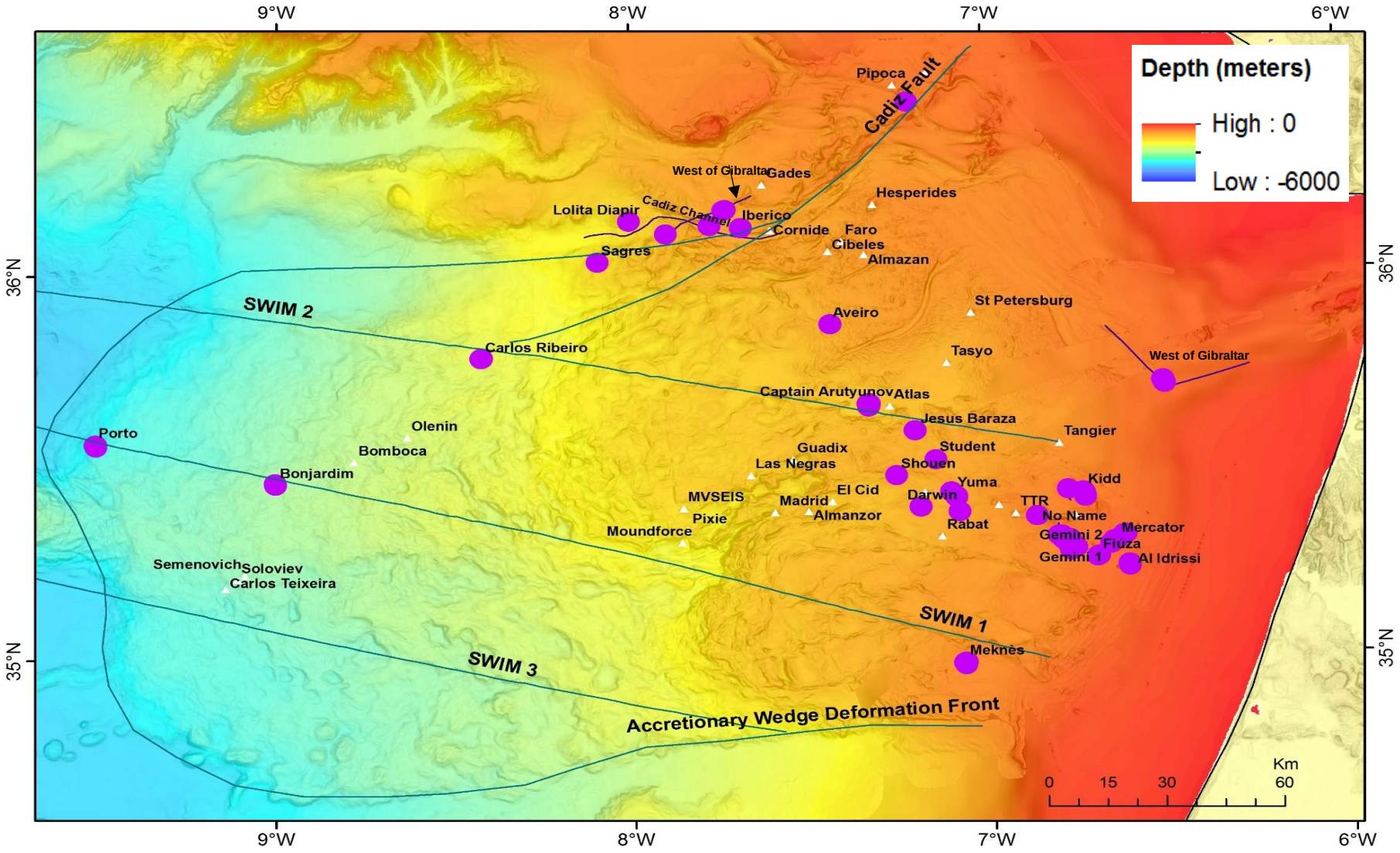

Figure 6.1 – Heterotrophic species distribution in the Gulf of Cadiz (Purple dots).

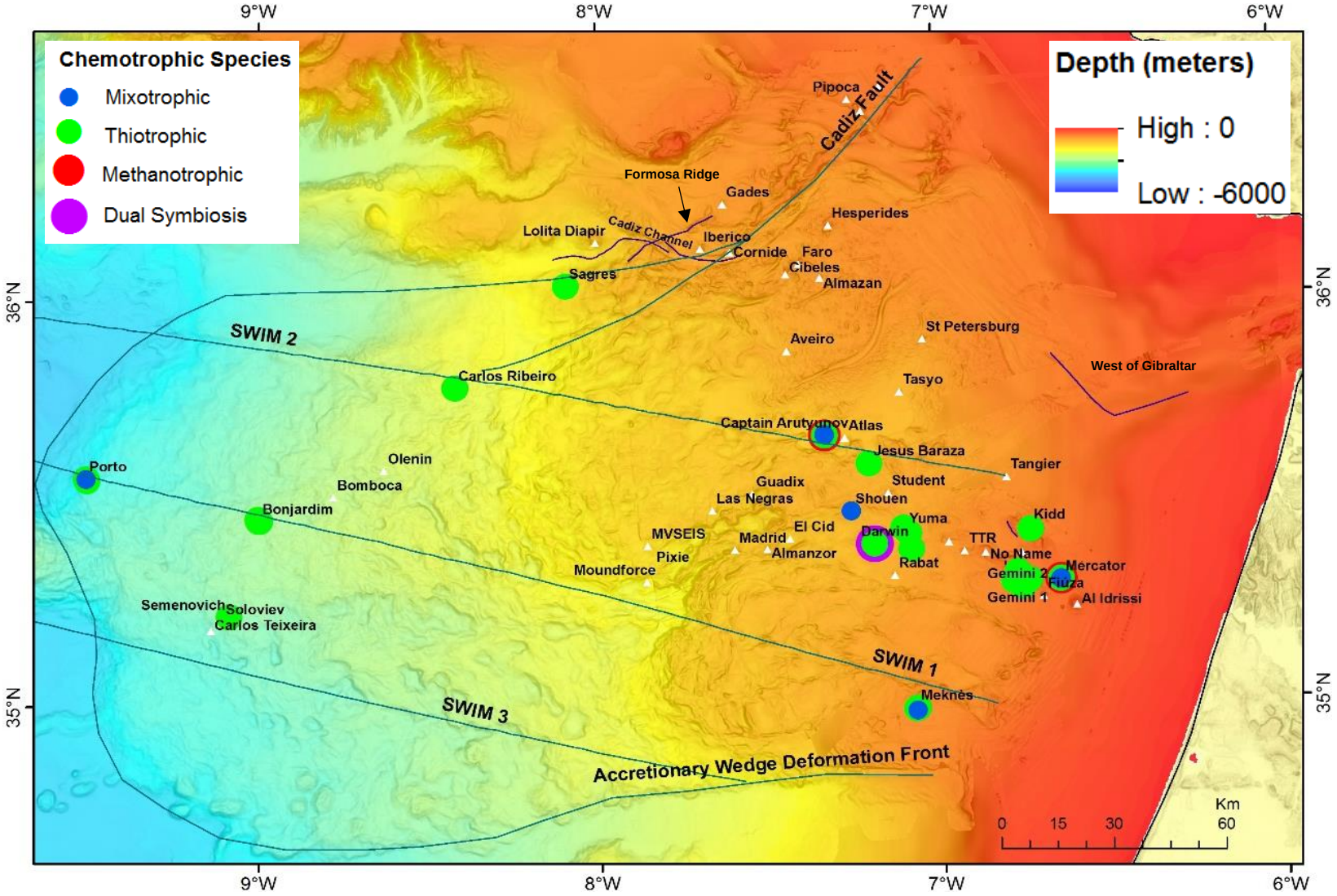

Figure 6.2 – Chemotrophic species distribution in the Gulf of Cadiz. Blue dots – Mixotrophic species; Green dots - Thiotrophic species; Red dots – Methanotrophic Species; Purple dot – Dual Symbiosis.

Chapter 7

Conclusions

The main conclusions of this work can be summarized as follows:

1- In general, the higher concentrations of species in the Gulf of Cadiz occur at low depths, from 200 to 1200 m and are mostly located in the mud volcanoes;

2- The heterotrophic species were found in most of the studied features of the Gulf of Cadiz, except in Semenovich MV, as expected, since they occur globally. The number of these species decreases with depth probably because the available food also becomes scarcer;

3- The thiotrophy is the dominant nutritional pathway of the chemotrophic species. It occurs due to the high availability of sulfur in the form of sulfide or sulfur in the methane seepage areas of the Gulf of Cadiz. Therefore these species only occur in mud volcanoes, except in Pen Duick Escarpment;

4- The methanotrophic species are only located in two mud volcanoes, Mercator (351 m) and Captain Arutyunov (1324 m), which indicates that the biogeochemical system in the Gulf of Cadiz is probably dominated by sulfur;

5- The highest concentration of chemotrophic species occur in mud volcanoes located on the SWIM 1 and SWIM 2 faults at water depths ≥ 1200 m. Thus suggesting that these faults act as preferential fluid conduits, feeding those species. In general, the methane seeps are especially common and active at water depths of 500–1000 m, where temperature and pressure combine to destabilize gas hydrates (Hester and Brewer, 2009), but in the Gulf of Cadiz this depth may be greater due to the influence of the warmer Mediterranean Outflow Water (Niemann *et al.* 2006; Sommer *et al.* 2009);

6- The main limitation of this work is the difference of sampling effort existing between features (one to 19 stations).

7.1. Future Work

- Complete the data with the same number of stations for all features;

- Identify the number of specimens in the collected samples for a more detailed statistics analysis;

- Acquire direct observation of the seafloor for the biologic communities on video;

- Use the same gear and sampling technique in all features;

- Collect gas samples at the stations studied in this work.

Bibliographic References

Alves J.M.R., Carton X. and Ambar I. (2011), Hydrological Structure, Circulation and Water Mass Transport in the Gulf of Cadiz, *International Journal of Geosciences* 2, 432-456;

Akhmetzhanov A.M., Ivanov M.K., Kenyon N.H. and Mazzini A. (2007), Deep-water cold seeps, sedimentary environments and ecosystems of the Black and Tyrrhenian Seas and the Gulf of Cadiz, *UNESCO*, Intergovernmental Oceanographic Commission technical series 72, 1-99;

Akhmetzhanov A.M., Kenyon N.H., Ivanov M.K., Westbrook G. and Mazzini A. (2008) Deep-water depositional systems and cold seeps of the Western Mediterranean, Gulf of Cadiz and Norwegian continental margins, *UNESCO*, Intergovernmental Oceanographic Commission technical series 76, 2-59;

Blazewicz-Paszkowycz M., Bamber R.N. and Cunha M.R. (2011a), New tanaidomorph Tanaidacea (Crustacea: Peracarida) from submarine mud-volcanoes in the Gulf of Cadiz (North-east Atlantic), *Zootaxa* 2769, 1-53;

Blazewicz-Paszkowycz M., Bamber R.N. and Cunha M.R. (2011b), Apseudomorph tanaidaceans (Crustacea: Peracarida) from mud-volcanoes in the Gulf of Cadiz (North-east Atlantic) *Zootaxa* 2919, 1-36;

Bode A., Varela M., Casas B. and González N. (2002), Intrusions of eastern North Atlantic central waters and phytoplankton in the north and northwestern Iberian shelf during Spring, *Journal of Marine Systems* 36, 197-218;

Bozec A., Lozier M.S., Chassignet E.P. and Halliwell G.R. (2011), On the variability of the Mediterranean Outflow Water in the North Atlantic from 1948 to 2006, *Journal of Geophysical Research* 116, 1-18;

Cao M., Qin K., Li G., Evans N.J. and Jin L. (2014), Abiogenic Fischer–Tropsch synthesis of methane at the Baogutu reduced porphyry copper deposit, western Junggar, NW-China, *Geochimica et Cosmochimica Acta* 141, 179-198;

Campbell K. A., Farmer J. D. and Des Marais D. (2002), Ancient hydrocarbon seeps from Mesozoic convergent margin of California: carbonate geochemistry, fluids and paleoenvironments, *Geofluids* 2, 63-96;

Cianca A., Santana R., Marrero J.P., Rueda M.J. and Llinás O. (2009), Modal composition of the central water in the North Atlantic subtropical gyre, *Ocean Science Discussions* 6, 2487-2506;

Cordes E.E., Cunha M.R., Galéron J., Mora C., Roy K.O., Sibuet M., Van Gaever S., Vanreusel A. and Levin L.A. (2010), The influence of geological, geochemical, and biogenic habitat heterogeneity on seep biodiversity, *Marine Ecology* 31, 51-65;

Cunha M. R., Rodrigues C. F., Genio L., Hilario A., Ravara A. and Pfannkuche O. (2013), Macrofaunal assemblages from mud volcanoes in the Gulf of Cadiz: abundance, biodiversity and diversity partitioning across spatial scales, *Biogeosciences* 10, 2553-2568;

Duarte J. C., Valadares V., Terrinha P., Rosas F., Zitellini N. and Gràcia E. (2009), *Anatomy and tectonic significance of WNW-ESE and NE-SW lineaments at a transpressive plate boundary (Nubia-Iberia)*, Trabajos de Geología, Universidad de Oviedo 29, 237-241;

Duarte J.D.C. (2011), *Tectonics of the Gulf of Cadiz: The Role of the Gibraltar Arc in the Reactivation of the SW Iberia Margin*, Universidade de Lisboa, Faculdade de Ciências, Departamento de Geologia, Tese de Doutoramento, 2-6;

Duarte J.C., Rosas F.M., Terrinha P., Gutscher M-A., Malavieille J., Silva S. and Matias L. (2011), Thrust-wrench interference tectonics in the Gulf of Cadiz (Africa-Iberia plate boundary in the North-East Atlantic): Insights from analog models, *Marine Geology* 289, 153-149;

Dworschak P.C. and Cunha M.R. (2007), A new subfamily, Vulcanocalliacinae n.subfam., for *Vulcanocalliax arutyunovi* n.gen., n.sp. from a mud volcano in the Gulf of Cádiz (Crustacea, Decapoda, Callianassidae), *Zootaxa* 1460, 35-46;

Etiope G. and Lollar B.S. (2013), Abiotic Methane on Earth, *Reviews of Geophysics* 51, 276-299;

Fischer D., Sahling H., Nothen K., Bohrmann G., Zabel M., and Kasten S. (2012), Interaction between hydrocarbon seepage, chemosynthetic communities, and bottom water redox at cold seeps of the Makran accretionary prism: insights from habitat-specific pore water sampling and modeling, *Biogeosciences* 9, 2013-2031;

Foubert A., Depreiter D., Beck T., Maignien L., Pannemans B., Frank N., Blamart D. and Henriet J-P. (2008), Carbonate mounds in a mud volcano province off north-west Morocco: Key to processes and controls, *Marine Geology* 248, 74-96;

García M., Hernández-Molina F.J., Llave E., Stow D.A.V., León R., Fernández-Puga M.C., Diaz del Río V. and Somoza L. (2009), Contourite erosive features caused by the Mediterranean Outflow Water in the Gulf of Cadiz: Quaternary tectonic and oceanographic implications, *Marine Geology* 257, 24-40;

Gardner J. M. (2001), Mud volcanoes revealed and sampled on the Western Moroccan continental margin, *Geophysical Research Letters* 28(2), 339-342;

Gartman A., Findlay J.A. and Luther III G.W. (2014), Nanoparticulate pyrite and other nanoparticles are a widespread component of hydrothermal vent black smoker emissions, *Chemical Geology* 366, 32-41;

Génio L., Johnson S.B., Vrijenhoek R.C., Cunha M.R., Tyler P.A., Kiel S. and Little C.T.S. (2008), New Record of ‘‘*Bathymodiolus*’’ *Mauritanicus* Cosel 2002 from the Gulf of Cadiz (Ne Atlantic) Mud Volcanoes, *Journal of Shellfish Research* 27 (1), 53-61;

Génio L., Warén A., Matos F. L. and Cunha M. R. (2013), The snails’ tale in deep-sea habitats in the Gulf of Cadiz (NE Atlantic), *Biogeosciences* 10, 5159-5170;

Grauls D. (2001), Gas hydrates: importance and applications in petroleum exploration, *Marine and Petroleum Geology* 18, 519-523;

Grünke S., Lichtschlag A., Beer D., Felden J., Salman V., Ramette A., Schulz-Vogt H. N. and Boetius A. (2012), Mats of psychrophilic thiotrophic bacteria associated with cold seeps of the Barents Sea, *Marine Geology* 155, 9-43;

Haffert L., Haeckel M., Liebetrau V., Berndt C., Hensen C., Nuzzo M., Reitz A., Scholz F., Schönfeld J., Perez-Garcia C. and Weise S.M. (2013), Fluid evolution and authigenic mineral paragenesis related to salt diapirism – The Mercator mud volcano in the Gulf of Cadiz, *Geochimica et Cosmochimica Acta* 106, 261-286;

Hanson R.S. and Hanson T.E. (1996), Methanotrophic Bacteria, *Microbiological Reviews*, 439-471;

Hensen C., Nuzzo M., Hornibrook E., Pinheiro L.M., Bock B., Magalhães V. H. and Brückmann W. (2007), Sources of mud volcano fluids in the Gulf of Cadiz—indications for hydrothermal imprint, *Geochimica et Cosmochimica Acta* 71, 1232-1248;

Hester, K. C and Brewer, P. G. (2009), Clathrate hydrates in nature, *Annual Review of Marine Science* 1, 303-327;

Hernández-Molina F.J., Llave E., Stow D.A.V., García M., Somoza L., Vázquez J.T., Lobo F.J., Maestro A., Díaz del Río V., León R., Medialdea T and, Gardner J. (2006), The contourite depositional system of the Gulf of Cádiz: A sedimentary model related to the bottom current activity of the Mediterranean outflow water and its interaction with the continental margin, *Elsevier*, Deep Sea Research 2 (53), 1420-1463;

Hernández-Molina F.J., Serra N., Stow D. A. V., Llave E., Ercilla G. and Van Rooij D. (2011), Along-slope oceanographic processes and sedimentary products around the Iberian margin, *Geo-Mar Lett* 31, 315-341;

Hernández-Molina F.J., Llave E., Fontan A.,. Brackenridge R.E, Stow D.A.V., Ercilla G., Medialdea T., García M., Sandoval N., Preu B., Arlucea M. P.,. Nombela M.A, Alejo I., Francés G., Mena A., Casas D., Somoza L., León R., Vázquez J. T., Juan C., Van Rooij D., Matias H., Bruno M., Serra N. and CONTOURIBER Team (2012), *First evidence of a main channel generated by the Mediterranean Outflow Water after its exit from the Gibraltar Strait*, 1813-1816;

Hernández-Molina F.J., Llave E., Preu B., Ercilla G., Fontan A., Bruno M., Serra N., Gomiz J.J., Brackenridge R.E., Sierro F.J., Stow D.A.V., García M., Juan C., Sandoval N. and Arnaiz A. (2014), *Contourite processes associated with the Mediterranean Outflow Water after its exit from the Gibraltar Strait: Global and conceptual implications*, 2nd Deep-Water Circulation Congress, Ghent, Belgium, 99-100;

Hilário A. and Cunha M.R. (2008), On some frenulate species (Annelida: Polychaeta: Siboglinidae) from mud volcanoes in the Gulf of Cadiz (NE Atlantic), *Scientia Marina* 72 (2), 361-371;

IFM-Geomar (2006), Maria S. Merian 1/3, Cruise Report, Wischhofstr, Germany: Leibniz-Institut für Meereswissenschaften, 12. April – 19. May, 10-12;

Ivanov M.K., Kenyon N.H., Laberg J-S. and Blinova V.N. (2010), Cold seeps, coral mounds and deepwater depositional systems of the Alboran Sea, Gulf of Cadiz and Norwegian continental margin, *UNESCO*, Intergovernmental Oceanographic Commission technical series 94, 1-144;

Johnston, A. C. (1996), Seismic moment assessment of earthquakes in stable continental regions – III, New Madrid 1811–1812, Charleston 1886, and Lisbon 1755, *Geophysical Journal Internacional*, *126*, 314–344;

Judd A.G. (2001), *Pockmarks in the UK sector of the North Sea*, Strategic Environmental Assessment – SEA 2, 10-11;

Judd, A. G. (2003), The global importance and context of methane escape from the seabed. *Geo-Marine Letters* 23, 147-154;

Kelley, D. S. (2001), *Black Smokers: Incubators on the Seafloor*, Department of Oceanography, University of Washington, 184-189;

Kenyon N.H., Ivanov M.K., Akhmetzhanov A.M. and Akhmanov G.G. (2000), Multidisciplinary Study of Geological Processes on the North East Atlantic and Western Mediterranean Margins, *UNESCO*, Intergovernmental Oceanographic Commission technical series 56, 5-102;

Kenyon N.H., lvanov M.K., Akhmetzhanov A.M. and Akhmano G.G. (2001), Interdisciplinary Approaches to Geoscience on the North East Atlantic Margin and Mid-Atlantic Ridge, *UNESCO*, Intergovernmental Oceanographic Commission technical series 60, 5-104;

Kenyon N.H., Ivanov M.K., Akhmetzhanov A.M. and Akhmanov G.G. (2002), Geological Processes in the Mediterranean and Black Seas and North East Atlantic, *UNESCO*, Intergovernmental Oceanographic Commission technical series 62, 5-89;

Kenyon N.H., Ivanov M.K., Akhmetzhanov A.M. and Akhmanov G.G. (2003), Interdisciplinary Geoscience Research on the North East Atlantic Margin, Mediterranean Sea and Mid-Atlantic Rigde, *UNESCO*, Intergovernmental Oceanographic Commission technical series 67, 5-110;

Kenyon N.H., Ivanov M.K., Akhmetzhanov A.M. and Kozlova E.V. (2006), Interdisciplinary geoscience studies of the Gulf of Cadiz and Western Mediterranean basins, Mediterranean Sea and Mid-Atlantic Rigde, *UNESCO*, Intergovernmental Oceanographic Commission technical series 70, 1-115;

Khélifi N., Sarnthein M., Frank M., Andersen N. and Garbe-Schönberg D. (2014), Late Pliocene variations of the Mediterranean outflow, *Marine Geology*, 1-41;

Lascelles D.F. (2007), Black smokers and density currents: A uniformitarian model for the genesis of banded iron-formations, *Elsevier*, Orc Geology Reviews 32, 381-411;

León R., Somoza L., Medialdea T., Maestro A., Díaz-del-Río V. and Fernández-Puga M.C. (2006), Classification of sea-floor features associated with methane seeps along the Gulf of Cádiz continental margin, *Deep-Sea Research* 2 (53); 1464-1481;

León R., Somoza L., Giménez-Moreno C.J., Dabrio C.J., Ercilla G., Praeg D., Díaz-del-Río v. and Gómez-Delgado M. (2009), A predictive numerical model for potential mapping of the gas hydrate stability zone in the Gulf of Cadiz, *Marine and Petroleum Geology* 26, 1564-1579;

Levin L.A. (2005), Ecology of Cold Seep Sediments: Interactions of Fauna with Flow, Chemistry and Microbes, *Oceanography and Marine Biology: An Annual Review* 43, 1-4;

Libes S.M. (1992), An Introdution to Marine Biogeochemistry, *Journal of Chemical Education*, 69 (9), A251;

Lollar B.S., Westgate T. D., Ward J. A., Slater G. F. and Lacrampe-Couloume G. (2002), Abiogenic formation of alkanes in the Earth's crust as a minor source for global hydrocarbon reservoirs, *Nature* 416;

Magalhães V.H.S. (2007), *Authigenic carbonates and fluid escape structures in the Gulf of Cadiz*, Universidade de Aveiro, Departamento de Geociências, Tese de Doutoramento, 19-21;

Magalhães V.H., Pinheiro L.M., Ivanov M.K., Kozlova E., Blinova V., J. Kolganova, Vasconcelos C., McKenzie J.A., Bernasconi S.M., Kopf A.J., Díaz-del-Río V., González F. J. and Somoza L. (2012), Formation processes of methane-derived authigenic carbonates from the Gulf of Cadiz, *Sedimentary Geology* 243-244, 155-168;

Maldonado A., Somoza L. and Pallarés L. (1999) The Betic orogen and the Iberian–African boundary in the Gulf of Cadiz: geological evolution (central North Atlantic), *Marine Geology* 155, 9-43;

Mauritzen C., Morel Y. and Paillet J. (2001), On the influence of Mediterranean Water on the Central Waters of the North Atlantic Ocean, *Deep-Sea Research* 1 (48), 347-381;

Medialdea T., Somoza L., Pinheiro L.M., Fernández-Puga M.C., Vázquez J.T., León R., Ivanov M.K., Magalhaes V., Díaz-del-Río V. and Vegas R. (2009), Tectonics and mud volcano development in the Gulf of Cádiz, *Marine Geology* 261, 48-63;

Mhammedi N.A., El Moumni1 B., El Hmaidi A., Raissouni1 A. and El Arrim A. (2008), Mineralogical and geochemical study of mud volcanoes in north Moroccan atlantic margin, *African Journal of Environmental Science and Technology* 2 (11), 387-396;

Mhammedi N.A., Villa R.M., Falagán C., Mata M.P., Somoza L., López-González N., Casas D. and Sánchez-Bellón A. (2010), Mineralogy of Methane- Related Sediments of the Atlantic Moroccan Shelf, *Revista de la Sociedad Española de Mineralogía* 10, 1-2;

Mol L., Hilário A., Van Rooij D. and Henriet J-P. (2012), Habitat Mapping of a Cold-Water Coral Mound on Pen Duick Escarpment (Gulf of Cadiz), *Elsevier* 46, 646-654;

Moore, C.H. and Wade, W.J. (2013), Carbonate Reservoirs Porosity and Diagenesis in a Sequence Stratigraphic Framework. In: Loon, A. J. v. (Ed.), Developments in sedimentology, Second Edition, *Elsevier*, 374;

Mulder T., Gonthier E., Lecroart P., Hanquiez V., Marches E. and Voisset M. (2009) Sediment failures and flows in the Gulf of Cadiz (eastern Atlantic), *Marine and Petroleum Geology* 26, 660-672;

Murton B.J. and Biggs J. (2003), Numerical modelling of mud volcanoes and their flows using constraints from the Gulf of Cadiz, *Marine Geology* 195, 223-236;

Naudts L., Greinert J., Artemov Y., Beaubien S.E., Borowski C. and De Batist M. (2008), Anomalous sea-floor backscatter patterns in methane venting areas, Dnepr paleo-delta, NW Black Sea, *Marine Geology* 251, 253-267;

Navarro G., Ruiz J., Huertas I.E., García C.M., Criado-Aldeanueva F. and Echevarría F. (2006), Basin-scale structures governing the position of the deep fluorescence maximum in the Gulf of Cádiz, *Deep-Sea Research* 2 (53), 1261 - 1281;

Niemann H., Duarte J., Hensen C., Omoregie E., Magalhães V.H., Elvert M., Pinheiro L.M., Kopf A. and Boetius A. (2006), Microbial methane turnover at mud volcanoes of the Gulf of Cadiz, Elsevier, *Geochimica et Cosmochimica Acta* 70, 5336-5355;

Nuzzo M., Hornibrook E.R.C., Gill F., Hensen C., Pancost R.D., Haeckel M., Reitz A., Scholz F., Magalhães V.H., Brückmann W. and Pinheiro L.M. (2009), Origin of light volatile hydrocarbon gases in mud volcano fluids, Gulf of Cadiz — Evidence for multiple sources and transport mechanisms in active sedimentary wedges, *Chemical Geology* 266, 350-363;

Oliver G., Rodrigues C.F. and Cunha M.R. (2011), Chemosymbiotic bivalves from the mud volcanoes of the Gulf of Cadiz, NE Atlantic, with descriptions of new species of Solemyidae, Lucinidae and Vesicomyidae, *ZooKeys* 113, 1-38;

Omoregiea E.O., Niemanna H., Mastalerz V., Lange G.J., Stadnitskaia A., Mascle J., Foucher J-P. and Boetius A. (2009), Microbial methane oxidation and sulfate reduction at cold seeps of the deep Eastern Mediterranean Sea, *Marine Geology* 261, 114-127;

Orange D.L., Yun J., Maher N., Barry J. and Greene G. (2002), Tracking California seafloor seeps with bathymetry, backscatter and ROVs, *Continental Shelf Research* 22, 2273–2290;

Ovsyannikov D.O., Sadekov A.Yu. and Kozlova E.V. (2003), Rock fragments from mud volcanic deposits of the Gulf of Cadiz : an insight into the Eocene-Pliocene sedimentary succession of the basin, *Marine Geology* 195, 211-221;

Padin X.A., Castro C.G., Ríos A.F., and Pérez F.F. (2011), Oceanic CO2 uptake and biogeochemical variability during the formation of the Eastern North Atlantic Central water under two contrasting NAO scenarios, *Journal of Marine Systems* 84, 96-105;

Petersen J.M. and Dubilier N. (2009), Methanotrophic symbioses in marine invertebrates, *Environmental Microbiology Reports* 1(5), 319–335;

Pinheiro L.M., Ivanov M.K., Sautkin A., Akhmanov G., Magalhães V.H., Volkonskaya A., Monteiro J.H., Somoza L., Gardner J., Hamouni N. and Cunha M.R. (2003), Mud volcanism in the Gulf of Cadiz: results from the TTR-10 cruise, *Marine Geology* 195, 131-151;

Pollard R.T., Griffrrhs M.J., Cunningham S.A., Read J.F., Péres F.F. and Ríos A.F. (1996), Vivaldi 1991 - A study of the formation, circulation and ventilation of Eastern North Atlantic Central Water, *Program Oceanographic* 37, 167-192;

Potter J., Rankin A.H. and, Treloar P.J. (2004), Abiogenic Fischer–Tropsch synthesis of hydrocarbons in alkaline igneous rocks; fluid inclusion, textural and isotopic evidence from the Lovozero complex, N.W. Russia, *Lithos* 75, 311-330;

Potter J., Salvi S., Longstaffe F.J. (2013), Abiogenic hydrocarbon isotopic signatures in granitic rocks: Identifying pathways of formation, *Lithos* 182-183, 114-124;

Rodrigues C. F., Oliver P. G. and Cunha M. R. (2008), Thyasiroidea (Mollusca: Bivalvia) from the mud volcanoes of the Gulf of Cadiz (NE Atlantic), *Zootaxa* 1752, 41-56;

Rodrigues C.F., Webster G., Cunha M. R., Duperron S. and Weightman A. J. (2010), Chemosynthetic bacteria found in bivalve species from mud volcanoes of the Gulf of Cadiz, *FEMS Microbiol Ecol* 73, 486–499;

Rodrigues C.F., Paterson G.L.J., Cabrinovic A. and Cunha M.R. (2011), Deep-sea ophiuroids (Echinodermata: Ophiuroidea: Ophiurida) from the Gulf of Cadiz (NE Atlantic), *Zootaxa* 2754, 1-26;

Rodrigues C. F., Hilário A. and Cunha M. R. (2013), Chemosymbiotic species from the Gulf of Cadiz (NE Atlantic): distribution, life styles and nutritional patterns, *Biogeosciences* 10, 2569-2581;

Rosas F.M., Duarte J.C., Terrinha P., Valadares V. and Matias L. (2009), Morphotectonic characterization of major bathymetric lineaments in Gulf of Cadiz (Africa–Iberia plate boundary): Insights from analogue modelling experiments, *Marine Geology* 261, 33-47;

Rosas F.M., Duarte J.C., Neves M.C., Terrinha P., Silva S., Matias L., Gràcia E., Bartolome R. (2012), Thrust–wrench interference between major active faults in the Gulf of Cadiz (Africa–Eurasia plate boundary, offshore SW Iberia): Tectonic implications from coupled analog and numerical modeling, *Tectonophysics* 548–549, 1–21;

Sauer S., Knies J., Lepland A., Chand S., Eichinger F., Schubert C.J. (2015), Hydrocarbon sources of cold seeps off the Vesterålen coast, northern Norway, *Chemical Geology* 417, 371–382;

Singh A.D., Rai A.K., Tiwari M., Naidu P.D., Verma K., Chaturvedi M., Niyogi A. and Pandey D. (2015), Fluctuations of Mediterranean Outflow Water circulation in the Gulf of Cadiz during MIS 5 to 7: Evidence from benthic foraminiferal assemblage and stable isotope records, *Global and Planetary Change* 133, 125-140;

Schmidt M., Hensen C., MÖrz T., Müller C., Grevemeyer I., Wallmann K., Mau S., Kaul N. (2005), Methane hydrate accumulation in "Mound 11" mud volcano, Costa Rica forearc, *Marine Geology* 216, 83–100;

Sommer S., Linke P., Pfannkuche O., Schleicher T., Deimling S.J.V., Reitz A., Haeckel M., Flögel S. and Hensen C. (2009), Seabed methane emissions and the habitat of frenulate tubeworms on the Captain Arutyunov mud volcano (Gulf of Cadiz), *Marine Ecology Progress Series* 382, 69-86;

Somoza L., Díaz-del-Río V. Léon R., Ivanov M., Fernández-Puga M.C., Gardner J.M., Hernández-Molina F.J., Pinheiro L.M., Rodero J., Lobato A., Maestro A., Vázquez J.T., Medialdea T. and Fernández-Salas L.M. (2003), Seabed morphology and hydrocarbon seepage in the Gulf of Cádiz mud volcano area: Acoustic imagery, multibeam and ultra-high resolution seismic data, *Marine Geology* 195, 153-176;

Stadnitskaia A., Ivanov M. K., Blinova V., Kreulen R. and Van Weering T.C.E. (2006), Molecular and carbon isotopic variability of hydrocarbon gases from mud volcanoes in the Gulf of Cadiz, NE Atlantic, *Marine and Petroleum Geology* 23, 281-296;

Stadnitskaia A., Ivanov M.K. and Damsté J.S.S. (2008), Application of lipid biomarkers to detect sources of organic matter in mud volcano deposits and post-eruptional methanotrophic processes in the Gulf of Cadiz, NE Atlantic, *Marine Geology* 255, 1-14;

Stolper D.A., Martini A.M., Clog M., Douglas P.M., Shusta S.S., Valentine D.L., Sessions A.L. and Eiler J.M. (2015), Distinguishing and understanding thermogenic and biogenic sources of methane using multiply substituted isotopologues, *Geochimica et Cosmochimica Acta* 161, 219-247;

Herzig P.M. and Hannington M.D., Input from the Deep: Hot Vents and Cold Seeps, Schulz H. D. and Zabel M., Editors (2000), Marine Geochemistry, *Springer*, 1ª Eds, 402;

Tassi, F., Fiebig, J., Vaselii, O. and Nocentini, M. (2012), Origins of methane discharging from volcanic-hydrothermal, geothermal and cold emissions in Italy. *Chemical* Geology 310-311, 36-48;

Terrinha P., Matias L., Vicente J., Duarte J., Luís J., Pinheiro L., Lourença N., Diez S., Rosa F., Magalhães V., Valadares V., Zitellini N., Roque C., Victor L.M. and MATESPRO Team (2009), Morphotectonics and strain partitioning at the Iberia-Africa plate boundary from multibeam and seismic reflection data, *Marine Geology* 267, 156-174;

Thiebot, E. and Gutscher, M. A. (2006), The Gibraltar Arc seismogenic zone (part 1): constraints on a shallow east dipping fault plane source for the 1755 Lisbon earthquake provided by seismic data, gravity and thermal modeling, *Tectonophysics* 426, 135–152;

Toucanne S., Mulder T., Schönfeld J., Hanquiez V., Gonthier E., Duprat J., Cremer M., Zaragosi S. (2007), Contourites of the Gulf of Cadiz: A high-resolution record of the paleocirculation of the Mediterranean outflow water during the last 50,000 years, Palaeogeography, Palaeoclimatology, *Palaeoecology* 246, 354-366;

Van Rensbergen P., Depreiter D., Pannemans B. and Henriet J-P. (2005a), Seafloor expression of sediment extrusion and intrusion at the El Arraiche mud volcano field, Gulf of Cadiz, *Journal of Geophysical Research* 110, 1-19;

Van Rensbergen P. Depreiter D., Pannemans B., Moerkerke G., Van Rooij D., Marsset B., Akhmanov G., Blinova V., Ivanov M., Rachidi M., Magalhaes V., Pinheiro Luis, Cunha M., Henriet J-P. (2005b), The El Arraiche mud volcano field at the Moroccan Atlantic slope, Gulf of Cadiz, *Marine Geology* 219, 1-17;

Van Rooij D.V., Blamart D., De Mol L., Mienis F., Pirlet H., Wehrmann L.M., Barbieri R., Maignien L., Templer S.P., de Haas H., Hebbeln D., Frank N., Larmagnat S., Stadnitskaia A., Stivaletta N., Van Weering T., Zhang Y., Hamoumi N., Cnudde V., Duyck P., Henriet J.-P. and The Microsystems

MD 169 shipboard party (2011), Cold-water coral mounds on the Pen Duick Escarpment, Gulf of Cadiz: The MiCROSYSTEMS project approach, *Marine Geology* 282, 102-117:

Van Sebille E., Baringer M.O., Johns W.E., Meinen C.S., Beal L.M., Jong M.F., and Van Ake H.M. (2011), Propagation pathways of classical Labrador Sea water from its source region to 26°N, *Journal of Geophysical Research* 116, 1-18;

Vandorpe T., Van Rooij D., Haas H. (2014), Stratigraphy and paleoceanography of a topography-controlled contourite drift in the Pen Duick area, southern Gulf of Cádiz, *Marine Geology* 349, 136–151;

Vanneste H., Kelly-Gerreyn B.A., Connelly D.P., James R.H., Haeckel M., Fisher R.E., Heeschen K. and Mills R.A. (2011), Spatial variation in fluid flow and geochemical fluxes across the sediment–seawater interface at the Carlos Ribeiro mud volcano (Gulf of Cadiz), *Geochimica et Cosmochimica Acta* 75, 1124-1144;

Vanneste H., Kastner M.b, James R.H., Connelly D.P., Fisher R.E., Kelly-Gerreyn B. A., Heeschen K., Haeckel M. and Mills R. A. (2012), Authigenic carbonates from the Darwin Mud Volcano, Gulf of Cadiz: A record of palaeo-seepage of hydrocarbon bearing fluids, *Chemical Geology* 300-301, 24-39;

Vanneste H., James R.H., Kelly-Gerreyn B.A., Mills R.A. (2013), Authigenic barite records of methane seepage at the Carlos Ribeiro mud volcano (Gulf of Cadiz), *Chemical Geology* 354, 42-54;

Vanreusel A., Andersen A.C., Boetius A., Connelly D., Cunha M.R., Decker C., Heeschen k., Hilario A., Kormas K.Ar., Maignien L., Olu K., Pachiadaki M., Ritt B., Rodrigues C., Sarrazin J., Tyler P., Van Gaever S. and Vanneste H. (2009), Biodiversity of Cold Seep Ecosystems Along the European Margins, *Oceanography* 22 (1), 118-135;

Von Cosel R. (2002), A new species of bathymodioline mussel (Mollusca, Bivalvia, Mytilidae) from Mauritania (West Africa) with comments on the genus Bathymodiolus Kenk and Wilson, 1985. *Zoosystema* 24 (2), 259-271;

Wehrmann L.M., Templer S.P., Brunner B., Bernasconi S.M., Maignien L. and Ferdelman T.G. (2011), The imprint of methane seepage on the geochemical record and early diagenetic processes in cold-water coral mounds on Pen Duick Escarpment, Gulf of Cadiz, *Marine Geology* 282, 118-137;

Wenau S. (2013), *Seismic and acoustic imaging of fluid seepage structures in different sedimentological and tectonic settings in the Lower Congo Basin*, Universidade de Bremen, Departamento de Geociências, Dissertação de Doutoramento em Ciências Naturais, 10-15;

Wienberg C., Hebbeln D., Fink H.G., Mienis F., Dorschel B., Vertino A., Correa M.L. and Freiwald A. (2009), Scleractinian cold-water corals in the Gulf of Cadiz—First clues about their spatial and temporal distribution, *Deep-Sea Research* I 56, 1873–1893;

Zitellini N., Gràcia E., Matias L., Terrinha P., Abreu M.A., DeAlteriis G., Henriet J.P., Dañobeitia J.J., Masson D.G., Mulder T., Ramella R., Somoza L. and Diez S. (2009), The quest for the Africa–Eurasia plate boundary west of the Strait of Gibraltar, *Earth and Planetary Science Letters*, 1-9.

Appendixes

ANEXO I – Main Matrix

Table 1 – The main matrix showing all geological features and their respective species.

Family	Species	AI	Fiú	Gem	WoG	Mer	LdT	VR	Kid	PDE	NN	AA	Mek	Ibe	Stu	Gin	Yum	FR	Av	JB	Sho	Dar	CC	CA	Sag	CR	Bom	Sem	Por	Total
Class Polychaeta		0	0	1	0	1	1	0	1	0	0	0	1	0	0	0	1	0	0	0	0	1	0	1	1	1	1	1	1	13
Siboglinidae	*Siboglinum* sp.2	0	0	0	0	0	0	0	0	0	0	0	1	0	0	0	0	0	0	0	0	0	0	0	0	0	0	0	0	1
Siboglinidae	*Bobmarleya gadensis*	0	0	0	0	0	0	0	0	0	0	0	0	0	0	0	0	0	0	0	0	0	0	0	0	1	0	0	0	1
Siboglinidae	*Lamellisabella denticulata*	0	0	0	0	0	0	0	0	0	0	0	0	0	0	0	0	0	0	0	0	0	0	0	0	0	0	0	1	1
Siboglinidae	*Polybrachia* sp.1	0	0	0	0	1	0	0	0	0	0	0	0	0	0	0	0	0	0	0	0	0	0	0	0	0	1	0	0	2
Siboglinidae	*Polybrachia* sp.2	0	0	0	0	0	0	0	0	0	0	0	0	0	0	0	0	0	0	0	0	0	0	1	0	0	0	0	0	1
Siboglinidae	*Polybrachia* sp.3	0	0	0	0	0	0	0	0	0	0	0	0	0	0	0	0	0	0	0	0	0	0	0	0	0	0	0	1	1
Siboglinidae	*Polybrachia* Va	0	0	0	0	0	0	0	0	0	0	0	0	0	0	0	0	0	0	0	0	0	0	0	0	1	0	1	0	2
Siboglinidae	*Polybrachia* Vb	0	0	0	0	0	0	0	0	0	0	0	0	0	0	0	0	0	0	0	0	0	0	0	1	0	0	0	0	1
Siboglinidae	*Polybrachia* Vc	0	0	0	0	0	0	0	0	0	0	0	0	0	0	0	0	0	0	0	0	0	0	0	0	0	1	0	0	1
Siboglinidae	*Siboglinum* cf. *poseidoni*	0	0	0	0	0	0	0	0	0	0	0	0	0	0	0	0	0	0	0	0	0	0	1	0	0	0	0	0	1
Siboglinidae	*Siboglinum* Ia	0	0	1	0	0	0	0	0	0	0	0	0	0	0	0	1	0	0	0	0	1	0	0	0	0	0	0	0	3
Siboglinidae	*Siboglinum* Ib	0	0	1	0	1	1	0	1	0	0	0	0	0	0	0	0	0	0	0	0	0	0	0	1	1	1	0	0	7
Siboglinidae	*Siboglinum* Ic	0	0	0	0	0	0	0	0	0	0	0	0	0	0	0	0	0	0	0	0	0	0	0	0	0	1	1	0	2
Siboglinidae	*Siboglinum* Id	0	0	0	0	1	0	0	0	0	0	0	0	0	0	0	0	0	0	0	0	0	0	1	0	0	0	0	0	2
Siboglinidae	*Siboglinum* Ie	0	0	0	0	0	0	0	0	0	0	0	0	0	0	0	0	0	0	0	0	1	0	0	0	0	0	0	0	1
Siboglinidae	*Siboglinum* If	0	0	0	0	0	0	0	0	0	0	0	1	0	0	0	0	0	0	0	0	0	0	0	0	0	0	0	1	2
Siboglinidae	*Siboglinum* sp.1	0	0	0	0	1	0	0	0	0	0	0	0	0	0	0	0	0	0	0	0	0	0	0	0	0	0	0	0	1

Siboglinidae	*Spirobrachia tripeira*	0	0	0	0	0	0	0	0	0	0	0	0	0	0	0	0	0	0	0	0	0	0	0	0	0	0	0	1	1
Classe Bivalvia		0	0	0	0	1	0	0	1	1	0	0	1	0	0	1	1	0	0	1	1	1	0	1	0	1	0	0	1	12
Lucinidae	*Lucionoma asapheus*	0	0	0	0	1	0	0	0	0	0	0	0	0	0	0	0	0	0	0	0	0	0	0	0	0	0	0	0	1
Mytilidae	*Bathymodiolus mauritanicus*	0	0	0	0	0	0	0	0	0	0	0	0	0	0	0	0	0	0	0	0	1	0	0	0	0	0	0	0	1
Solemyidae	*Acharax gadirae*	0	0	0	0	0	0	0	0	1	0	0	0	0	0	1	1	0	0	1	0	0	0	1	0	1	0	0	1	7
Solemyidae	*Solemya (Petrasma) elarraichensis*	0	0	0	0	1	0	0	1	1	0	0	1	0	0	1	1	0	0	0	0	0	0	0	0	0	0	0	0	6
Thyasiridae	*Axinulus croulinensis*	0	0	0	0	1	0	0	0	0	0	0	0	0	0	0	0	0	0	0	0	0	0	0	0	0	0	0	0	1
Thyasiridae	*Leptaxinus minutus*	0	0	0	0	1	0	0	0	0	0	0	0	0	0	0	1	0	0	0	0	1	0	0	0	0	0	0	0	3
Thyasiridae	*Mendicula ferruginosa*	0	0	0	0	1	0	0	0	0	0	0	0	0	0	0	0	0	0	0	0	0	0	0	0	0	0	0	0	1
Thyasiridae	*Spinaxinus* cf. *sentosus*	0	0	0	0	0	0	0	0	0	0	0	0	0	0	0	0	0	0	0	0	0	0	1	0	0	0	0	0	1
Thyasiridae	*Thyasira (Parathyasira) granulosa*	0	0	0	0	1	0	0	0	0	0	0	1	0	0	0	0	0	0	0	1	0	0	0	0	0	0	0	0	3
Thyasiridae	*Thyasira obsoleta*	0	0	0	0	1	0	0	0	0	0	0	0	0	0	0	0	0	0	0	0	0	0	1	0	1	0	0	1	4
Thyasiridae	*Thyasira tortuosa*	0	0	0	0	0	0	0	0	0	0	0	0	0	0	0	0	0	0	0	0	0	0	0	0	0	0	0	1	1
Thyasiridae	*Thyasira vulcolutre*	0	0	0	0	0	0	0	0	0	0	0	0	0	0	0	0	0	0	0	0	0	0	1	0	1	0	0	0	2
Vesicomyidae	*Isorropodon megadesmus*	0	0	0	0	0	0	0	0	0	0	0	0	0	0	0	0	0	0	0	0	0	0	1	0	0	0	0	0	1
Vesicomyidae	*Isorropodon* sp. indeterminate	0	0	0	0	0	0	0	0	0	0	0	0	0	0	0	0	0	0	0	0	0	0	1	0	0	0	0	0	1
Class Gastropoda		1	1	1	1	1	0	0	1	1	1	1	0	1	1	0	0	1	0	1	0	1	0	1	1	1	1	0	1	19
Borsoniidae	*Drilliola loprestiana*	0	0	0	0	1	0	0	0	0	0	0	0	0	0	0	0	0	0	0	0	0	0	0	0	0	0	0	0	1
Buccinidae	*Chauvetia balgimae*	0	0	1	0	1	0	0	1	0	0	0	0	0	0	0	0	0	0	0	0	0	0	0	0	0	0	0	0	3

Buccinidae	*Neptunea contraria*	0	0	0	0	0	0	0	0	0	0	0	0	0	0	0	0	0	0	1	0	0	0	0	0	0	0	0	0	1
Calliotropidae	*Putzeysia* cf. *wiseri*	0	0	0	0	0	0	0	0	1	1	0	0	0	0	0	0	0	0	0	0	1	0	0	0	0	0	0	1	4
Cerithiopsidae	Cerithiopsidae sp. A	0	0	0	0	0	0	0	0	0	0	0	0	0	0	0	0	1	0	0	0	0	0	0	0	0	0	0	0	1
Chilodontidae	*Danilia tinei*	0	0	0	0	0	0	0	1	0	0	0	0	0	0	0	0	0	0	0	0	0	0	0	0	0	0	0	0	1
Cimidae	*Graphis gracilis*	0	0	0	0	0	0	0	0	0	0	0	0	0	0	0	0	0	0	0	0	1	0	0	0	0	0	0	0	1
Colloniidae	*Cantrainea peloritana*	0	0	0	0	0	0	0	0	0	0	0	0	0	0	0	0	0	0	0	0	1	0	1	0	0	0	0	0	2
Columbellidae	*Amphissa acutecostata*	0	0	0	0	0	0	0	0	1	1	0	0	1	1	0	0	0	0	0	0	0	0	1	0	0	0	0	0	5
Conoidea	Conoidea sp. A	0	0	0	0	0	0	0	0	0	0	0	0	0	0	0	0	0	0	0	0	0	0	1	0	0	0	0	0	1
Drilliidae	*Spirotropis monterosatoi*	0	1	0	0	1	0	0	1	0	0	0	0	0	0	0	0	0	0	0	0	0	0	0	0	0	0	0	0	3
Epitoniidae	*Claviscala* sp. A	0	0	0	0	0	0	0	0	0	0	0	0	0	0	0	0	0	0	0	0	0	0	0	1	0	0	0	0	1
Eulimidae	*Fusceulima minuta*	0	0	0	0	0	0	0	0	0	0	1	0	0	0	0	0	0	0	0	0	0	0	0	0	0	0	0	0	1
Eulimidae	*Melanella* sp. A	0	0	0	0	1	0	0	0	1	0	0	0	0	0	0	0	0	0	0	0	0	0	0	0	0	0	0	0	2
Fissurellidae	*Emarginula multistriata*	0	0	0	0	1	0	0	0	0	0	0	0	0	0	0	0	0	0	0	0	0	0	0	0	0	0	0	0	1
Fissurellidae	*Fissurisepta* cf. *granulosa*	0	0	0	0	0	0	0	0	0	0	0	0	1	0	0	0	0	0	0	0	1	0	0	0	0	0	0	0	2
Fissurellidae	*Puncturella* sp. A	0	0	0	0	0	0	0	0	0	0	0	0	0	0	0	0	0	0	0	0	0	0	1	0	0	0	0	0	1
Lepetellidae	*Lepetella* sp. A	1	0	0	0	0	0	0	0	0	0	0	0	0	0	0	0	0	0	0	0	0	0	0	0	0	0	0	0	1
Lepetidae	*Iothia* sp. A	0	0	0	0	0	0	0	0	0	0	0	0	0	0	0	0	0	0	0	0	1	0	0	0	0	0	0	0	1
Mangeliidae	*Benthomangelia macra*	0	0	0	0	0	0	0	0	0	0	0	0	0	0	0	0	0	0	0	0	0	0	0	0	1	0	0	0	1
Marginellidae	*Marginellidae* und.	0	1	1	0	1	0	0	1	1	0	0	0	0	0	0	0	0	0	0	0	0	0	0	0	0	0	0	0	5
Melanodrymiidae	*Leptogyra* sp. A	0	0	0	0	0	0	0	0	0	0	0	0	0	0	0	0	0	0	0	0	1	0	0	0	0	0	0	0	1
Muricidae	*Pagodula echinata*	0	0	0	0	1	0	0	1	0	0	0	0	0	0	0	0	0	0	0	0	1	0	1	0	0	0	0	0	4

Nystiellidae	*Iphitus marshalli*	0	0	0	0	0	0	0	0	1	0	0	0	0	0	0	0	0	0	0	0	0	0	0	0	0	0	0	0	1
Pyramidellidae	cf. *Odostomia* sp.	0	0	0	0	0	0	0	0	0	0	0	0	0	0	0	0	0	0	0	0	0	0	0	1	0	0	0	0	1
Pyramidellidae	*Eulimella* sp. A	0	0	0	0	1	0	0	0	0	0	0	0	0	0	0	0	0	0	0	0	0	0	0	0	0	0	0	0	1
Pyramidellidae	*Odostomia* sp. A	0	1	0	0	0	0	0	0	0	0	0	0	0	0	0	0	0	0	0	0	0	1	0	0	0	0	0	0	2
Pyramidellidae	Pyramidellidae spA	0	0	0	0	0	0	0	1	0	0	0	0	0	0	0	0	0	0	0	0	0	0	0	0	0	0	0	0	1
Pyramidellidae	*Syrnola* sp. A	0	0	0	0	1	0	0	0	0	0	0	0	0	0	0	0	0	0	0	0	0	0	0	0	0	0	0	0	1
Pyramidellidae	*Turbonilla* sp. A	0	0	0	0	0	0	0	0	1	0	0	0	0	0	0	0	0	0	0	0	0	0	0	0	0	0	0	0	1
Pyropeltidae	*Pyropelta* aff. *sibuetae*	0	0	0	0	0	0	0	0	0	0	0	0	0	0	0	0	0	0	0	0	0	1	0	0	0	0	0	0	1
Raphitomidae	*Gymnobela aquilarum*	0	0	0	0	0	0	0	0	0	0	0	0	0	0	0	0	0	0	0	0	0	0	0	0	0	0	1	0	1	2
Raphitomidae	*Taranis* cf. *alexandrina*	0	0	0	0	0	0	0	0	0	0	0	0	0	0	0	0	0	0	0	0	0	1	0	1	0	0	0	0	1	3
Rissoidae	*Alvania zylensis*	0	0	0	0	1	0	0	0	1	0	0	0	0	0	0	0	0	0	0	0	0	0	0	0	0	0	0	0	0	2
Rissoidae	*Alvania cimicoides*	0	0	0	0	1	0	0	0	1	0	0	0	0	0	0	0	0	0	0	0	0	0	0	0	0	0	0	0	0	2
Rissoidae	*Alvania electa*	0	0	0	0	0	0	0	1	0	0	0	0	0	0	0	0	0	0	0	0	0	0	0	0	0	0	0	0	0	1
Rissoidae	*Alvania tomentosa*	0	0	0	0	0	0	0	0	1	0	1	0	0	0	0	0	0	0	0	0	0	0	0	0	0	0	0	0	0	2
Rissoidae	*Obtusella intersecta*	0	0	0	0	0	0	0	0	0	0	0	0	0	0	0	0	0	0	0	0	0	0	0	1	0	0	0	0	0	1
Rissoidae	*Pseudosetia* sp. A	0	0	0	0	0	0	0	0	1	0	0	0	0	0	0	0	0	0	0	0	0	0	0	0	0	0	0	0	0	1
Rissoidae	*Pseudosetia* sp. C	0	0	0	0	0	0	0	0	0	0	0	0	0	0	0	0	0	0	0	0	0	1	0	0	1	0	0	0	1	3
Rissoidae	*Pseudosetia* sp. D	0	0	0	0	1	0	0	0	0	0	0	0	0	0	0	0	0	0	0	0	0	0	0	0	0	0	0	0	0	1
Rissoidae	*Punctulum porcupinae*	0	0	1	0	0	0	0	0	0	0	0	0	0	0	0	0	0	0	0	0	0	1	0	0	0	1	0	0	1	4
Scissurellidae	*Anatoma* sp. A	0	0	0	1	0	0	0	0	1	0	0	0	0	0	0	0	0	0	0	0	0	0	0	0	0	0	0	0	1	3
Scissurellidae	*Anatoma* sp. B	0	0	0	0	1	0	0	0	0	0	0	0	1	0	0	0	1	0	0	0	0	0	0	0	0	0	0	0	0	3
Seguenziidae	*Akritogyra* sp. A	0	0	0	0	0	0	0	0	0	0	0	0	0	0	0	0	0	0	0	0	0	0	0	1	0	0	0	0	0	1
Seguenziidae	cf. *Sahlingia* sp. A	0	0	0	0	0	0	0	0	0	0	0	0	0	0	0	0	0	0	0	0	0	0	0	1	0	0	0	0	0	1
Seguenziidae	*Lissotesta* sp. A	0	0	0	0	0	0	0	0	0	0	0	0	0	0	0	0	0	0	0	0	0	0	0	0	0	0	0	0	1	1
Seguenziidae	*Sahlingia* sp. A	0	0	0	0	0	0	0	0	0	0	0	0	0	0	0	0	0	0	0	0	0	0	0	0	0	0	0	0	1	1

Seguenziidae	*Sahlingia* sp. B	0	0	0	0	0	0	0	0	0	0	0	0	0	0	0	0	0	0	0	0	0	0	0	0	0	0	1	1
Seguenziidae	Seguenziidae sp. A	0	0	0	0	1	0	0	0	0	0	0	0	0	0	0	0	0	0	0	0	0	0	0	0	0	0	0	0	1
Solariellidae	*Solariella amabilis*	0	0	0	1	0	0	0	0	0	0	0	0	0	0	0	0	0	0	0	0	0	0	0	0	0	0	0	0	1
Triphoridae	*Strobiligera brychia*	0	0	0	0	0	0	0	0	0	1	0	0	0	0	0	0	0	0	0	0	0	0	0	0	0	0	0	0	1
Turbinidae	*Cirsonella* aff. *romettensis*	0	0	0	0	0	0	0	0	0	0	0	0	0	0	0	0	0	0	0	0	0	1	0	0	0	0	0	0	1
Turbinidae	*Moelleriopsis* cf. *messanensis*	0	0	0	0	0	0	0	0	0	0	0	0	0	0	0	0	0	0	0	0	0	1	0	0	0	0	0	1	2
Vetigastropoda und	*Vetigastropoda* sp. A	0	0	0	0	0	0	0	0	0	0	0	0	0	0	0	0	0	0	0	0	0	0	0	1	0	0	0	0	1
Xylodisculidae	*Xylodiscula* sp. A	0	0	0	0	0	0	0	0	0	0	0	0	0	0	0	0	0	0	0	0	0	1	0	1	0	0	0	0	2
Order Tanaidacea		0	1	0	1	1	0	0	1	1	1	0	1	0	0	0	1	1	1	1	0	0	1	1	0	0	1	0	0	14
Apseudidae	*Apseudes grossimanus*	0	0	0	0	0	0	0	1	0	1	0	1	0	0	0	1	0	0	0	0	0	0	0	0	0	0	0	0	4
Apseudidae	*Apseudes setiferus*	0	0	0	1	1	0	0	1	1	1	0	1	0	0	0	0	1	0	0	0	0	0	0	0	0	0	0	0	7
Apseudidae	*Atlantapseudes nigrichela*	0	1	0	0	1	0	0	1	1	0	0	1	0	0	0	0	0	1	0	0	0	1	1	0	0	0	0	0	8
Apseudidae	*Fageapseudes retusifrons*	0	1	0	0	1	0	0	1	0	0	0	0	0	0	0	0	0	0	0	0	0	0	0	0	0	0	0	0	3
Colletteidae	*Haplocope diapira*	0	0	0	0	1	0	0	0	0	0	0	0	0	0	0	0	0	0	0	0	0	0	0	0	0	0	0	0	1
Leptocheliidae	*Mesotanais pinguiculus*	0	0	0	0	0	0	0	0	0	1	0	1	0	0	0	0	0	0	1	0	0	0	0	0	0	0	0	0	3
Paratanaoidea inc sed	*Coalecerotanais alter*	0	0	0	0	0	0	0	0	0	0	0	0	0	0	0	0	0	0	0	0	0	0	1	0	0	0	0	0	1
Paratanaoidea inc sed	*Cristatotanais contoura*	0	0	0	0	1	0	0	0	0	0	0	0	0	0	0	1	0	1	0	0	0	0	1	0	0	0	0	0	4
Pseudotanaidae	*Pseudotanais (Pseudotanais) tympanobaculum*	0	0	0	0	1	0	0	1	0	0	0	0	0	0	0	0	0	0	0	0	0	0	1	0	0	1	0	0	4
Sphyrapodidae	*Pseudosphyrapus*	0	0	0	0	0	0	0	0	0	0	0	0	0	0	0	0	0	0	1	0	0	0	0	0	0	0	0	0	1

Sphyrapodidae	*Pseudosphyrapus* sp. A	0	0	0	0	0	0	0	1	0	0	0	0	0	0	0	0	0	0	0	0	0	0	0	0	0	0	0	0	1
Sphyrapodidae	*Sphyrapus malleolus*	0	1	0	0	1	0	0	1	0	0	0	1	0	0	0	0	0	0	0	0	0	0	0	0	0	1	0	0	5
Sphyrapodidae	*Sphyrapus meknes*	0	0	0	0	0	0	0	0	0	0	0	1	0	0	0	0	0	0	0	0	0	0	0	0	0	0	0	0	1
Tanaellidae	*Araphura macrobelone*	0	0	0	0	0	0	0	1	0	0	0	0	0	0	0	0	0	0	0	0	0	0	1	0	0	0	0	0	2
Typhlotanaidae	*Torquella iberica*	0	0	0	0	0	0	0	0	0	0	0	1	0	0	0	0	0	0	0	0	0	0	0	0	0	0	0	0	1
Typhlotanaidae	*Typhlotanais guca*	0	1	0	0	1	0	0	1	0	0	0	0	0	0	0	0	0	0	0	1	0	0	0	0	0	0	0	0	4
Typhlotanaidae	*Typhlotanais kyphosis*	0	1	0	0	1	0	0	1	0	0	0	0	0	0	0	0	0	0	0	0	0	0	1	0	0	0	0	0	4
Order Decapoda		0	0	0	0	0	0	0	0	0	0	0	0	0	0	0	0	0	0	0	0	0	0	1	0	0	0	0	0	1
Callianassidae	*Vulcanocalliax arutyunovi*	0	0	0	0	0	0	0	0	0	0	0	0	0	0	0	0	0	0	0	0	0	0	1	0	0	0	0	0	1
Class Ophiuroidea		1	1	0	1	1	0	1	1	1	1	0	1		0	1	1	1	0	1	1	1	0	1	0	1	0	0	1	18
Amphilepididae	*Amphilepis ingolfiana*	0	1	0	0	1	0	0	1	1	0	0	0	0	0	0	1	0	0	0	0	0	0	0	0	0	0	0	0	5
Amphiuridae	*Amphioplus hexabrachiatus*	0	1	0	0	1	0	0	1	1	0	0	0	0	0	0	1	0	0	0	0	1	0	1	0	0	0	0	0	7
Amphiuridae	*Amphipholis squamata*	0	1	0	1	1	0	0	1	1	1	0	1	0	0	1	1	1	0	1	0	1	0	1	0	0	0	0	0	13
Amphiuridae	*Amphiura chiajei*	0	0	0	0	1	0	0	1	0	0	0	0	0	0	0	0	0	0	0	0	0	0	0	0	0	0	0	0	2
Amphiuridae	*Amphiura filiformis*	1	1	0	1	1	0	0	0	1	0	0	0	0	0	0	0	0	0	0	0	0	0	0	0	0	0	0	0	5
Amphiuridae	*Amphiura grandisquama*	0	0	0	0	0	0	1	0	1	0	0	0	0	0	0	0	0	0	0	0	0	0	0	0	0	0	0	0	2
Amphiuridae	*Amphiura* sp. A	0	0	0	1	0	0	0	1	1	0	0	1	0	0	0	1	0	0	0	0	1	0	1	0	0	0	0	0	7
Amphiuridae	*Amphiura* und.	0	0	0	0	1	0	0	1	0	0	0	0	0	0	0	1	0	0	0	0	0	0	0	0	0	0	0	0	3
Amphiuridae	Amphiuridae und.	0	1	0	1	1	0	0	1	0	0	0	1	0	0	0	1	0	0	0	0	1	0	0	0	0	0	0	0	7
Ophiacanthidae	*Ophiacantha aristata*	0	0	0	0	0	0	0	0	0	0	0	0	0	0	0	0	0	0	0	0	0	0	1	0	0	0	0	0	1
Ophiacanthidae	*Ophiopristis gadensis*	0	0	0	0	0	0	0	0	0	0	0	0	0	0	0	0	0	0	0	0	0	0	1	0	0	0	0	0	1

Ophiactidae	*Ophiactis abyssicola*	0	0	0	0	0	0	0	0	0	0	0	0	0	0	0	0	0	0	0	0	0	0	1	0	0	0	0	0	1
Ophiactidae	*Ophiactis balli*	1	0	0	1	0	0	0	0	0	0	0	0	0	0	0	0	0	0	0	0	0	0	0	0	0	0	0	0	2
Ophiolepididae	*Ophiomusium lymani*	0	0	0	0	0	0	0	0	0	0	0	0	0	0	0	0	0	0	0	0	0	0	0	0	0	0	0	1	1
Ophiuridae	*Ophiura (Dictenophiura) carnea*	0	0	0	0	1	0	0	0	0	0	0	0	0	0	0	0	0	0	0	0	0	0	0	0	0	0	0	0	1
Ophiuroidea und.	*Ophiuroidea* und.	0	0	0	0	1	0	0	1	0	0	0	1	0	0	0	1	0	0	0	1	0	0	1	0	1	0	0	0	7

Annex II – Examples of species of different taxa

Order Decapoda

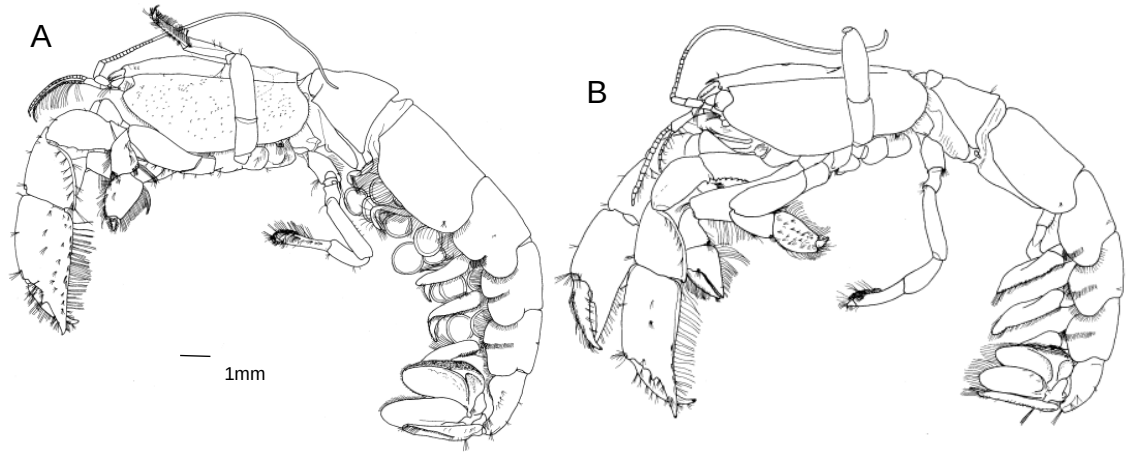

Figure 1 – Specie *Vulcanocalliax arutyunovi* (from Dworschak and Cunha, 2007). A - Female holotype; B – Male holotype.

Class Polychaeta

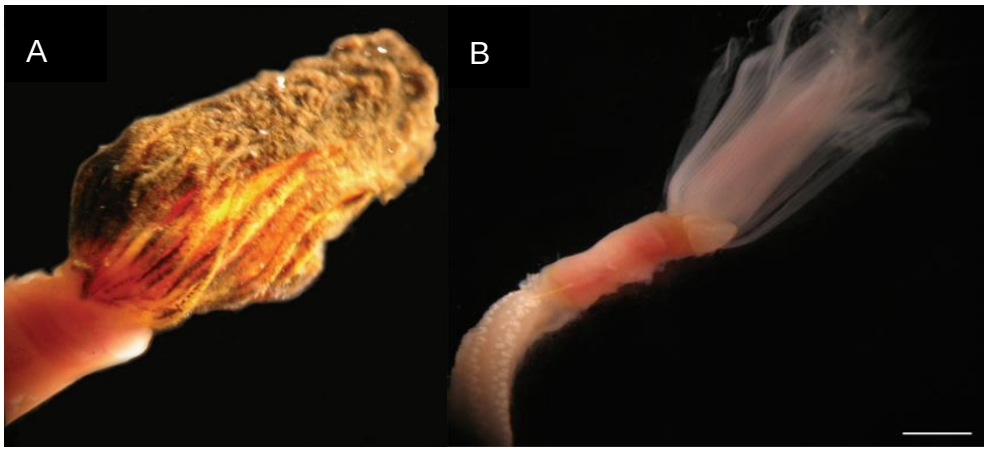

Figure 2 – A: Specie *Bobmarleya gadensis*; B: Specie *Spirobrachia tripeira*; 0.5 mm (from Hilário and Cunha, 2008).

Class Bivalvia

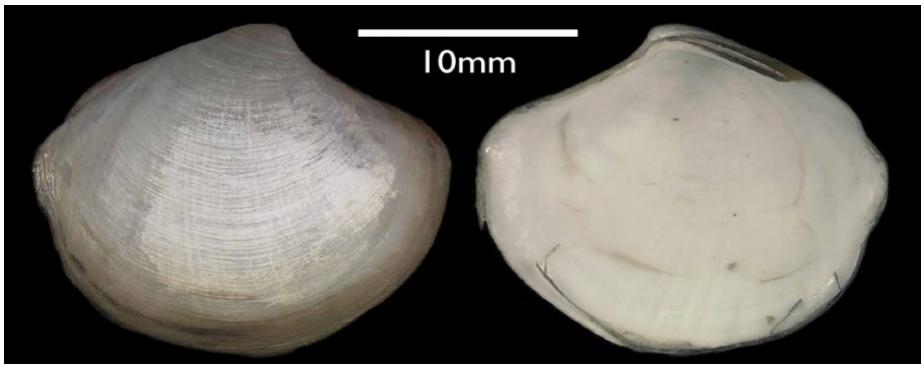

Figura 3 – Specie *Thyasira vulcolutre* (from Rodrigues *et al.* 2008).

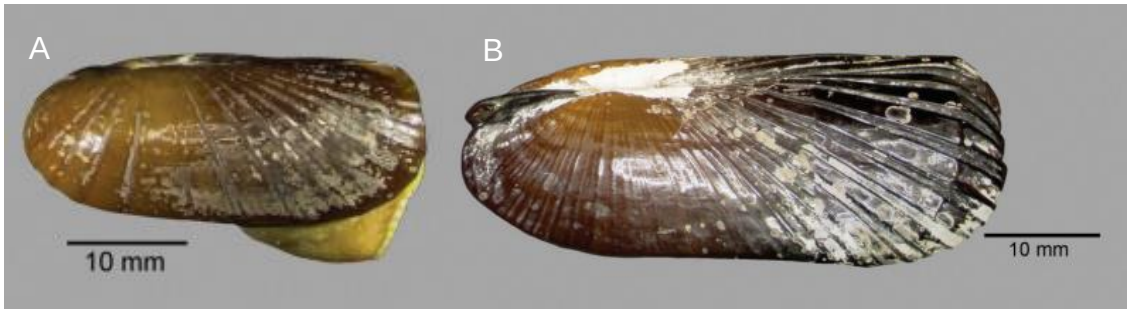

Figure 4 – A - Specie *Solemya* (*Petrasma*) *elarraichensis;* B - Specie *Acharax gadirae* (from Oliver *et al.* 2011).

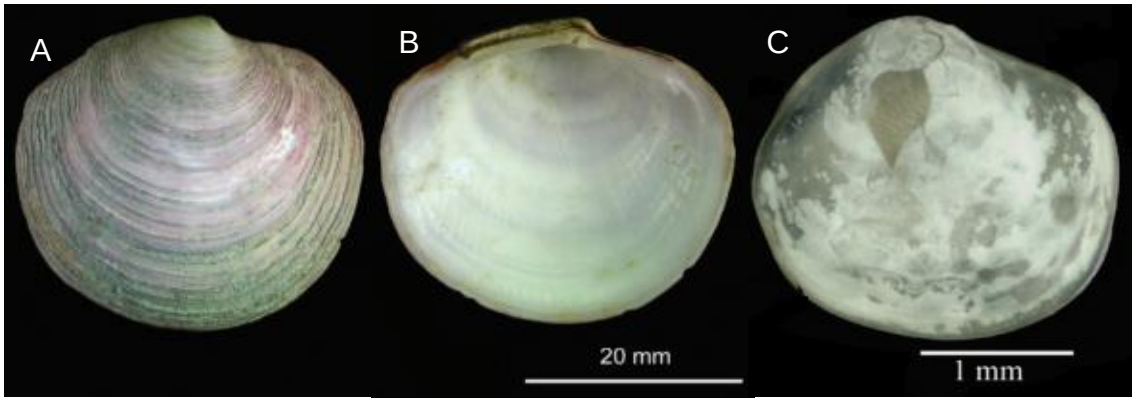

Figure 5 – Specie *Lucinoma asapheus.* A – Exterior aspect; B – Interior aspect. C - Specie *Spinaxinus* cf. *sentosus* (from Oliver *et al.* 2011).

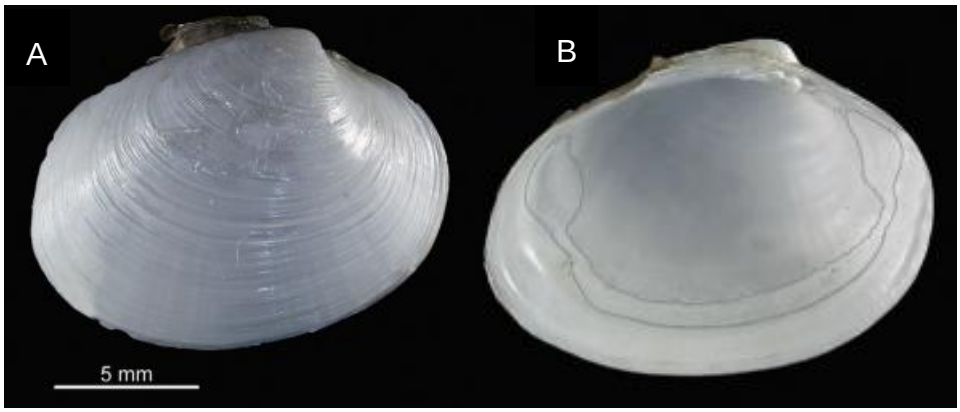

Figure 6 – Specie *Isorropodon megadesmus.* A – Exterior aspect; B – Interior aspect (from Oliver *et al.* 2011).

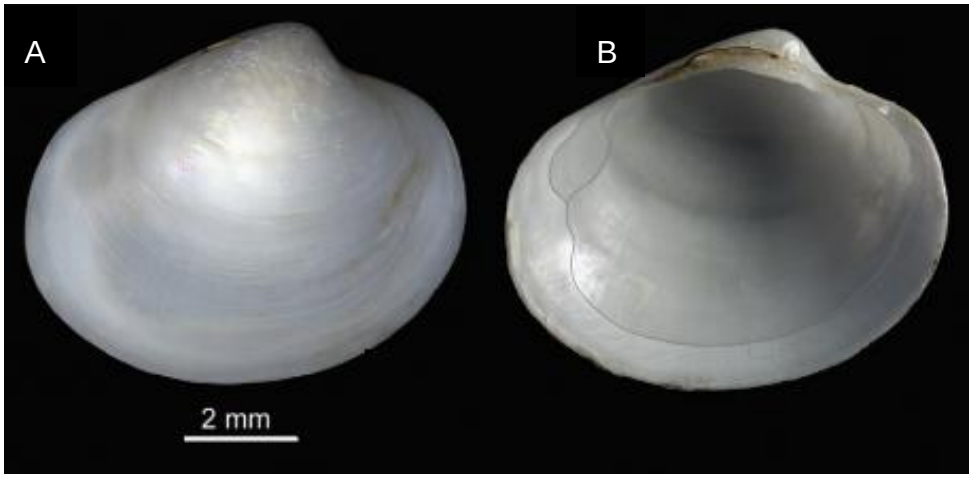

Figure 7 – Specie *Isorropodon* sp. indeterminate. A – Exterior aspect; B – Interior aspect (from Oliver *et al.* 2011).

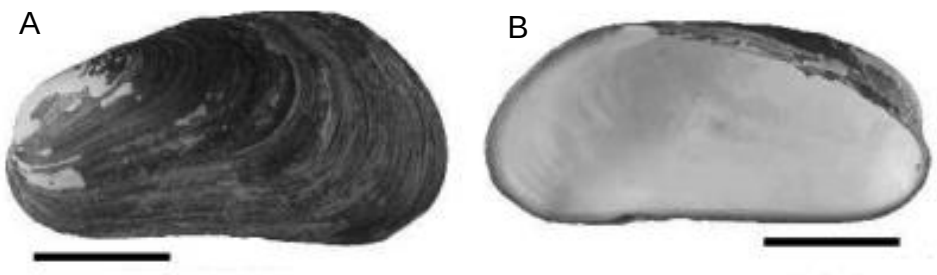

Figure 8 - Specie *"Bathymodiolus"* sp. A - Exterior aspect; B – Interior aspect. Scale bar 1 cm (from Génio *et al.* 2008).

Order Tanaidacea

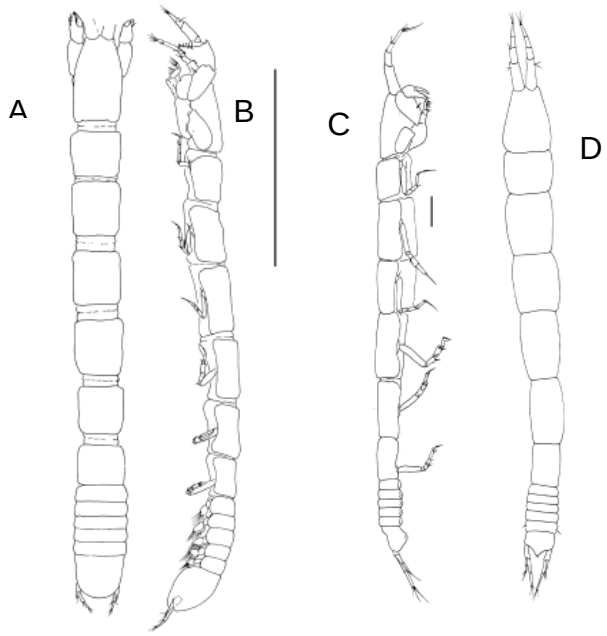

Figure 9 – Specie *Araphura macrobelone*. A - Dorsa aspect; B - Lateral aspect; Scale line = 1 mm. Specie *Haplocope diapira.* C - Lateral aspect; D – Dorsal aspect. Scale line = 0.1 mm (from Blazewicz-Paszkowycz *et al.* 2011a).

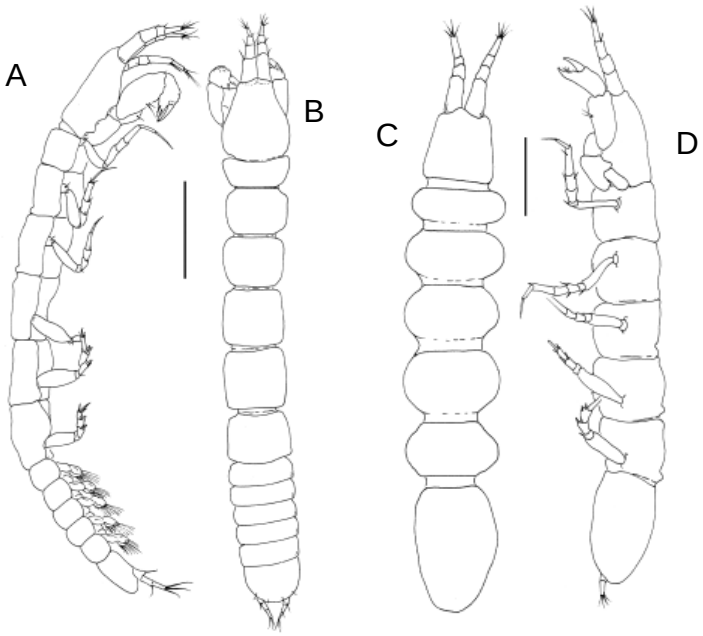

Figure 10 – Specie *Cristatotanais contoura.* A – Lateral aspect; B - Dorsal aspect; Scale line = 0.1 mm. Specie *Coalecerotanais alter.* C - Dorsal aspect; D - Lateral aspect. Scale line: = 0.1 mm (from Blazewicz-Paszkowycz *et al.* 2011a).

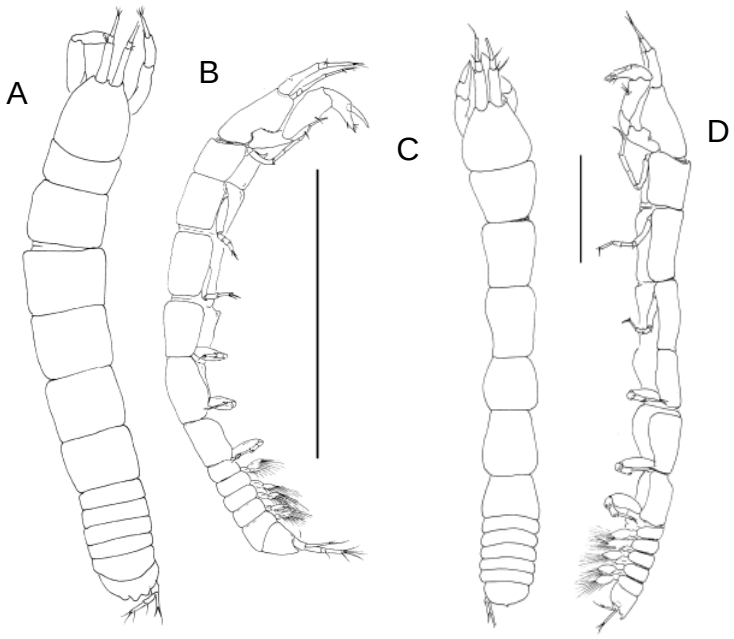

Figure 11 – Specie *Typhlotanais kyphosis* (from Blazewicz-Paszkowycz *et al.* 2011a). A – Dorsal aspect; B – Lateral aspect. Scale line = 1 mm. Specie *Torquella ibérica.* C – Dorsal aspect; D – Lateral aspect. Scale line = 1 mm.

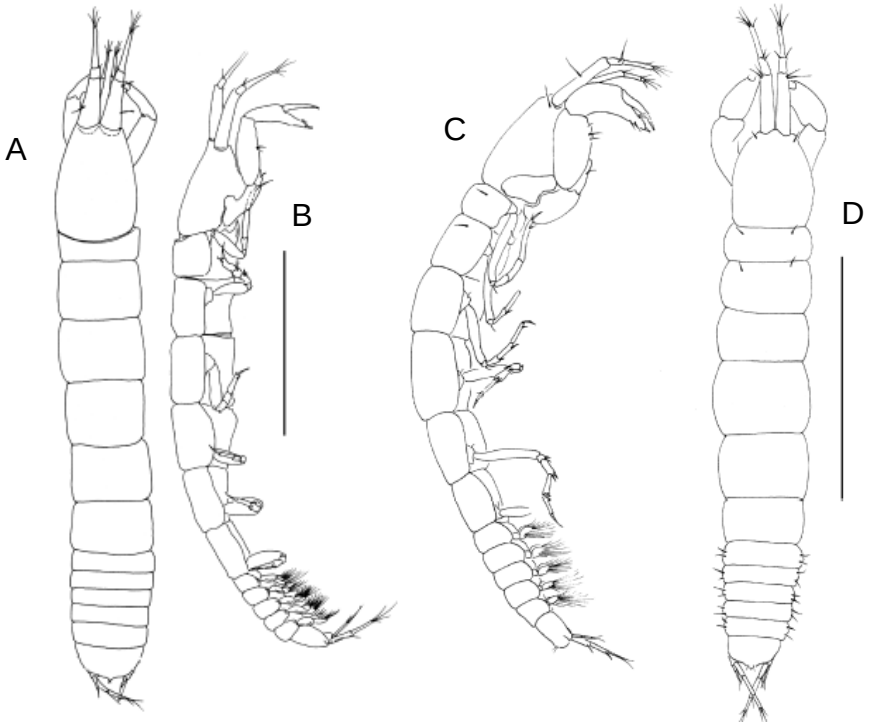

Figure 12 – Specie *Typhlotanais guca* (from Blazewicz-Paszkowycz *et al.* 2011a). A – Dorsal aspect; B – Lateral aspect. Scale line = 1 mm. Specie *Mesotanais pinguiculus.* C – Lateral aspect; D – Dorsal aspect; Scale line = 1 mm.

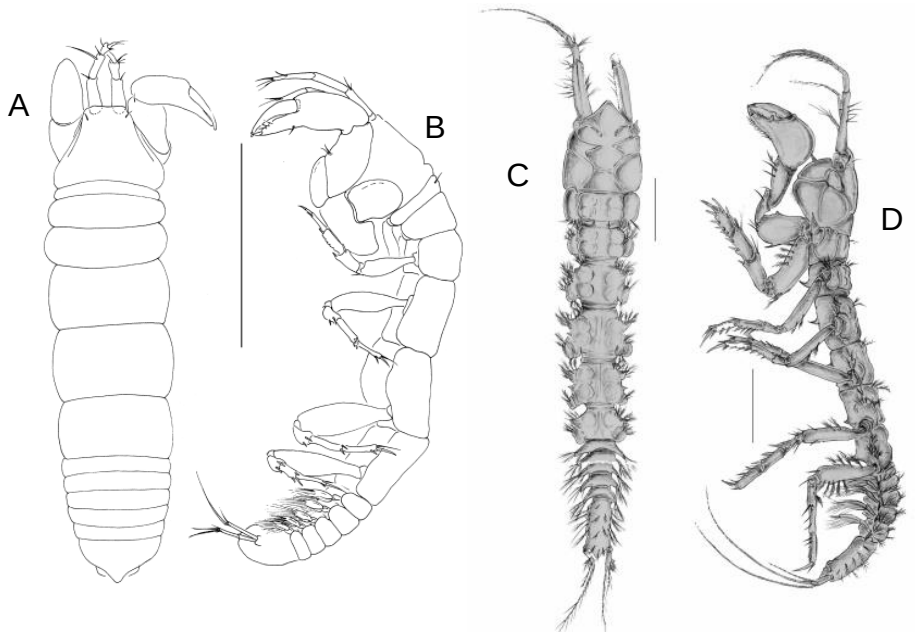

Figure 13 - Specie *Pseudotanais (Pseudotanais) tympanobaculum*. A – Dorsal aspect; B – Lateral aspect. Scale line = 1 mm (from Blazewicz-Paszkowycz *et al.* 2011a). Specie *Apseudes setiferus*. C – Dorsal aspect; D – Lateral aspect. Scale lines = 1 mm (from Blazewicz-Paszkowycz *et al.* 2011b).

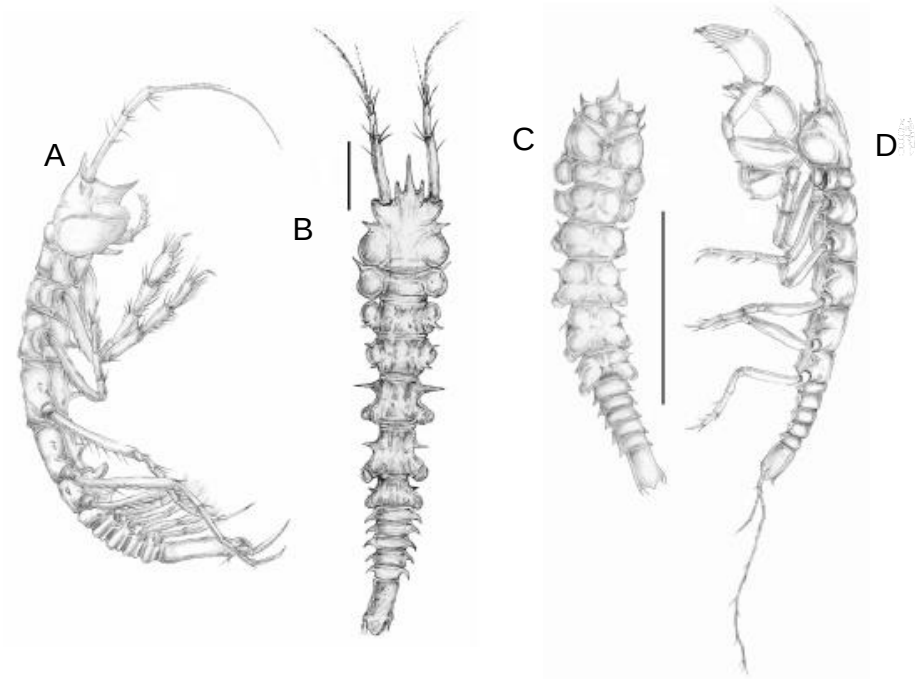

Figure 14 - Specie *Apseudes grossimanus*. A – Lateral aspect; B – Dorsal aspect. Scale line = 1 mm. Specie *Atlantapseudes nigrichela.* C – Dorsal aspect; D – Lateral aspect. Scale line = 2 mm (from Blazewicz-Paszkowycz *et al.* 2011b).

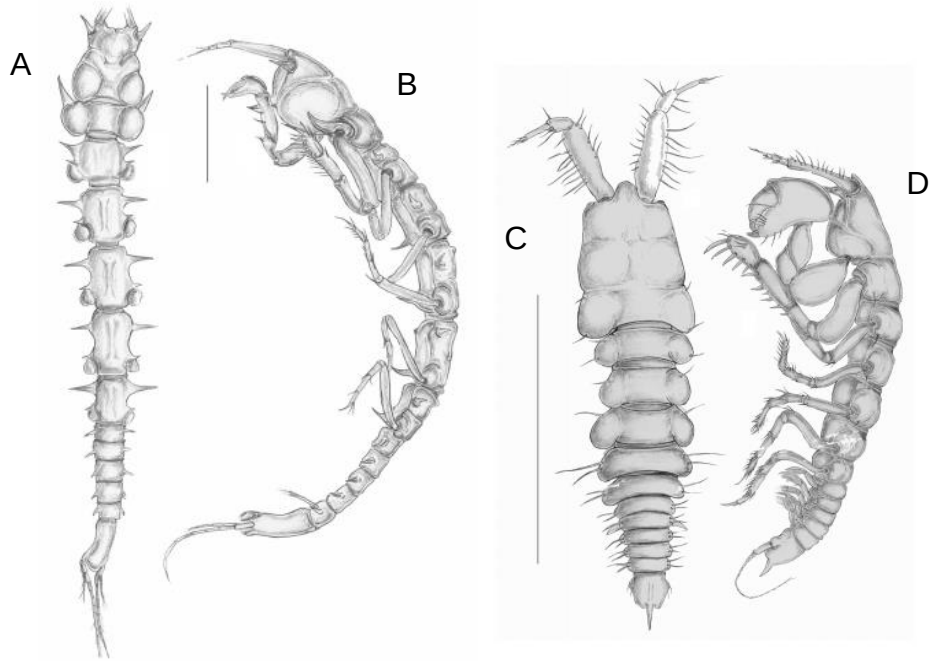

Figure 15 - Specie *Fageapseudes retusifrons*. A – Dorsal aspect; B – Lateral aspect. Scale line = 1 mm. Specie *Sphyrapus malleolus.* C – Dorsal aspect; D – Lateral aspect. Scale line = 1 mm (from Blazewicz-Paszkowycz *et al.* 2011b).

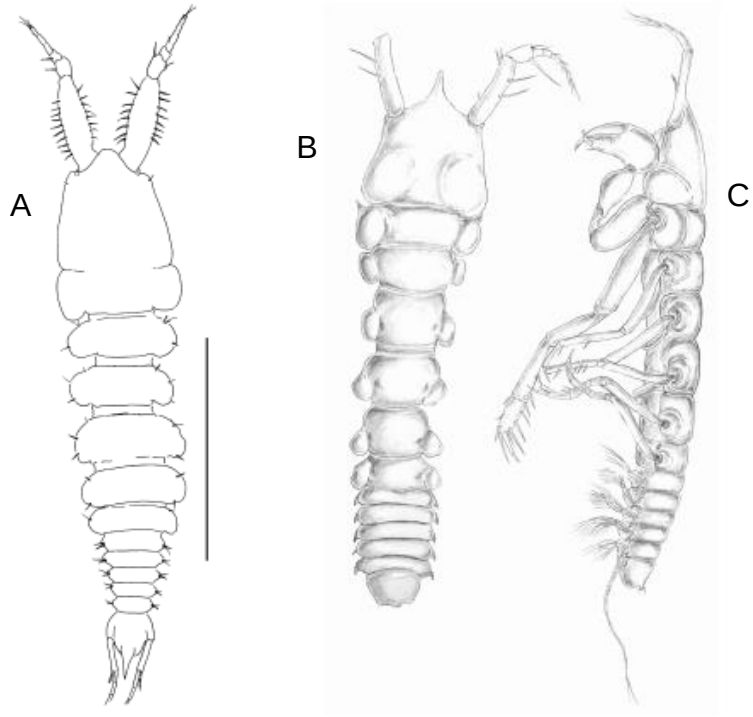

Figura 16 – Specie *Sphyrapus meknes*. A – Dorsal aspect. Scale line = 1 mm. Specie *Pseudosphyrapus* sp. A. B - Dorsal aspect; C - Lateral aspect (from Blazewicz-Paszkowycz *et al.* 2011B).

Class Ophiuroidea

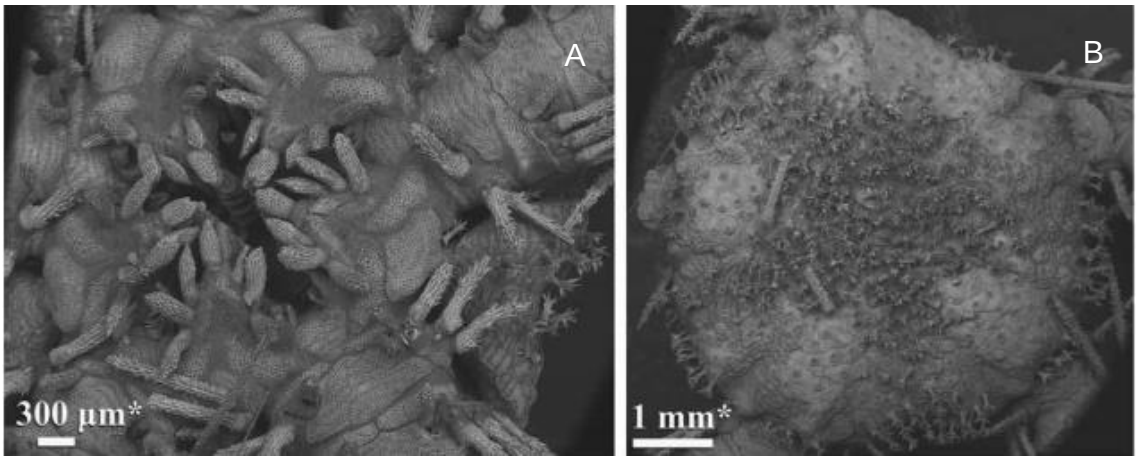

Figure 17 - Specie *Ophiacantha aristata.* A - Ventral aspect; B - Dorsal aspect (from Rodrigues *et al.* 2011).

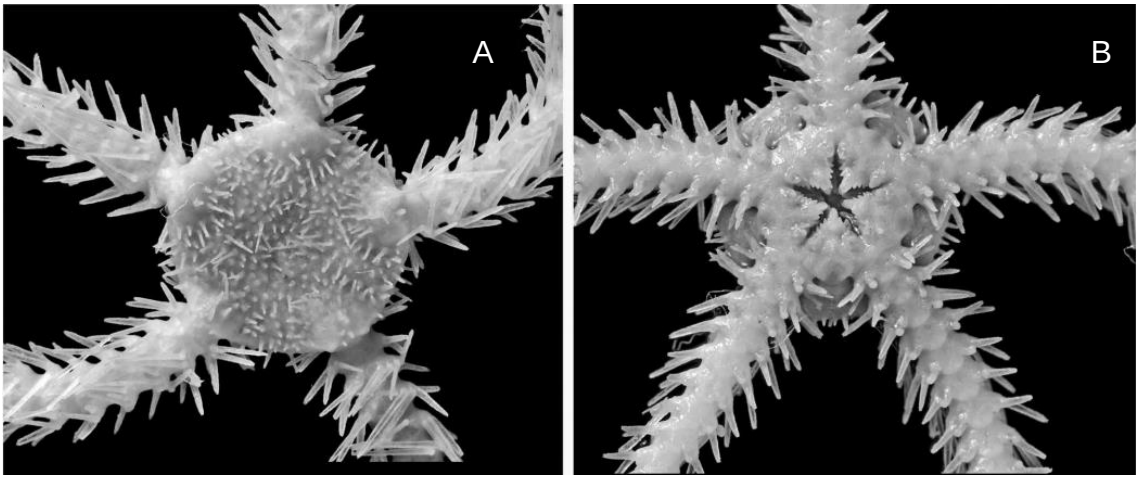

Figure 18 - Specie *Ophiopristis gadensis.* A - Ventral aspect; B - Dorsal aspect. Scale bars = 1 cm (from Rodrigues *et al.* 2011).

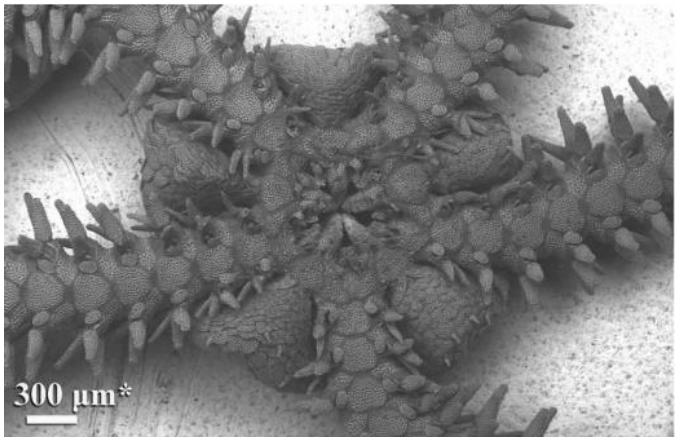

Figure 19 – Specie *Ophiactis abyssicola* - Ventral aspect (from Rodrigues *et al*. 2011).

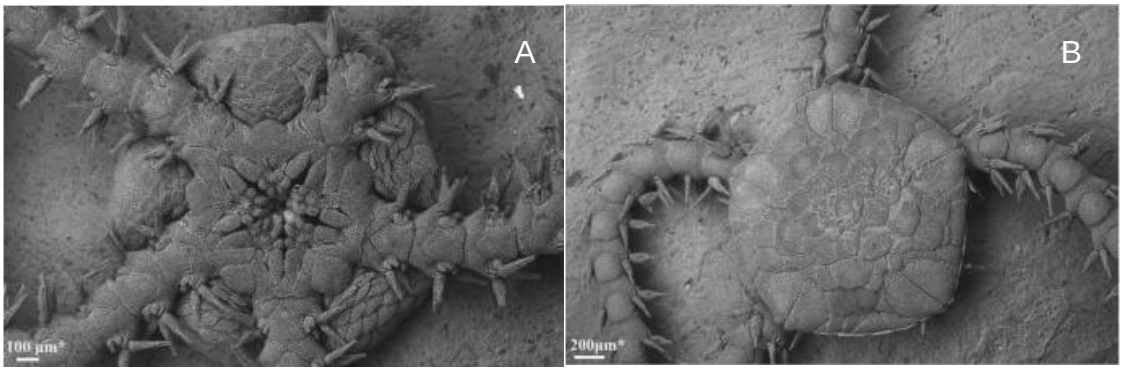

Figure 20 - Specie *Amphipholis squamata* (from Rodrigues *et al.* 2011). A - Ventral aspect; B - Dorsal aspect.

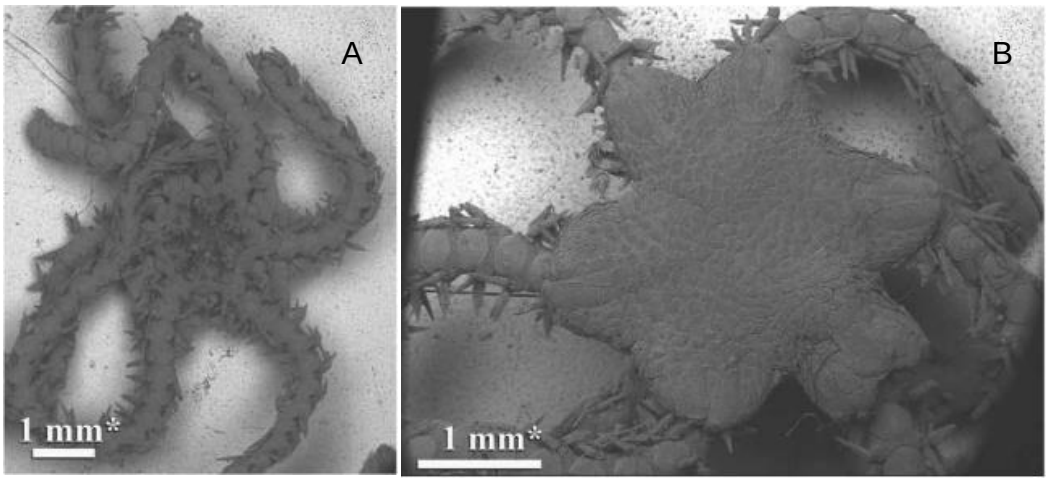

Figure 21 – Specie *Amphioplus hexabrachiatus* (from Rodrigues *et al*. 2011). A - Ventral aspect; B - Dorsal aspect.

Class Gastropoda

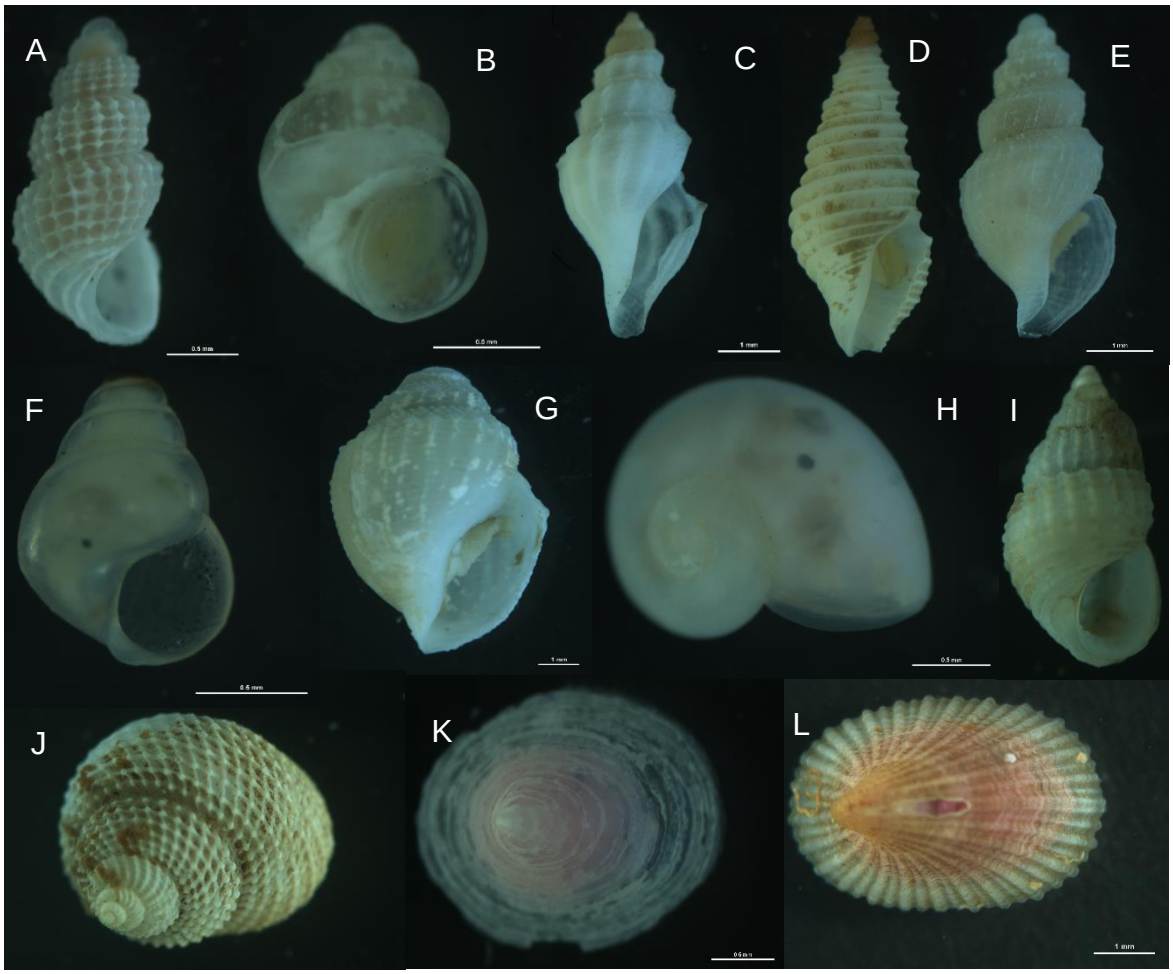

Figure 22 – A - Specie *Alvania tomentosa*; Scale bars = 5 mm. B - Specie *Obtusella intersecta;* Scale bars = 5 mm. C - Specie *Benthomangelia macra;* Scale bars = 1 mm. D - Specie *Drilliola loprestiana.* E - Specie Taranis cf. alexandrina; Scale bars = 1 mm. F - Genus *Pseudosetia*; Scale bars = 0,5 mm. G - Specie *Gymnobela Aquilarum;* Scale bars = 1 mm. H - Specie *Moelleriopsis* cf. *messanensis*; Scale bars = 0,5 mm. I - Family Rissoidae. J - Specie *Putzeysia* cf. *wiseri.* K - Specie *Pyropelta* aff. *sibuetae*; Scale bars = 0,5 mm. L - Genus *Puncturella*; Scale bars = 1 mm (Luciana Génio and Fábio Matos, CESAM, Biology department, Aveiro University).